ISSN 2730-2695

THAI GEOSCIENCE JOURNAL

Vol. 2 No. 2 July 2021

NEW NORMAL

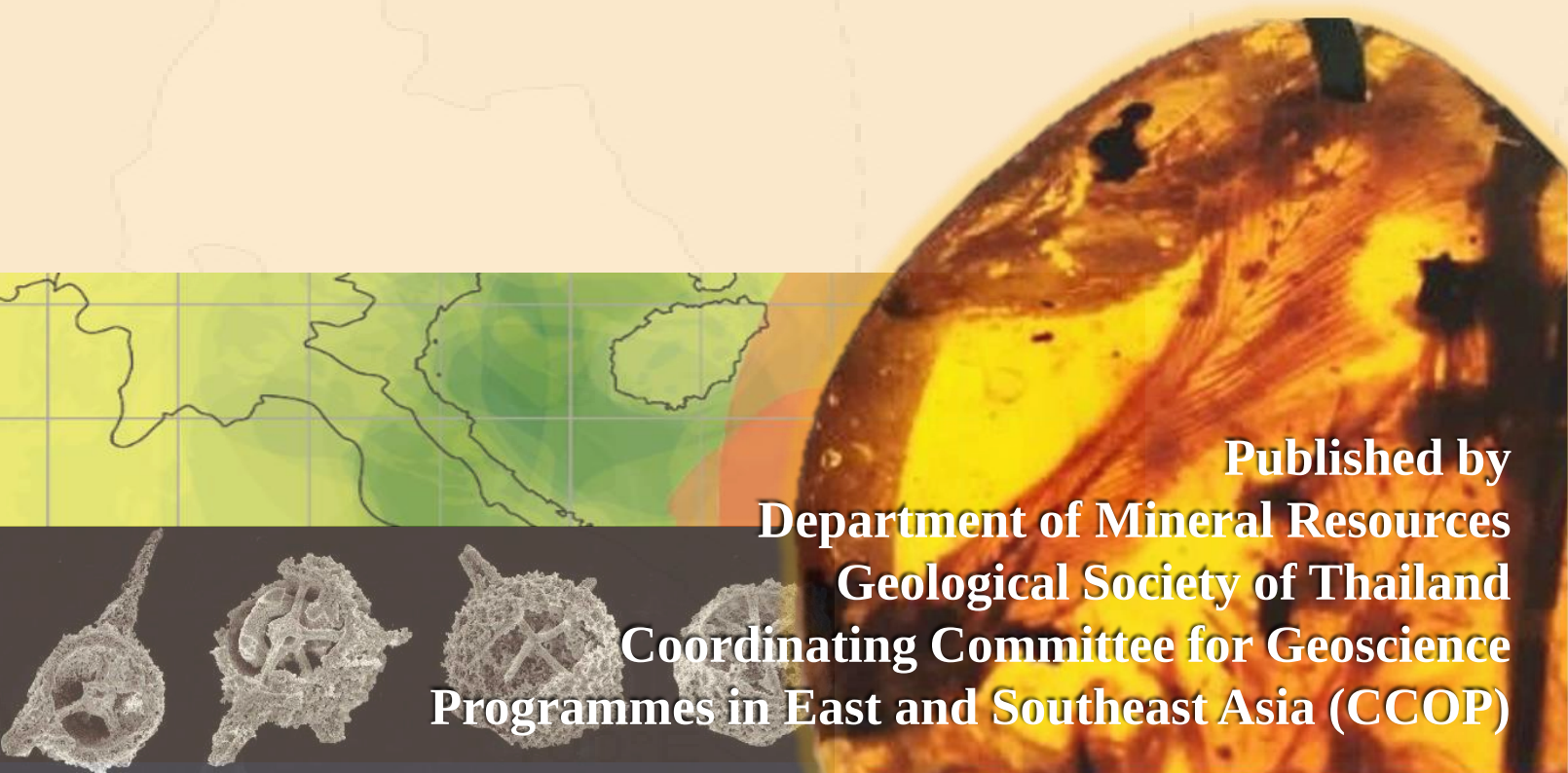

Published by
Department of Mineral Resources
Geological Society of Thailand
Coordinating Committee for Geoscience Programmes in East and Southeast Asia (CCOP)

Editorial Committee

On the cover

1) Combined positive and negative data for source crater location. Greener areas = higher probability. Yellower areas = lower probability. Red / orange areas = no probability. (*Aubrey Whymark , p.22, fig. 23*)

2) Bird-Feather in Khamti amber (photomicrographs by Thet Tin Nyunt; dark field, 40×) (*Thet Tin Nyunt et al., p.68, fig. 9)*

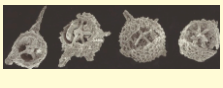

3) Radiolarian SEM photos of Mississippian chert from southern peninsular Thailand. All scale bars indicate 100 μm. (*Katsuo Sashida et al., p.77, fig. 5*)

THAI GEOSCIENCE JOURNAL

Vol. 2 No. 2
July 2021

Published By
Department of Mineral Resources • Geological Society of Thailand
Coordinating Committee for Geoscience Programmes in East and Southeast Asia (CCOP)

Thai Geoscience Journal website at http://www.dmr.go.th/tgjdmr

Preface

The Thai Geoscience Journal, Volume 2 Number 2, online in July 2021, constitutes our One Year Anniversary issue. We propose continuing our journal with several kinds of geological and geoscience objectives and with an increased distribution. We need more co-operation with global geoscience organizations. In this issue we welcome the Coordinating Committee for Geoscience Programmes in East and Southeast Asia (CCOP) as our co-organizers of the TGJ. We have the honor to warmly welcome Dr. Young Joo Lee, Director of CCOP as our Honorary Editor along with his colleagues to our editorial team.

The COVID-19 pandemic situation has changed the life and behavior of people around the world. The New Normal has changed with most of us working at home (WFH) along with social distancing. Our New Normal geological life means that it is difficult and dangerous to go in the field. In this situation, we will probably do more research about data management instead and write articles from our stored data and then hopefully send the results to TGJ.

We sincerely hope that the COVID-19 pandemic will soon be over and bring back our life even though it will not be quite the same. We hope to find a new way of life and learn to be happy again. Finally, we are pleased to invite all geologists, scientists and researchers to publish in our TGJ.

Thank you very much.

(Dr. Sommai Techawan)
Director-General of the Department of Mineral Resources
President of the Geological Society of Thailand

From the editor

Welcome to the Thai Geoscience Journal, Volume 2, Number 2. It is almost one year since the first TGJ issue in July 2020. We have connected our TGJ to the Coordinating Committee for Geoscience Programmes in East and Southeast Asia (CCOP) as the co-organizer for this publication and we will be working together on this and subsequent issues. We very much appreciate the kind cooperation of Dr. Young Joo Lee, Director of CCOP, and Dr. Dhiti Tulyatid, Regional Expert, CCOP.

This issue includes many geological articles from the CCOP's annual meeting and other researchers. The New Normal geoscience article discussing Covid-19 and the world's population is very relevant to the current situation. The paper on the Australasian tektite forming crater is a continuing theme from TGJ Vol.2 No.1 and may inspire researchers who are interested in this new theory. This issue also includes various and interesting articles such as the 3D geological mapping in Tokyo, Japan, mineral resources studies (monazite and xenotime in Malaysia, and gemmology in Myanmar), and Carboniferous radiolarians in Thailand.

Finally, we would like to express our appreciation to all of our TGJ Vol.2 No.2's authors for publishing your valuable articles in TGJ. As the TGJ editor in chief, I would like to express my thanks to TGJ's honorary, advisory, associate editors, and reviewers for their kind support. Special thanks are due to the editorial secretary team who have worked very hard on every TGJ issue. We continue to strive to make TGJ a high international standard journal and welcome all researchers to be TGJ members and to be part of our geoscience community.

Thank you very much.

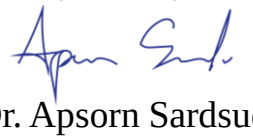

(Dr. Apsorn Sardsud)
Editor in Chief
Thai Geoscience Journal

Thai Geoscience Journal
Vol. 2 No. 2
July 2021
ISSN 2730-2695

LIST OF CONTENTS

Thai Geoscience Journal website at http://www.dmr.go.th/tgjdmr
Printed: 2twin Printing tel +66 2 185 9953, July 2021

Thai Geoscience Journal 2(2), 2021, p. 1-29

ISSN-2730-2695; DOI-10.14456/tgj.2021.2

A review of evidence for a Gulf of Tonkin location for the Australasian tektite source crater

Aubrey Whymark*

Consultant Wellsite Geologist, Manila, Philippines.
Corresponding author: aubrey@tektites.info
Received 5 March 2021; Accepted 17 June 2021.

Abstract

Australasian tektites (AAT) occur across Southeast Asia, Australia, the Indian Ocean, and southwest Pacific Ocean. AAT form the youngest and most extensive major tektite strewn field. Unlike other tektite strewn fields, AAT have no known source crater. Review of the literature establishes that a single ~ 43 km post-impact diameter crater exists, possibly significantly enlarged by slumping. The obliquity of the impact that formed the AAT would result in a crater that is less pervasive in depth but with greater downrange shock effects and melt ejection. Multiple lines of evidence, historically viewed in isolation, were examined, concatenated, contextualized, and discussed. Tektite morphology and distribution; microtektite regressions; geochemical considerations, comparisons, and iso--concentration regressions; lithological characteristics; age of source rock; and regional geological considerations are reviewed. The source material is predicted to be an abnormally thick sequence of rapidly deposited, poorly compacted, deltaic to shallow marine, shales to clay-rich siltstones of early Pleistocene to Pliocene age. The impact likely occurred in a shallow marine environment. Forty--two maps of positive and negative parameters are presented and overlain. These indicate the AAT source crater probably lies in the central to northwestern Yinggehai - Song Hong Basin / Gulf of Tonkin. This geochemically optimal setting is characterized by exceptionally high sedimentation rates that explain the ^{10}Be and Rb-Sr age discrepancy, the seawater signature, and apparent absence of a crater by rapid burial.

Keywords: Australasian tektite, Gulf of Tonkin, impact crater, Pleistocene, Song Hong Basin, Yinggehai Basin.

1. Introduction

Tektites are naturally occurring, holohyaline macroscopically homogenous, droplets formed by the melting and ballistic ejection of silica--rich target rocks by large cosmic impacts. Australasian tektites (AAT) form a young and extensive strewn field covering over 10% of the Earth's surface. All major tektite groups, apart from the AAT, have been geochemically associated with terrestrial impact craters. AAT have been extensively studied, drawing data from diverse and disparate fields, each yielding conclusion in isolation. This article attempts to concatenate all available evidence to identify the probable AAT source crater location.

2. Constraints

2.1 Presence of a Crater: All other known tektite strewn fields are associated with craters. The existence of silica-rich ballistic ejecta with low-angle trajectories and velocities exceeding 5 km/s (Chapman, 1964) demonstrates a direct transfer of energy, as opposed to an aerial burst (Wasson, 2003), or impact plume (Wasson, 2017) scenario. An impact crater is concluded to exist.

2.2 Single or Multiple Craters: The distance of ejection can be related to crater size, which in turn is a function of the mass and velocity of the impactor (Elliott, Huang, Minton, & Freed, 2018). Other factors, such as obliquity of impact and target composition, also influence distance of ejection and are discussed in Section 2.6. The distance between the most northerly Indochinese macro-tektites and most southerly Australian macro-tektites exceeds 8,500 km. The implication is that at least one large impact crater is present. A thorough review of the geochemistry of tektites (Schnetzler & Pinson Jr, 1963), concluded that a random process of formation or multiple separate impacts could

be excluded. Nd and Sr isotopic variations indicate a single impact event (Blum, Papanastassiou, Koeberl, & Wasserburg, 1992; Shaw & Wasserburg, 1982). Rare-earth elements (REE) indicate a single reasonably uniform source (Koeberl, 1994; Koeberl, Kluger, & Kiesl, 1985). It is concluded that a single large crater in a relatively homogenous source rock exists. Associated smaller craters in the same source rock cannot be excluded but are not required.

2.3 Age: AAT are 786 ± 2 ka based on $^{40}Ar/^{39}Ar$ dating of tuffs at ODP Site 758 and relative stratigraphic position to Termination IX (Mark et al., 2017) or 788.1 ± 3 ka based on the $^{40}Ar/^{39}Ar$ age data from four AAT (Jourdan, Nomade, Wingate, Eroglu, & Deino, 2019). The impact occurred during a glaciation where the continental shelf would be subaerially exposed or covered by very shallow seas. The young age means that geological evidence of the structure could not have been eroded away. The structure exists, even if buried. The recent age of ejecta means that the tektite distribution suffers little stratigraphic outcrop bias. Plate tectonic shift of the crater and ejecta has a low significance over this short period of time, but in high resolutions should be considered.

2.4 The Crater Size: Utilizing microtektite data and the methodology of Stöffler, Gault, Wedekind, & Polkowski (1975), which is calibrated to known impacts and thus has a high expectation for accuracy, a post-impact crater diameter of 32 ± 14 km is derived (Glass & Pizzuto, 1994), or 33 ± 8 km (Prasad, Mahale, & Kodagali, 2007). If un-melted ejecta estimates are considered, which should provide an even more accurate estimate, a 39 to 44 km (Glass, 2003) and 43 ± 9 km (Glass & Koeberl, 2006) diameter crater estimate is derived. Studying the compositional range of condensate droplets (bottle-green microtektites), which reflect plume cooling rate and therefore plume size, a 40 to 60 km diameter crater was estimated (Elkins-Tanton, Kelly, Bico, & Bush, 2002).

Tektite distribution can be compared with tektite / spherule strewn fields that have a known crater, but source rock, fluid content, sea depth, and impactor parameters, particularly velocity and obliquity of impact may have varied. It can be crudely ascertained that the AAT source crater is likely larger than the 24 km diameter (Schmieder & Kring, 2020) Ries Crater, significantly smaller than the 100 km diameter (Schmieder & Kring, 2020) Popigai Crater, and broadly comparable with the 40 to 45 km (Schmieder & Kring, 2020) Chesapeake Bay Crater, with slumped outer rim of 80 to 90 km (Collins & Wünnemann, 2005).

In conclusion, a crater with 43 ± 9 km diameter (Glass & Koeberl, 2006) should be sought. If the crater is in a continental shelf setting then, post-impact, it may be slumped to 80 to 90 km or more in diameter.

2.5 Obliquity of Impact / Crater Geometry: The AAT impact was oblique, and this is very adequately demonstrated by asymmetric morphological and geochemical variations of tektites that indicate the source crater is in the broad Indochinese portion of the strewn field. The obliquity of the impact would reduce the depth and volume of melted and shocked materials at the impact site and enhance the volume of ejected melt (including tektites) (Pierazzo & Melosh, 2000). However, highly oblique impacts (<5°) may have a negative effect on tektite production as the first formed ejecta must travel a greater distance to traverse the atmosphere.

To establish whether the impact was a highly oblique (<5°) grazing impact, or an oblique (5° to 30°) impact the distal ejecta pattern should be reviewed. The AAT strewn field has a downrange lobe of ejecta, mirroring forbidden zones, and butterfly lobes, typical of impacts below 45° (Gault & Wedekind, 1978). The bilateral symmetry of the downrange ejecta is broadly along a 164° azimuth and the butterfly lobes are ~62° offset from the center of the downrange ejecta. In grazing impacts that produce elliptical craters a 90° offset from the center of the downrange ejecta would be anticipated (Gault & Wedekind, 1978).

Highly oblique grazing impacts result in increased projectile contamination of the target melt (Artemieva & Pierazzo, 2003; Stöffler, Artemieva, & Pierazzo, 2002), something not observed in AAT.

In a grazing impact there should be an uprange forbidden zone, but in less oblique impacts the uprange forbidden zone may close as the impact

proceeds (Schultz, Anderson, & Hermalyn, 2009; Schultz et al., 2007). Therefore, the presence of uprange tektites is an argument against a grazing impact. This will be discussed further as the evidence is presented.

AAT distribution suggests an oblique impact above 5° but, by comparison to Artemieva (2013), under 30°. An oblique impact is optimal for melt (tektite) ejection (Pierazzo & Melosh, 2000) and will limit downward shock effects at the impact site. The impact crater might be asymmetrical in its depth profile, deeper in a north-northwesterly direction, after Gault & Wedekind (1978). If there was subsequent slumping this may be influenced by the asymmetry of the post-impact crater profile and might result in an elliptical slumped crater. The above factors may result in a less pervasive crater with atypical morphology. This would make recognition more problematic.

2.6 Tektite Morphological Regression: AAT fall into three transitional but readily differentiable morphological groups, which can be compared with tektites in strewn fields with a known source crater. Distal tektites (e.g., Australites) were the first formed, highest velocity tektites. They underwent minimal plastic deformation as the molten body exited the atmosphere, suffered ablation during re-entry, then spallation. Medial tektites (e.g., Philippinites, Billitonites, and Bediasites) underwent moderate plastic deformation as the molten body exited the atmosphere, re-entry heating that was insufficient for ablation to occur, and then spallation. Proximal tektites (e.g., Indochinites, Moldavites, Georgiaites, Ivory Coast Tektites) underwent significant plastic deformation as they interacted with the atmosphere at lower altitudes, suffered minimal re-entry heating and minimal spallation. Muong Nong-type (MN-type) layered impact glass, whilst ballistically ejected, never formed discrete surface tension-controlled droplets due to lower melt temperature. MN-type layered impact glasses represent the lowest energy, theoretically most proximal, melts.

The lower ablation limit for tektites is about 5 km/s (Chapman, 1964). This is the defining boundary between medial and distal tektite morphologies. Within the AAT strewn field, the most northerly ablated downrange tektites are found in Sangiran, Java (Chapman, 1964). To the north (along an azimuth towards Indochina), tektites are not ablated and therefore re-entered at velocities below about 5 km/s. Taking Sangiran, Java, as the 5 km/s mark, and utilizing trajectory calculations from *Orbit 1.2 Software* (1998-2000), the crater likely lies somewhere between 3,319 km away (37° ejection angle) and 2,632 km away at 20° and 56.8° ejection angle (shown in Fig. 1). At ejection angles lower than 20° or higher than 56.8° (which are less likely) the crater will be even closer. A potential margin of error of hundreds (but not thousands) of kilometers exists, but this calculation indicates the most probable impact region and rules out the wildest crater guesses where modelled re-entry velocities do not match observed physical attributes of the tektites. Re-entry angles of tektites over Java were likely quite oblique with angles of 20° to 25° probably being realistic, implying a distance from the source crater of 2,632 km to 2,992 km, again within a margin of error being present.

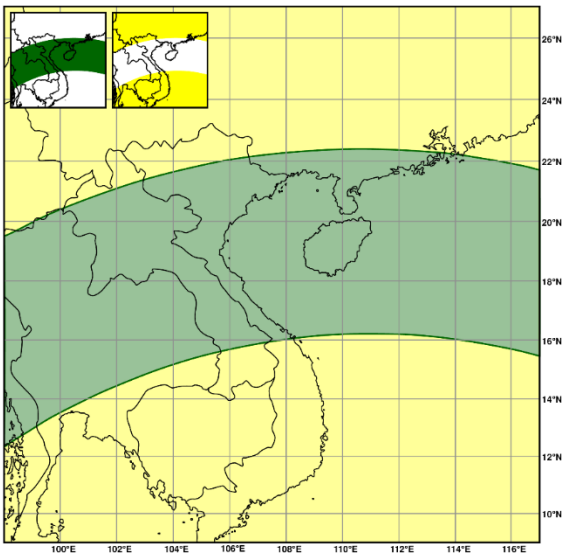

Fig. 1: Taking Sangiran, Java, as the 5 km/s mark, where the most northerly directly downrange ablated tektites exist, the crater likely lies somewhere between 3,319 km away (37° ejection angle) and 2,632 km away at 20° and 56.8° ejection angle. The AAT crater probably lies within the belt highlighted in green. The middle to southerly portion of the green shaded region is most probable based on a 20° to 25° re-entry angle for tektites in Java. The yellow area is lower probability. Inset: Data used in map overlay. Green = Probable regions; Yellow = Less favorable regions for the AAT impact.

Increased target rock compressibility can enhance melt production (Stöffler, Hamann, & Metzler, 2018). Obliquity of impact can enhance

melt ejection (Pierazzo & Melosh, 2000). Water-rich surface layers can potentially enhance melt production and ejection (K. T. Howard, 2011). These factors, together with the size of the impact, result in greater tektite abundance (assuming suitable source rocks) and distance of ejection (asymmetrically in the case of oblique impact). Regardless of scaling, the distal, medial, and proximal tektite morphological divisions would be expected to be found at broadly the same distance from the impact location. This is because the morphological divisions are primarily related to re-entry heating, controlled principally by velocity. A re-entry tektite must travel from the crater location to a fall location. It can theoretically do so by any combination of angle and velocity that achieves the defined distance. Ejection angles of 15° to 50° result in tektite velocities of: 2.87 to 3.74 km/s to land at 900 km; 3.70 to 4.50 km/s to land at 1,650 km; and 6.40 to 7.05 km/s to land at 6,800 km from the impact location (*Orbit 1.2 Software*, 1998-2000). Velocity values are reasonably constrained regardless of the ejection angle.

Oblique impacts result in a low-angle downrange ejection of the highest velocity melts compared to vertical impacts that result in higher angle omnidirectional ejection of melt (Gault & Wedekind, 1978). The melt will travel further in oblique impacts, but at lower angles. In more energetic oblique impacts, sufficient energy is present in the later stage of impact to yield high-angle omnidirectional melts as well as the initial higher velocity low-angle downrange melt ejecta. So, at a set distance from the impact crater the ejecta may be low-angle melts derived from a smaller oblique crater or (low and) high-angle melts derived from a larger oblique or vertical impact. Morphological differences would be anticipated between low- and high-angle melt ejecta. Low-angle tektites will encounter greater atmospheric interaction. This manifests morphologically in cascading to smaller bodies in a hot melt, or by plastic deformation in a cooler more viscous melt during exit, and in a longer duration of heating during re-entry.

The question arises whether magnitude and obliquity of impact, which may affect ejection angle, influences the distance at which morphological groups theoretically occur. In short, it does, but to a minimal degree: this methodology will not offer precision but is expected to deliver a broadly accurate result. This is because re-entry velocity does not vary dramatically in response to expected re-entry angles at a fixed location. It is the tektite velocity that defines the boundary between distal and medial forms. The medial to proximal boundary is a little more complex: again, the medial morphology requires a certain re-entry velocity / heating, but spallation can be over-ridden by the glass temperature in the re-entry phase. If the glass retained sufficient temperature from formation, crack growth and spallation are inhibited. Scaling may have greater influence in the proximal realm, but the prerequisite for sufficient velocity to produce medial cores validates that all medial cores should be found at similar distances from the source. Variations in core morphology are illustrated in Fig. 11 of Chapman (1964). Uncertainty in comparisons may be reduced further by comparing tektites from similar craters in terms of magnitude, obliquity, and target.

The distance of proximal and medial North American tektites from the Chesapeake Bay source crater can be compared with Australasian tektites. The two impacts are comparable in terms of calculated magnitude and can be inferred to have similar target rock characteristics as both impacts yield widespread tektites. The asymmetry of the North American tektite distribution suggests the Chesapeake Bay impact was oblique, although likely less oblique than the AAT impact. Within the North American strewn field, the medial tektite morphologies are found at distances of 1,955 km to 2,180 km (O'Keefe, 1963) southwest from the point of impact. The proximal North American tektites are found predominantly to the southwest at distances of 635 km to 930 km (Povenmire, 2010; Povenmire & Strange, 2006). The comparable Chesapeake Bay impact is used to evaluate the AAT impact crater location.

The Central European strewn field yields proximal tektites at distances of 185 km to 430 km (Čada, Houzar, Hrazdil, & Skála, 2002; Trnka & Houzar, 2002) from the Ries source crater. The Ivory Coast strewn field yields tektites at distances of 255 to 320 km (Gentner, 1966)

from the Bosumtwi source crater. These smaller impacts demonstrate that true tektites can occur in closer proximity to the crater.

The North American Bediasites are morphological equivalents to Philippinites, Malaysianites, Brunei tektites, Billitonites and northern Indonesianites. In North America similar morphologies occur at distances of 1,955 to 2,180 km (O'Keefe, 1963) from the impact site and do not occur within 930 km (Povenmire, 2010) from the impact site. All locations within 930 km of medial tektite occurrences can be eliminated as shown in red in Fig. 2. It can be established that by 1,955 km there are no proximal tektite morphologies (the true number is likely much less but cannot be calibrated). The source crater must be within 1,955 km of all proximal tektite morphologies. This further restricts the potential source area (green region in Fig. 2). A focal point can be established by assuming all proximal tektites occur within 930 km of the impact site. The actual number is somewhere between 930 and 1,955 km but likely close to the lower limit for the AAT when cross referenced with other evidence presented in this article. The focal point is therefore an area of highest probability but does not rule out surrounding areas. This approach is demonstrated by the dark green region in Fig. 2.

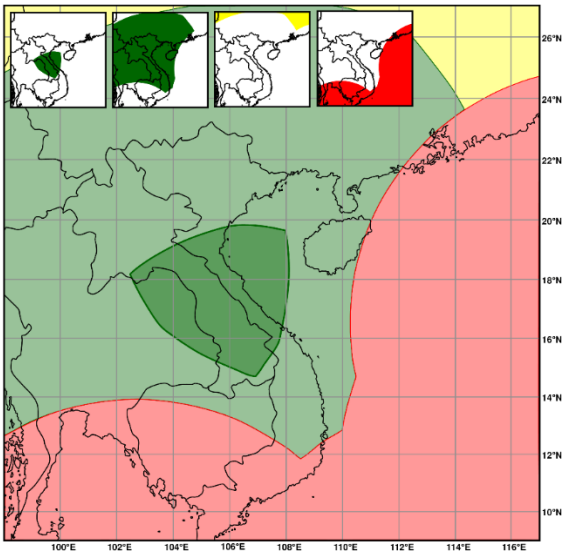

Fig. 2: A map utilizing data from the North American strewn field and comparing it with morphological groups of tektites in the Australasian region. All medial tektites (e.g., Philippinites) should be at least 930 km from the source crater, ruling out the areas in red. Medial tektite locations used: 16.386186° N, 119.892056° E, Bolinao, Philippines; 10.955550° N, 119.405150° E, northern Palawan, Philippines; 4.952386° N, 114.835486° E, Brunei; -2.923631° S, 108.206319°E, Belitung, Indonesia; 4.750000° N, 103.166667° E, Malay Peninsula, Malaysia. All proximal tektites (e.g., Indochinites) should be within 1,955 km of the source crater: possible areas are in green. If it is assumed that all proximal tektites occur within 930 km of the source crater (a number likely marginally too low) then the darker green area is the most probable crater location (in reality, this is almost certainly a broader area focused on this region as 930 km represents a minimum value). The yellow area is lower probability. Inset: Data used in map overlay. Green = Probable regions; Yellow = Less favorable regions; Red = Incompatible regions for the AAT impact.

2.7 Distribution of MN-Type Layered Impact Glass: Muong Nong-type (MN-type) layered impact glasses are the lowest temperature ballistically (Huber, 2009; Koeberl, 1992; Schnetzler, 1992) ejected melts. These impact glasses are not entirely homogenized, are volatile-rich in comparison to tektites, contain relict mineral grains, and have alternating layers of different composition (Koeberl, 1986). Logically, MN-type tektites are expected to occur in proximity to the source crater. A triangular wedge-shaped ~65,000 km^2 area was noted in northeastern Thailand, southern Laos, and central Vietnam where MN-type layered impact glasses occur in the absence (or near-absence) of true splash-form tektites (Fiske et al., 1999; Schnetzler & McHone, 1996) (see Fig. 3). Further afield a mixture of MN-type layered impact glasses and splash-form tektites occur. Then further out, importantly in all directions, only splash-form tektites, in the absence of MN-type layered impact glasses, occur (Fig. 3). This triangular wedge-shaped area of MN-type layered impact glasses has been assumed by many to represent the center of the proximal tektite distribution and the impact crater should lie close by. However, this region of MN-type impact glasses is neither in the most northwesterly part of the strewn field nor in the center of the proximal splash-form tektite and MN-type impact glass distribution: instead, it is rather unsatisfactorily to the southwest of center.

The triangular wedge of MN-type layered impact glasses can be followed to the southwest (see Fig. 3) and it appears to be the proximal part of the prominent southwesterly butterfly ray. This ray extends into the central Indian Ocean and beyond, almost reaching the southernmost tip of Africa. The triangular wedge of MN-type

layered impact glasses points towards an origin in the Gulf of Tonkin, possibly forming arcuate rays in a cardioid (heart)-shaped pattern, with reference to Schultz et al. (2009, 2007). A mirroring wedge of MN-type layered impact glasses would be expected on the southeasterly butterfly ray that extends through northern Manila and Paracale in the Philippines, onwards in the direction of Micronesia in the southern Pacific Ocean. This mirroring wedge of MN-type layered impact glasses cannot be observed, if present, as it falls in the Gulf of Tonkin and South China Sea. In support of its presence, rare examples of MN-type layered impact glasses have been found along the same trajectory in Manila and Paracale in the Philippines (Chapman & Scheiber, 1969; Whymark, 2020). It is apparent, as seen in all oblique crater ray systems, that ejecta distribution is not equal. This scenario is depicted in Fig. 3.

Regardless of whether the triangular wedge--shaped area of MN-type layered tektites is accepted as the center of distribution or whether this region is accepted as the proximal part of the southwesterly butterfly ray, with the center of distribution in the Gulf of Tonkin, it is evident the lowest temperature melts are not concentrated in the most northwesterly area of tektite distribution (i.e., Yunnan and Guangxi regions of China and northern Vietnam) (Fig.4). This observation is critical as it implies a crater located in the center of the proximal part of the strewn field and implies the presence of uprange ejecta.

2.8 Tektite Crater Rays: Ejecta rays can be seen emanating from craters on geologically less active planetary bodies (e.g., the Moon, Mercury, Ganymede). Increased gravity and increased atmospheric density (e.g., Venus) will act to suppress ejecta rays (Schultz, 1992). The Earth has slightly greater gravity than Venus but the atmosphere on Earth is significantly less dense. Tektite droplets, forming from the ejecta curtain at altitude, would be less inhibited on Earth, compared with Venus. The presence of distal AAT (e.g., Australites) that re-entered the atmosphere (Chapman, 1964) is proof that AAT ejecta was not wholly suppressed by the Earth's gravity and atmosphere. The distance that AAT ejecta has travelled, by comparison to crater rays

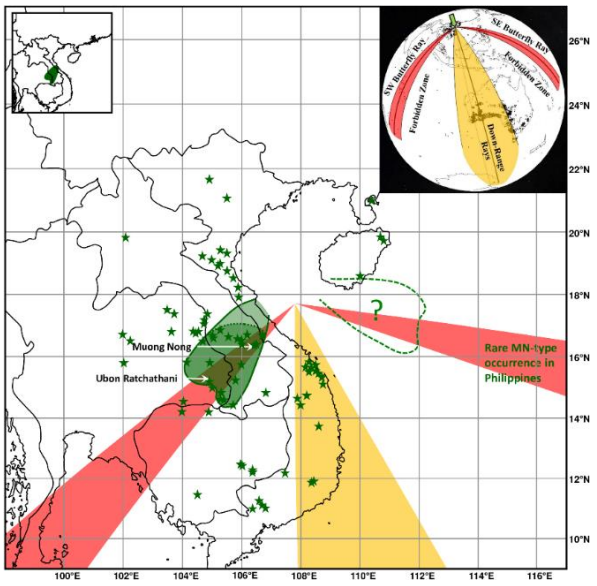

Fig. 3: The distribution of MN-type layered impact glasses (green stars). The green region is predominantly MN-type layered impact glasses in the absence (or near-absence) of splash-form tektites (Fiske et al., 1999; Schnetzler & McHone, 1996). This region has traditionally been taken as the center of the Australasian strewn field. In fact, it may represent one of two butterfly rays emanating from the Gulf of Tonkin (suggested by green dashed line) (Whymark, 2020). The most prominent rays are indicated, with an assumed crater position in the Gulf of Tonkin as per Whymark (2013) (note that this location is not proven). Note how the green region of MN-type layered impact glass and prominent localities such as Muong Nong and Ubon Ratchathani lie beneath this inferred ray. Inset: Data used in map overlay. Green = Probable regions for the AAT impact.

on other planetary bodies, indicates that tektites are part of a crater ray system as opposed to randomly distributed.

In Australia, the prominent linear tektite concentration that runs through South Australia, Victoria, and into Tasmania has a distinct high calcium (HCa) geochemical profile (Chapman, 1971). The combined linear tektite distribution and distinct geochemistry indicate this feature is an ejecta ray. The presence of at least one AAT ejecta ray suggests the existence of a crater ray system. Tektite distribution patterns, in terms of location, abundance, and maximum tektite size, hint at a further two ejecta rays in Western Australia. In the Philippines, a prominent ray is suggested from Zambales, through northern Manila, Rizal Province (Tanay, Siniloan), Paracale, Catanduanes, and onwards into the Pacific Ocean. Notably, this ray yields the largest splash-form tektites in existence (Whymark, 2015). Further, less distinct,

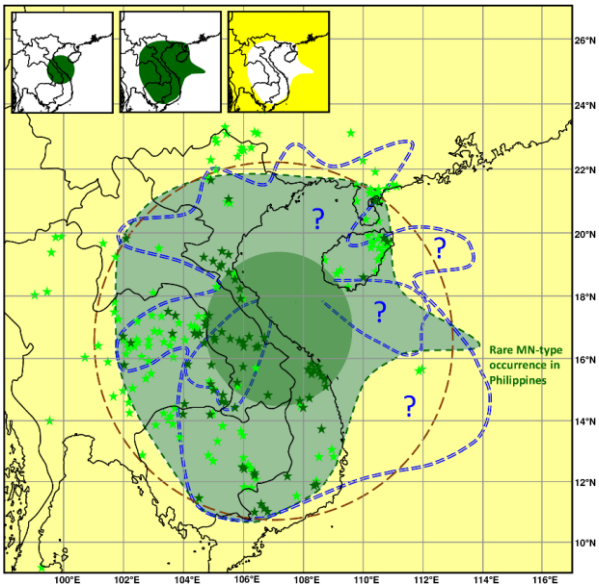

Fig. 4: Possible solutions for the distribution of MN-type layered impact glasses. Dark green stars represent MN-type layered impact glass occurrence. Bright green stars represent splash-form or undifferentiated tektite occurrence. Note how splash-form morphologies continue to occur at distance, surrounding the centrally located MN-type layered impact glasses. The outer limit of the observed distribution on MN-type layered impact glasses is shown by the dark green dashed line. The brown dashed line represents the circular best fit. The absence of data to the east and southeast leaves a degree of uncertainty as to the center of distribution. The presence of MN-type layered impact glass in the Philippines is suggestive that there is another triangular wedge of MN-type layered impact glass along the southeasterly butterfly ray in the Gulf of Tonkin and South China Sea. The triangular wedge of predominantly MN-type layered impact glass (Fiske et al., 1999; Schnetzler & McHone, 1996) is likely the proximal part of the southwesterly butterfly ray as opposed to the center of tektite distribution. This scenario is shown by the blue dashed line. Regardless of the precise scenario, the center of distribution likely lies somewhere in the darker green shaded region. The yellow area is lower probability. Inset: Data used in map overlay. Green = Probable regions; Yellow = Less favorable regions for the AAT impact.

rays may be present in the Philippines. In the Malay Peninsula, an ejecta ray may be present but is not sufficiently distinct to confidently deduce an accurate azimuth. Microtektite distribution has been widely accepted to indicate two mirroring butterfly rays (Glass & Koeberl, 2006; Prasad et al., 2007). The southeast butterfly ray extends from the northern Manila-Paracale region out into the Pacific Ocean towards Nauru. The southwest butterfly ray extends from the prominent Muong Nong-type layered impact glass localities of Muong Nong, Laos, and Ubon Ratchathani, Thailand, into the Indian Ocean to a region south of Madagascar.

Sufficient evidence exists from observation (e.g., Chapman, 1971; Dunn, 1912; Fenner, 1935) and from modelling (e.g., Artemieva, 2013) to indicate an uneven AAT distribution, in the form of ejecta rays, in medial and distal tektites and even possibly in the proximal setting (Izokh & An, 1983). A non-random tektite distribution implies that some tektite localities are related to one another (by means of occurring at different distances along the same ejecta ray). This theoretically allows for a best-fit impact location to be calculated. In doing so, stratigraphic outcrop bias (minimal in the young AAT ejecta); water transportation and redistribution (randomized on a global scale); the Coriolis effect (high tektite velocities (Chapman, 1964) result in minimal loft time); and post-impact plate tectonics, must be considered. Since the AAT impact, Australia is believed to have moved 54 km northwards with a slight clockwise rotation (B. C. Howard, 2016). These values become significant when regressing back thousands of kilometers and lead to a significant easterly shift in projections.

The use of a non-random tektite distribution pattern, corrected for the Coriolis effect and continental drift, should allow an accurate crater

position to be calculated. This is beyond the scope of this article but is highlighted for future research to provide additional layers of data.

2.9 Microtektite Regression: Microtektites are found in the oceanic environment. Terrestrial microtektites, other than those in salt lakes or ice, are rapidly destroyed by dissolution in meteoric waters. Microtektite regressions therefore utilize a patchy distribution of distal oceanic borehole locations. Numerous microtektite regression studies have followed the same methodology but have progressively used a greater number of localities. The most recent study (Prasad et al., 2007), utilizing the greatest number of localities, is therefore the most accurate, superseding previous studies (see Fig. 5, large ellipse). The R^2 regression process was repeated using the same methodology and data set from Prasad et al. (2007), but with a higher density mesh (0.25° spacing) to create a more detailed map and focal region (Fig. 5, small ellipse).

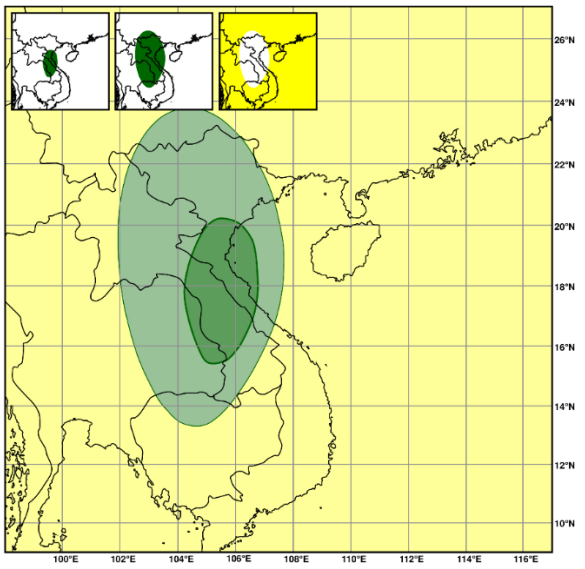

Fig. 5: An R^2 microtektite regression map based on 61 localities from Prasad et al. (2007) (light green). Utilizing identical methodology and dataset, but with a higher density of regression points, a focal point was calculated (dark green). The impact crater likely lies within the green region, with the darkest green region being most probable. The yellow area is lower probability. Inset: Data used in map overlay. Green = Probable regions; Yellow = Less favorable regions for the AAT impact.

Prasad et al. (2007) utilized 61 localities, of which only 15 were from the easterly portion of the strewn field and 46 from the westerly portion. The distance from the approximated source region also varied, with many easterly localities being more proximal. Ultimately, insufficient microtektite localities are available, particularly on the northern (continental) and eastern portion of the strewn field, to precisely locate the crater. A notable observation is that with increased microtektite localities the regressed crater location has varied quite considerably, and whilst becoming increasingly refined, the focal point of regression still has the possibility of readily shifting from its current location with the addition of new microtektite abundance data.

2.10 Target Lithology: Tektites, being a type of natural glass, require a network former (primarily silica), and therefore the source rock is necessarily a silica-rich rock. If the impactor strikes a silica-poor rock, then tektites cannot form. Terrestrial weathering processes act to concentrate silica in sedimentary rocks and their metamorphic descendants. Tektites form through shock melting so the temperature attained will be dependent on the compressibility of the rock: according to Stöffler, Hamann, & Metzler (2018) "…at a given shock pressure, the shock temperature of highly porous rocks can be up to an order of magnitude higher than those of dense crystalline rocks" (p. 2). Recently deposited water-rich siliciclastic sediments, common on the continental shelf, are therefore optimal for tektite production (K. T. Howard, 2011). Older siliciclastic sedimentary rocks are still suitable but are denser at surface (due to previous burial compaction) and so less compressible, followed by metamorphosed siliciclastic sedimentary rocks. Silica-rich igneous rocks, with low compressibility, could still form tektites but a much smaller volume of melt would attain sufficient temperature to fully melt.

Clues as to the tektite source material can be derived through the study of associated unmelted and partially melted lithologies, mineral grains in tektites and impact glasses (particularly in lower temperature melts), and through analysis of the geochemistry of fully melted tektites. Rock fragments recovered from the Australasian microtektite layer were found to be well sorted, quartz-rich, fine-grained (silt- to fine sand-sized) sedimentary rock (Glass & Barlow, 1979; Glass & Koeberl, 2006). A derivation from shales, graywackes, and lithic arenites has been suggested

(Glass, Huber, & Koeberl, 2004; Koeberl, 1992). In agreement, K. T. Howard (2011) suggested a mixture of shale-like material and a very quartz--rich material. A minor carbonate (dolomite) component was suggested to explain the CaO (positively correlated with MgO) variation (Amare & Koeberl, 2006).

Coarse-grained sedimentary rocks such as sandstones and conglomerates, as have been commonly described from Jurassic sediments in the central Indochinese region (Blum et al., 1992; Javanaphet, 1969; Sieh et al., 2020) (Fig. 6), are unsuitable source materials for AAT despite theoretically being suitable for tektite formation. This is further confirmed by REE analyses. Interlayered silts and shales may be suitable source materials, but not when considered in this heterogeneous context.

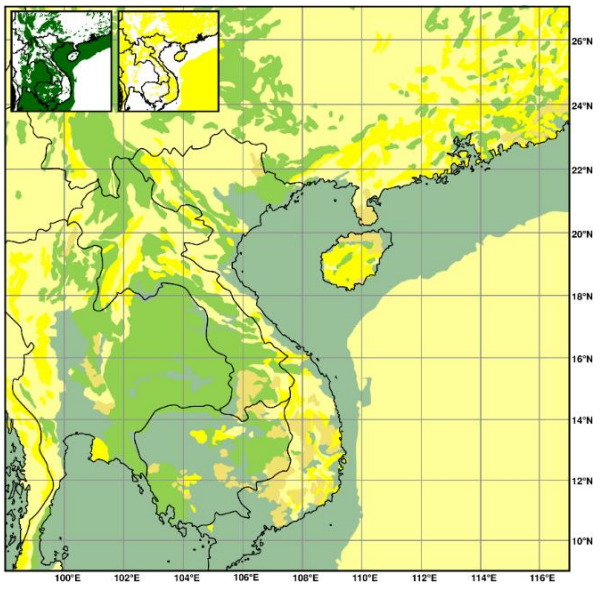

Fig. 6: A geological map outlining potentially suitable and unsuitable rock types for AAT. Mesozoic rocks (lime green), including Middle Jurassic strata. Quaternary outcrops and continental shelf areas (dull sea-green) which likely yield recent sediments. Green regions yield rocks of potentially suitable ages (dependent on various Rb/Sr and ^{10}Be interpretations) and may be compatible with the site of impact. Intrusive igneous rocks (bright yellow) are unlikely source materials and impact melts should not be surface exposed. Extrusive volcanic rocks (beige) are unlikely source regions due to geochemical incompatibility. Dull yellow regions represent outcropping rocks of incompatible age and incompatible deeper sea sediments. Yellow / beige regions have a low compatibility with the site of impact. After Liu et al. (2016). Inset: Data used in map overlay. Green = Probable regions; Yellow = Less favorable regions for the AAT impact.

Based on principal component analysis (PCA) using major-element tektite composition an admixture of sandstone and basalt was proposed by Sieh et al. (2020). As discussed in Section 2.15, thorough mixing is demonstrably poor in tektites (Glass & Simonson, 2013, p. 113; Koeberl, 1992). AAT REE data is incompatible with sandstone (Fig. 7) and basalt sources (Fig. 8) (Koeberl, 1992). Sr-Nd isotopic data is incompatible with basalts (N. Hoang, Flower, & Carlson, 1996; N. Hoang, Hauzenberger, Fukuyama, & Konzett, 2018). PCA did, however, highlight compositional variations between early (distal) and late (proximal) formed tektites, reinforcing trends also seen in REE and Sr-Nd isotopes, indicative of a lithological variation with depth of excavation if a ballistic equivalent of 'inverted' stratigraphy is accepted. Igneous rocks as a target material are highly improbable from a geochemical (presented subsequently) and wide AAT distribution perspective. Impact-related melts should not be surface exposed in a recent impact that has suffered minimal erosion. Igneous provinces are improbable source regions (Fig. 6).

2.11 Rare-Earth Elements: Koeberl et al. (1985) states that rare-earth elements (REE) are known to be of "great genetic significance" (p. 108). REE are refractory elements, and their abundance pattern has not changed in the process of melting (Koeberl et al., 1985). Chondrite (McDonough & Sun, 1995) normalized REE patterns of averaged tektite values can be compared with various rock types. Koeberl et al. (1985) concluded that AAT '…follow very closely the pattern exhibited by the post-Archean upper crust average sediments and are very likely to have originated from such a source' p. 107. Averaged shale groupings (Condie, 1993; Howard, 2011; Koeberl et al., 1985; Lodders & Fegley, 1998), see Fig. 7, were highly comparable with AAT values. Graywacke values (Condie, 1993; Koeberl et al., 1985), see Fig. 7, conformed to the later stage splash-form and layered tektites. Sandstones (Condie, 1993; Koeberl et al., 1985), see Fig. 7, had low REE values, incompatible as a sole source for AAT.

REE values for basalt (including Bolaven Plateau basalts), see Fig. 8, did not reproduce the AAT REE pattern (Condie, 1993; N. Hoang

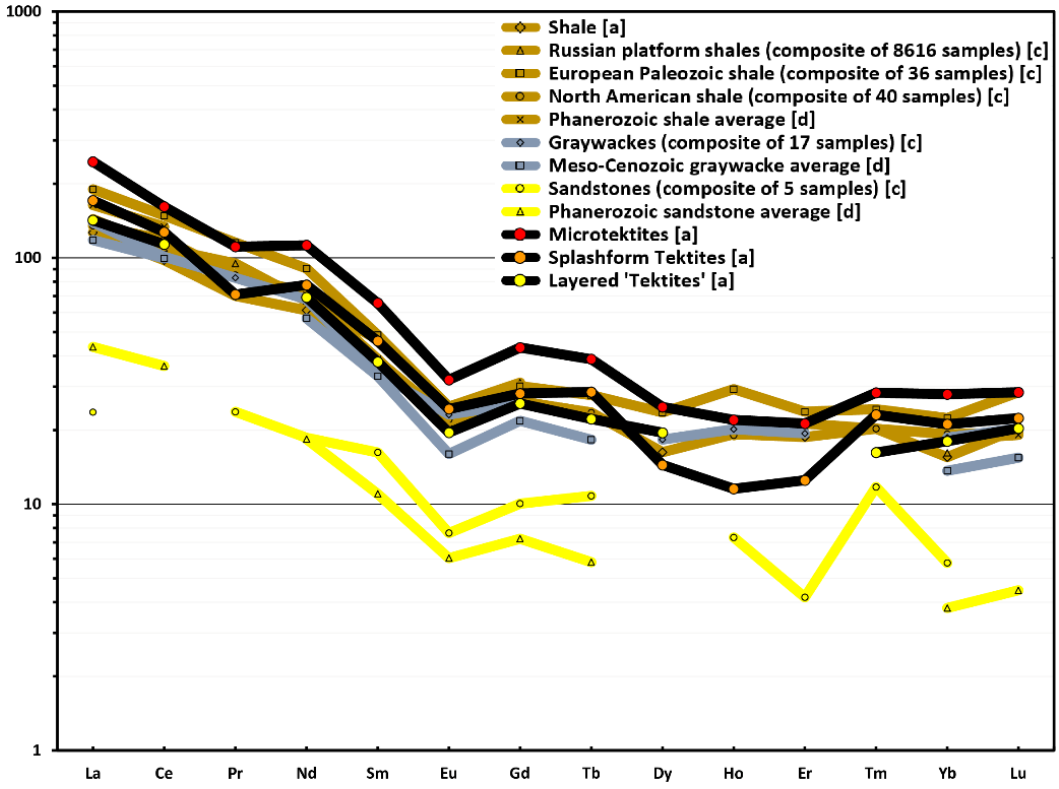

Fig. 7: Chondrite (McDonough & Sun, 1995) normalized rare-earth element patterns of average tektite values [a] (K. T. Howard, 2011) compared with shale, graywacke, and sandstone values. [a] K. T. Howard (2011) after Lodders & Fegley (1998); [c] Koeberl et al. (1985); [d] Condie (1993).

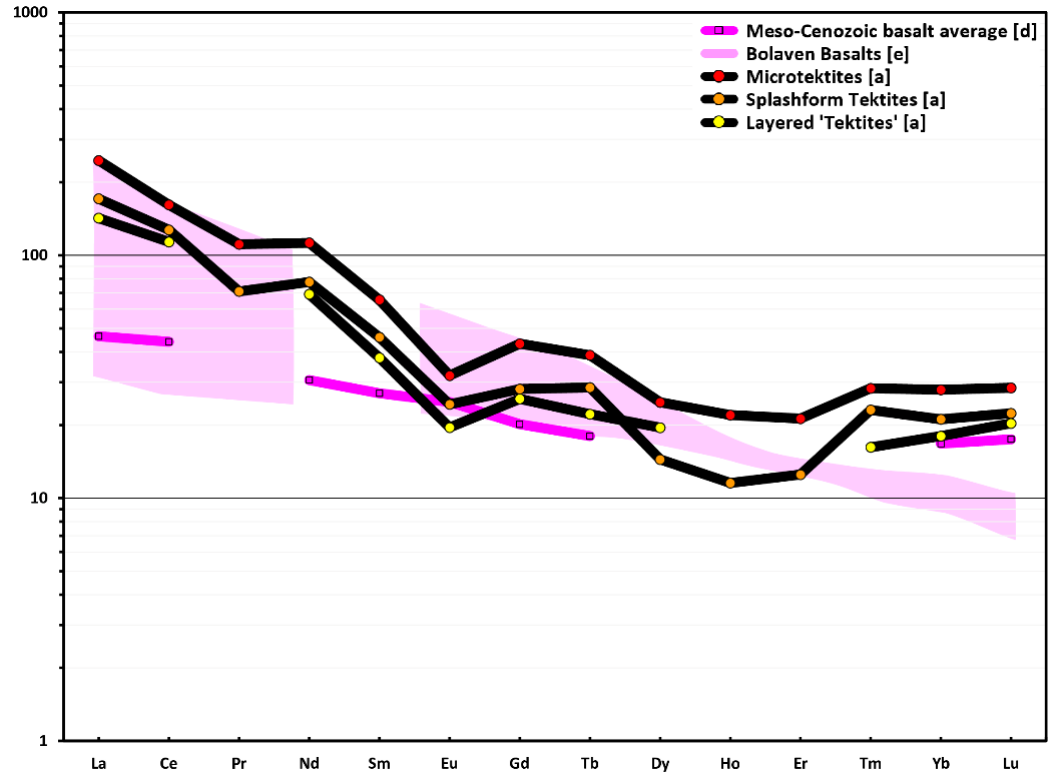

Fig. 8: Chondrite (McDonough & Sun, 1995) normalized rare-earth element patterns of average tektite values [a] (K. T. Howard, 2011) compared with Meso-Cenozoic basalt values: [d] Condie (1993). Various plotted Bolaven basalt compositions are duplicated from [e] N. Hoang et al. (2018).

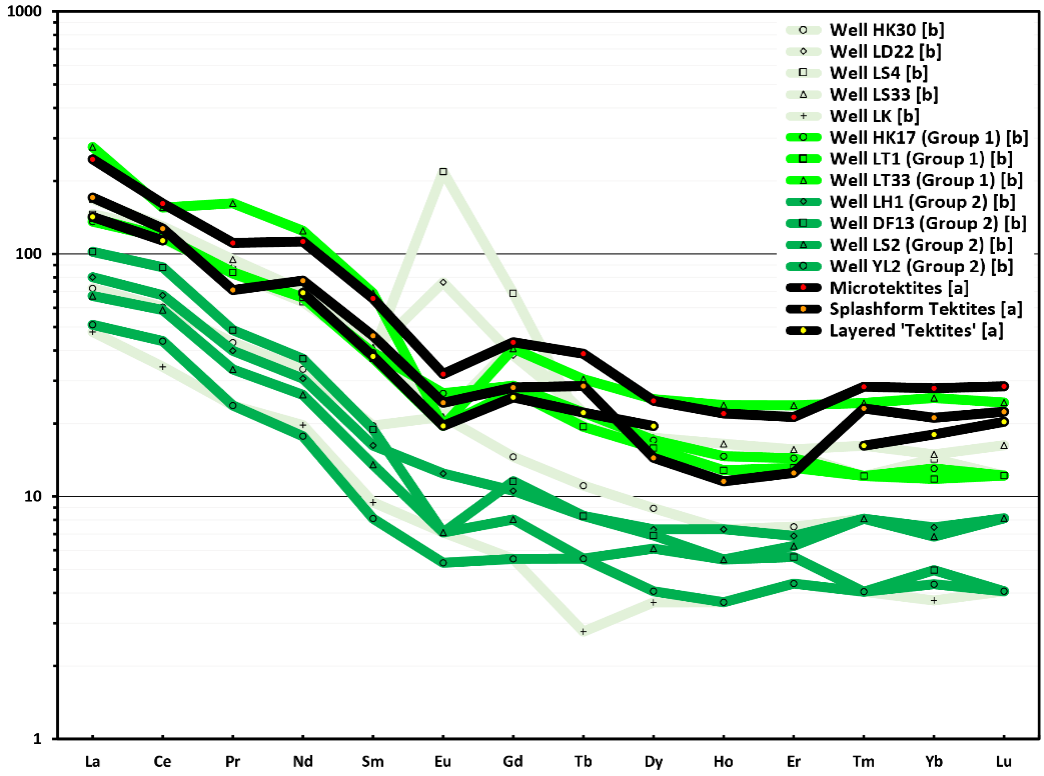

Fig. 9: Chondrite (McDonough & Sun, 1995) normalized rare-earth element patterns of average tektite values [a] (K. T. Howard, 2011) compared with Upper Miocene sediment values: [b] (Cao et al., 2015). Bright green wells were categorized by (Cao et al., 2015) as Group 1 wells with relatively high REE concentrations. Dark green wells were categorized by (Cao et al., 2015) as Group 2 wells with relatively low REE concentrations. Pale green wells were uncategorized, falling into both Group 1 and 2 with some anomalies.

et al., 2018). Basic igneous rocks can be excluded as a potential source material for AAT (wholly or in part) based on REE (N. Hoang et al., 1996, 2018; Koeberl, 1992) (Fig. 8). Koeberl (1992) states: 'Mixing of local soils, or with some related loess samples, cannot reproduce the tektite REE patterns, and any basaltic, oceanic, or extraterrestrial rocks can be excluded as source rocks…' p. 1033. Figs. 7 & 8 demonstrate that REE patterns of sandstones and basalts, either in isolation or in combination, are incompatible with AAT.

All shales have similar REE patterns, so it is not possible to determine the exact precursor rock / formation from which AAT originated (Koeberl et al., 1985). It can simply be determined that the source rock was shale-rich and post-Archean (Koeberl et al., 1985). Averaged tektite values from K. T. Howard (2011), suggest that earlier formed microtektites have, on average, higher REE concentrations than splash-form tektites, which in turn have higher REE concentrations than the last formed layered 'tektites' (Figs. 7 - 9). If a ballistic equivalent of 'inverted' stratigraphy, a concept that is not proven but appears likely, is accepted then REE may indicate a subtle transition from shales to siltier / sandier inter-bedded shales or graywackes with greater depth of excavation.

Australasian tektite REE values can be compared with Upper Miocene sediments from boreholes in the Yinggehai Basin and Qiong-dongnan Basin (Cao, Jiang, Wang, Zhang, & Sun, 2015), see Fig. 9. AAT REE values were comparable with sediments containing high REE concentrations, categorized as Group 1 wells by Cao et al. (2015). Average AAT microtektite values closely matched well LT33. Average AAT splash-form and layered 'tektite' values were comparable with wells HK17 and LT1, see Fig. 9. In the sparse data set, in terms of geographic and stratigraphic extent, Group 1 wells corresponded with regions surrounding Hainan, but notably no data for comparison is available offshore Vietnam. Sediments close to the Red River mouth and in central Qiongdongnan

Basin showed low compatibility (Figs. 9 & 10). Cao et al. (2015) did not compare lithology to REE abundance. It is possible that compatible wells simply represent shale-rich sediments. Incompatible wells may represent sand-rich submarine or deltaic fans derived from rivers (Fig. 10). The most prominent river is the Red River which progrades into the northern part the Yinggehai - Song Hong (YGH-SH) Basin. Tektite REE data appears to preclude coarser siliciclastic sediment and, as such, may indicate a crater position away from a river mouth and its extended submarine fans.

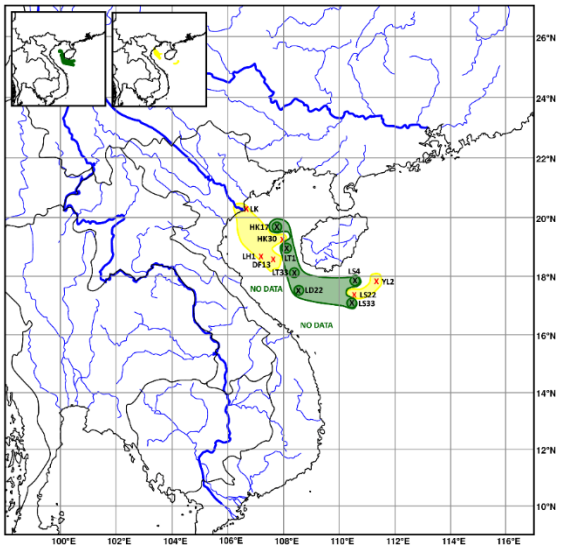

Fig. 10: REE compatibility of Upper Miocene sediments (Cao et al., 2015) with AAT (K. T. Howard, 2011). Wells with compatible Upper Miocene sediment are marked with a green circle and shaded green. Incompatible wells, likely representing sandier deposits, are marked with a red cross and shaded yellow. Stratigraphically results will vary. No data from Vietnamese wells. Modern rivers are depicted in blue, which are anticipated to deliver sand-rich sediments. Inset: Data used in map overlay. Green = Probable regions; Yellow = Less favorable regions for the AAT impact.

2.12 Strontium - Neodymium: Sr-Nd isotopic data can potentially be used to 'fingerprint' the source rock. As highlighted in Section 2.15, thorough mixing is demonstrably poor in tektites (Glass & Simonson, 2013, p. 113; Koeberl, 1992). The close grouping of Sr-Nd values in tektites (Fig. 11) would therefore be suggestive of a relatively homogenous target rock as opposed to thorough and efficient mixing of disparate melts (e.g., basalt and sandstone) in the brief seconds following impact. The constituents of fine-grained sedimentary rocks, identified as the probable source material (Section 2.10), are thoroughly mixed and homogenized by sedimentary transport processes resulting in consistency if derived from the same parent materials. Fig. 11 demonstrates reasonably homogenized sediments in basins, versus the diversity in immature river sediments. In the suggested absence of thorough mixing of tektite melts a relatively homogenous source rock is interpreted.

Cross plots of $^{87}Sr/^{86}Sr$ against εNd values were constructed to compare published AAT values (Ackerman et al., 2020; Blum et al., 1992; Shaw & Wasserburg, 1982) with published river sediment data (Clift et al., 2008; Jonell et al., 2017; Liu et al., 2007) and with surface sediments of the South China Sea region (Wei et al., 2012), see Fig. 11. Slight differences in $^{87}Sr/^{86}Sr$ and εNd values between proximal and distal tektites are potentially indicative of derivation of tektites from variable depths in a stratified, but generically related, target (Blum et al., 1992). These data indicated a compatibility of AAT with sediments at the Red River mouth and the East Vietnam and South China Seas (see Figs. 11 & 12). Samples were not available in the Yinggehai - Song Hong (YGH-SH) Basin but modern-day Red River drainage accounts for approximately 80% the total sediment supply of the YGH-SH Basin (Feng et al., 2018). When sediment supply exceeded accommodation space in the YGH-SH Basin, the sediment 'spilled' into the East Vietnam and South China Seas. By inference, a YGH-SH Basin source, located between compatible sources and sinks, is likely compatible.

Australasian tektite samples yielded εNd values between -10.9 and -12.2, averaging -11.58 (Ackerman et al., 2020; Blum et al., 1992; Shaw & Wasserburg, 1982). These consistent εNd values are indicative of a reasonably homogenous target material, or improbable scenario of a thoroughly mixed melt, from a single source crater. εNd values from the Red River mouth were -11.47 (Liu et al., 2007, 2016). AAT εNd values conformed closely with εNd values from the Red River mouth, YGH-SH Basin, Qiongdongnan Basin, Pearl River mouth and west Zhujiangkou Basin (fed by the Pearl River with Hainan

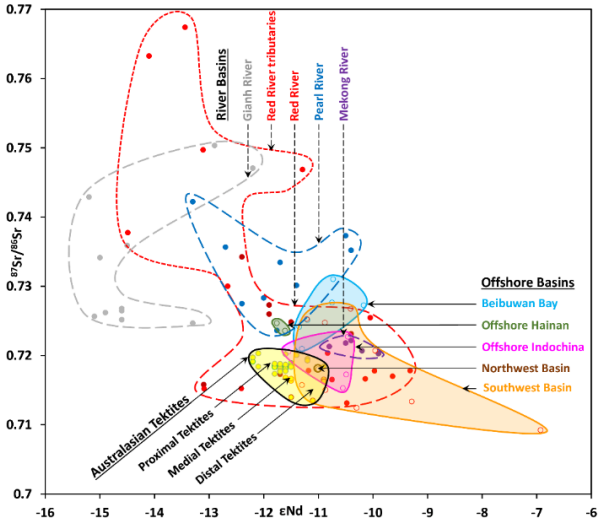

Fig. 11: Cross plot of Sr versus Nd isotope compositions of Australasian tektites and potential source materials from river basins and offshore basins. AAT overlap with Red River sediments, offshore Indochina, the Northwest Basin, and the Southwest Basin. No data was available for the YGH-SH Basin.

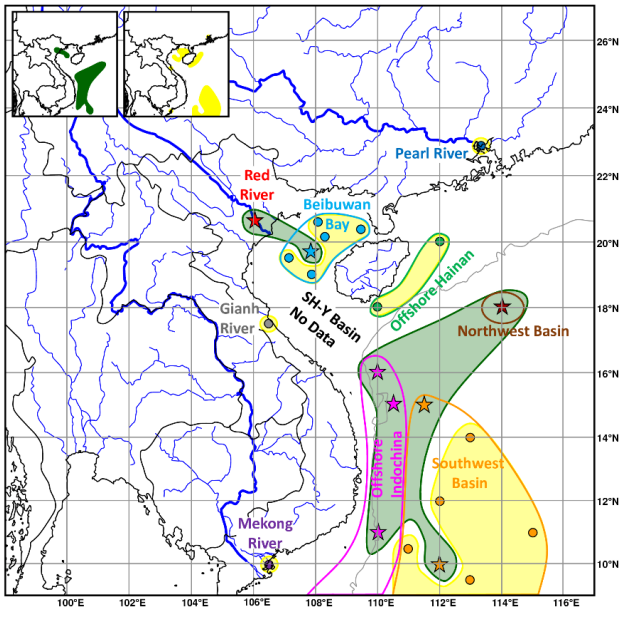

Fig. 12: Location of samples in cross plot (see Fig. 11) of Sr versus Nd isotope compositions for tektites (Ackerman et al., 2020; Blum et al., 1992; Shaw & Wasserburg, 1982) compared with basin sediments measured from offshore Hainan, Beibuwan Bay, offshore Indochina, Northwest Basin and Southwest Basin (Wei et al., 2012) and river sediments (Clift et al., 2008; Jonell et al., 2017; Liu et al., 2007). Samples with a star and green shaded areas are closely compatible with tektites. Samples denoted by a circle and yellow shaded areas indicate low compatibility with AAT. Modern rivers are depicted in blue. Inset: Data used in map overlay. Green = Probable regions; Yellow = Less favorable regions for the AAT impact.

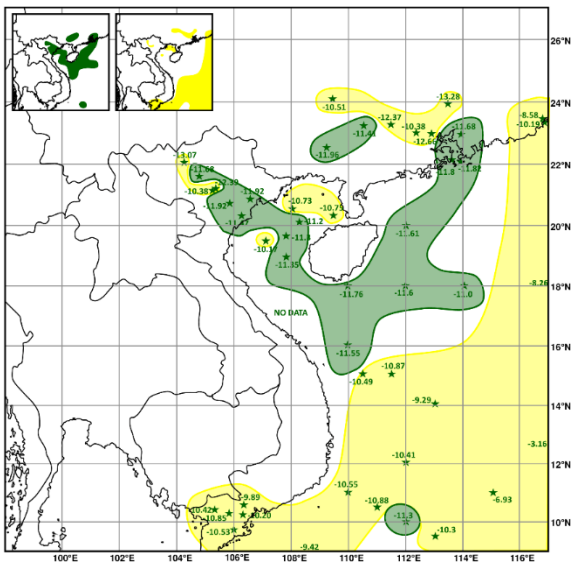

Fig. 13: Modern εNd values from (Liu et al., 2016). These values can be compared with tektite samples that yielded εNd values between -10.9 and -12.2, averaging -11.58 (Ackerman et al., 2020; Blum et al., 1992; Shaw & Wasserburg, 1982). Green areas represent suitable source areas. Yellow areas represent unlikely source areas. Inset: Data used in map overlay. Green = Probable regions; Yellow = Less favorable regions for the AAT impact.

influence). εNd values used to construct a map of potential source areas (see Fig. 13).

Sr-Nd isotopic data of southern Vietnamese Basalts (N. Hoang et al., 1996) can be compared with tektites (Ackerman et al., 2020; Blum et al., 1992; Shaw & Wasserburg, 1982). In southern Vietnamese basalts $^{87}Sr/^{86}Sr$ values average 0.744 (0.7036 to 0.7065), compared to AAT that average 0.7169 (0.7118 to 0.7213); $^{143}Nd/^{144}Nd$ values average 0.5128 (0.5126 to 0.5130), compared to AAT that average 0.5117 (0.5112 to 0.5121); εNd averages 3.72 (-0.9 to 7.6), compared to AAT that average -11.58 (-12.2 to -10.9) (Ackerman et al., 2020; Blum et al., 1992; N. Hoang et al., 1996; Shaw & Wasserburg, 1982). Values for Bolaven are not given, but $^{87}Sr/^{86}Sr$ and $^{143}Nd/^{144}Nd$ values of Bolaven basalts are plotted in N. Hoang et al. (2018) and fall centrally within the ranges of southern Vietnamese basalt values of N. Hoang et al. (1996). It is demonstrated that regional basalts are incompatible as a source material for AAT.

2.13 Major Element Geochemical Regression: The geographic distribution of SiO_2, Na_2O, and CaO concentrations in MN-type layered impact glasses and intermediate tektites are plotted from Schnetzler (1992) (Figs. 14 - 16). Schnetzler (1992) utilized a sparse data set with some approximated or poorly defined localities (SiO_2 = 22 localities / 166 analyses; Na_2O = 23 localities / 97 analyses; CaO = 24 localities / 98 analyses). The absence of data from the Gulf of Tonkin, East Vietnam Sea, and South China Sea potentially skews data westwards. Whilst trends are observed, the contours are somewhat subjective, and the possibility of erroneous localities cannot be dismissed. The use in map overlay, however, remains valid as the principle combines weak data to create a more robust argument through weight of evidence. The major element geochemical iso-concentrations in Schnetzler (1992) appear to trend to the center of the proximal tektite strewn field.

2.14 Beryllium-10 Regression: A trend of decreasing ^{10}Be content with proximity to the likely source area is observed (Table 1). This trend in ^{10}Be iso-concentrations within the AAT strewn field is increasingly being accepted as representing a ballistic equivalent of 'inverted' stratigraphy (Ma et al., 2004). An 'inverted' stratigraphy should be more evident if a thick sedimentary column has been sampled. ^{10}Be iso-concentrations of MN-type layered impact glasses were used by Ma et al. (2004) to calculate the crater position with the assumption that the crater would lie at the center of the lowest concentration of ^{10}Be (Fig. 17).

2.15 Target Lithology Age: Rb-Sr versus ^{10}Be: There is conflicting data regarding the stratigraphic age of the target material. Resolving this issue would significantly narrow down the crater search area. The conflicting data are:

- It was determined that the last major Rb-Sr fractionation event (i.e., weathering, transportation, and deposition) experienced by the sedimentary target materials occurred in a narrow range of stratigraphic ages ~170 Ma ago (Blum et al., 1992).
- The ^{10}Be content in tektites, half-life of 1.39 Ma (Chmeleff, Blanckenburg, Kossert, & Jakob, 2010; Korschinek et al., 2010), was recognized as being too high to be derived from a Middle Jurassic source rock (Blum et al., 1992). It was concluded by Ma et al. (2004) that the AAT source material "did not consist of older igneous or sedimentary rocks, but of unconsolidated materials or young sedimentary rocks" (p. 3887).

There are three solutions that might theoretically provide satisfactory outcomes (Fig. 18):

1) There is thorough mixing between Middle Jurassic rocks and a young surficial cover during melt production. If it were a young fluvial sediment cover a ~1:4 ratio of young fluvial sediment to Middle Jurassic rock (Blum et al., 1992) would be expected.
2) The source rock is solely Middle Jurassic in age. A weathered surface in the target area was exposed to meteoric waters for longer than the half-life of ^{10}Be and if ^{10}Be was not lost to erosion or solution then a ~200 m column of Middle Jurassic bedrock could yield the correct ^{10}Be content (Blum et al., 1992).
3) The source rock is a young unconsolidated sedimentary rock (Ma et al., 2004). This suggests that the Rb-Sr clock may not have been reset and represents the penultimate depositional cycle (at ~170 Ma) or an averaged Rb-Sr age (Cordani, Mizusaki, Kawashita, & Thomaz-Filho, 2004; Dickin, 2005).

Mixing is demonstrably poor in microtektites according to Glass & Simonson (2013): "There is not time for impact melt to be thoroughly mixed and homogenized prior to being ejected" (p. 113). Koeberl (1992) states that the lower temperature, MN-type layered impact glasses are "…compatible with incomplete mixtures of different target rocks" (p. 1056). It is assumed that microtektites represent early stage, typically shallow derived, melts whereas MN-type layered impact glasses represent later stage, on average more deeply excavated, melts. The compositional layering in MN-type impact glasses may reflect sedimentary bedding, indicative of melting with practically no mixing, implying ^{10}Be content at depth. It was remarked by Ma et al. (2004):

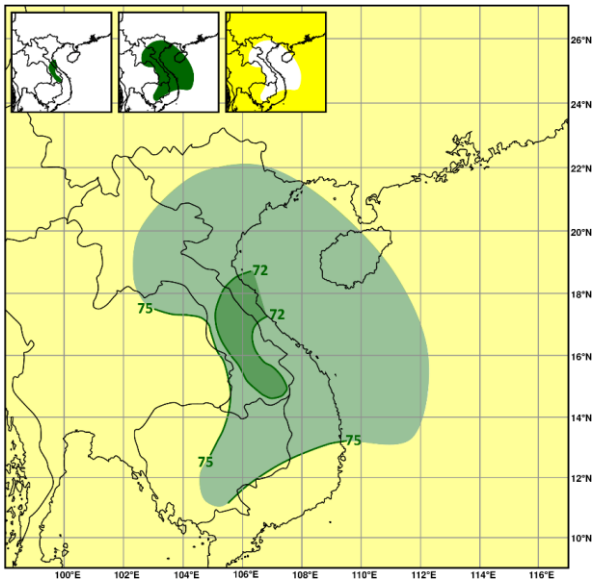

Fig. 14: The geographic distribution of SiO_2 concentrations in MN-type layered impact glasses and intermediate tektites based on 22 localities / 166 analyses (Schnetzler, 1992). Note the absence of data to the east and southeast due to the presence of seas. Green regions represent regions of higher probability and yellow areas denote lower probability for the presence of the AAT source crater. Inset: Data used in map overlay. Green = Probable regions; Yellow = Less favorable regions for the AAT impact.

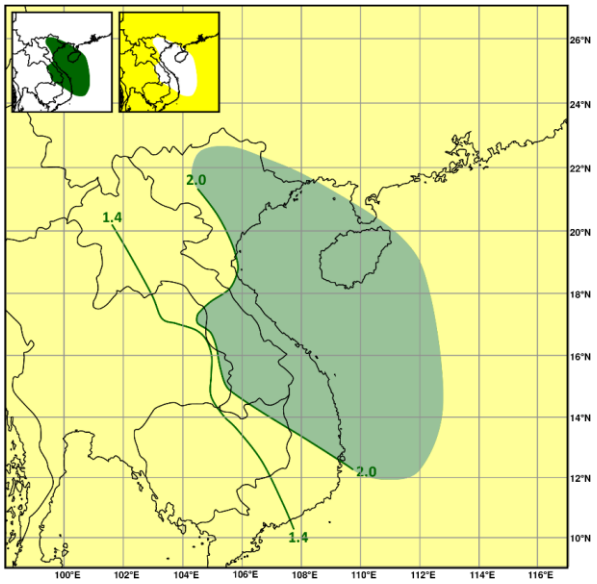

Fig. 15: The geographic distribution of Na_2O concentrations in MN-type layered impact glasses and intermediate tektites based on 23 localities / 97 analyses (Schnetzler, 1992). Note the absence of data to the east and southeast due to the presence of seas. Green regions represent regions of higher probability and yellow areas denote lower probability for the presence of the AAT source crater. Inset: Data used in map overlay. Green = Probable regions; Yellow = Less favorable regions for the AAT impact.

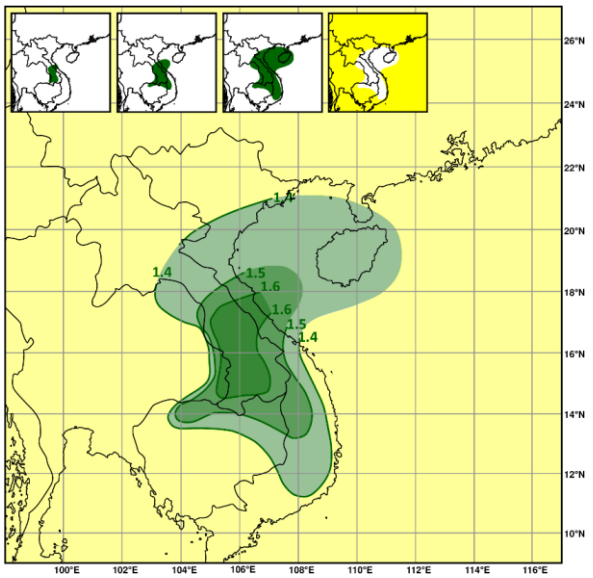

Fig. 16: The geographic distribution of CaO concentrations in MN-type layered impact glasses and intermediate tektites based on 24 localities / 98 analyses (Schnetzler, 1992). Note the absence of data to the east and southeast due to the presence of seas. Green regions represent regions of higher probability and yellow areas denote lower probability for the presence of the AAT source crater. Inset: Data used in map overlay. Green = Probable regions; Yellow = Less favorable regions for the AAT impact.

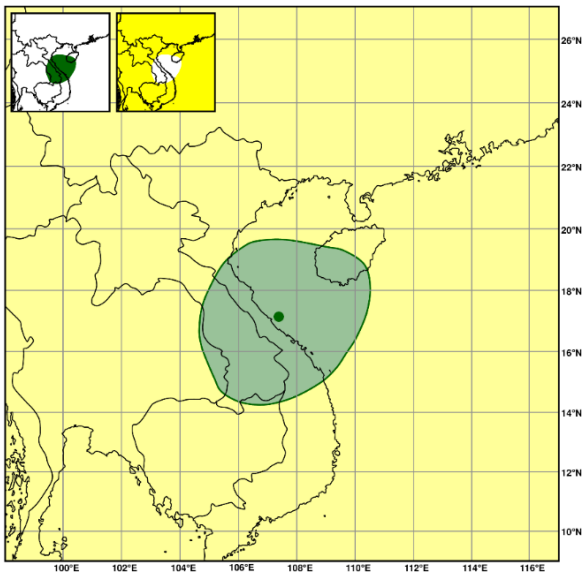

Fig. 17: Regression of ^{10}Be iso-concentrations (Ma et al., 2004) indicate the crater is within the shaded region, with the best fit at '•'. Note the absence of data to the east and southeast due to the presence of seas. The yellow shaded area denotes lower probability for the AAT source crater. Inset: Data used in map overlay. Green = Probable regions; Yellow = Less favorable regions for the AAT impact.

Table 1: Average ^{10}Be concentrations of tektites grouped by country. Sources: [1] = (Ma et al., 2004); [2] = (Rochette et al., 2018); [3] = (Koeberl, Nishiizumi, Caffee, & Glass, 2015). Note that corrections for *in situ* ^{10}Be production are minimal, not exceeding ~10 × 10^6 atom/g (Ma et al., 2004, after others).

Country	Average ^{10}Be (atoms/g)	Source
Laos	59 ±9 × 10^6 (uncorrected)	[1]
Thailand	71 ±17 × 10^6 (uncorrected)	[1]
Vietnam	73 ±13 × 10^6 (uncorrected)	[1]
China	85 ±24 × 10^6 (uncorrected)	[1]
Indonesia	115 ±27 × 10^6 (uncorrected)	[1]
Philippines	121 ±22 × 10^6 (uncorrected)	[1]
Australia	136 ±30 × 10^6 (uncorrected)	[1]
Microtektites:		
Antarctica	184 ±8 × 10^6 (corrected for *in situ* production)	[2]
S. China Sea	260 ±60 ×10^6	[3]

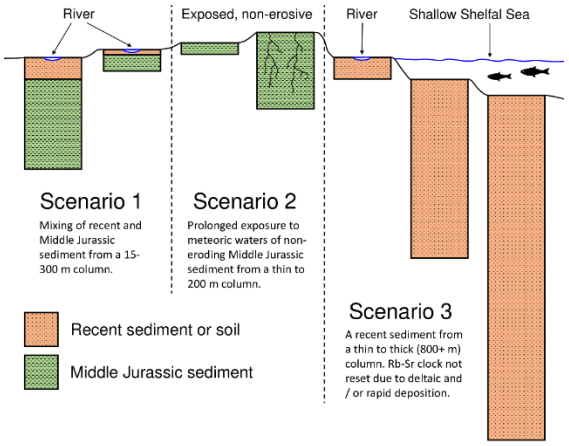

Fig. 18: Three scenarios that satisfactorily explain the Rb-Sr and ^{10}Be values.

"assuming that during crater formation neither the precursor grains nor the material melted mixed efficiently on a scale of tens of meters (N. A. Artemieva and E. Pierazzo, personal communication, 2002) we conclude that the vertical extent or thickness (as opposed to the absolute depth) of the hypothetical region that participated in tektite formation was likely between 15 and 300 m." (p. 3892).

The assumption made in Ma et al. (2004) was that if mixing is poor then high ^{10}Be values in tektite demonstrate a surficial origin (15 to 300 m). This has been supported by numerous authors: ~200 m (Blum et al., 1992); X0 m (Trnka, 2020); first tens of cm's of soil / sediment for Antarctica microtektites (Rochette et al., 2018). This assumption, however, is incorrect as it assumes an impact on land or in a region of normal sedimentation. Within the region of most probable impact (i.e., Indochinese to southern Chinese region) the YGH-SH Basin in the Gulf of Tonkin demonstrates exceptionally high sedimentation rates and therefore presumable abnormally high ^{10}Be content at great depth. Sediments predominantly comprise siliciclastic continental material in a deltaic to shallow marine setting. High ^{10}Be values in AAT do not demonstrate a surficial origin unless the source crater geology is known. ^{10}Be content does, however, potentially allow a crude understanding of stratigraphy at the unknown impact location if depth of excavation of tektites can be independently estimated.

Artemieva (2008) states that: "Excavation depth (initial position of ejecta in the target) drops quickly with increasing ejection velocity: from 0.25 Dpr for 2 km/s to 0.02 Dpr for 11 km/s" (p. 1) (Dpr = diameter of projectile). The trajectories of tektites, neglecting atmospheric drag, were calculated (Schmitt, 2004): at 2 km/s material is ejected laterally 204 km at 15º and 75º; 312 km at 25º and 65º to a maximum of 408 km at 45º. Moldavites, from Ries Crater, occur at distances beyond ~185 km. Assuming ejection angles from 15º to 75º, neglecting atmospheric drag, corresponding velocities of 1.35 to 1.9 km/s are calculated for these Moldavites, suggestive that tektites are present in ejecta travelling at under (or certainly close to) 2 km/s.

Atmospheric drag will, to varying degrees, raise the launch velocities required to eject a body a certain distance, in turn reducing the

depth from which tektite could have been produced. In the early stages of impact, material is jetted (Vickery, 1993) and discrete tektite droplets form from the ejecta curtain at variable altitudes. The rarefied atmosphere is demon--strated by tektite bubble pressures (Matsuda, Maruoka, Pinti, & Koeberl, 1996; Mizote, Matsumoto, Matsuda, & Koeberl, 2003; Zähringer & Gentner, 1963). In larger impacts, such as the AAT impact, the influence of atmospheric drag is less prominent as the ejecta accelerates the atmosphere (Shuvalov & Dypvik, 2013). The large size of the AAT impact and the evidence of the formation of discrete tektite droplets at altitude significantly reduces, but does not eliminate atmospheric interaction, as manifested in the plastic deformation of tektite droplets, especially in proximal morphologies.

It is reasonable to assume that the AAT impact was comparable in size to the Chesapeake Bay impact (or possibly marginally larger), which is believed to have been produced by a 3.2 km diameter impactor (Kenkmann et al., 2009). An impactor of this diameter might excavate tektite producing ejecta to a depth of 800+ m, after Artemieva (2008), assuming no / shallow seas and suitable glass-forming lithologies in the stratigraphy. Three possible impact scenarios can now be presented:

A) The impact was a highly oblique grazing impact (< 5º) resulting in an elliptical crater. Consequently, tektites were only produced from surficial material.

B) The impact was oblique and resulted in a near-circular crater. However, tektites were only produced from the surficial layers as the strata at depth was incompatible with glass formation (e.g., limestone or anhydrite).

C) The impact was oblique and resulted in a near-circular crater. Tektites were produced from rock derived from the surface to ~800 m depth.

The arguments can be readily tested as the surficial (early stage) origin of tektites (A & B) necessitate that ejecta is predominantly downrange with a distinct uprange zone of avoidance (Gault & Wedekind, 1978; Schultz et al., 2009, 2007), i.e., an impact in northernmost Vietnam or Yunnan Province in China. Whereas C would eject tektites throughout the 360º azimuthal range (uprange and downrange) (Gault & Wedekind, 1978) with a crater in the center of the proximal strewn field (Ubon Ratchathani Province of Thailand, Savannakhét, Salavan, and Champasak Provinces of central-southern Laos, central Vietnam, and the Gulf of Tonkin).

Scenario A has been discussed and can be dismissed based on the azimuth of the butterfly lobes (Gault & Wedekind, 1978). Multiple parameters, including microtektite regression (Prasad et al., 2007), geochemical regression (Ma et al., 2004; Schnetzler, 1992), and MN--type layered impact glass distribution (Schnetzler, 1992) all point to a broadly central crater position either in the central-eastern part of Indochina or into the Gulf of Tonkin. This dictates that the proximal ejecta in this oblique impact is, in part, uprange and was therefore later stage, coming from depth as the circular crater opened-up. The observations of uprange AAT indicate the solution is Scenario C. Whilst tektites are typically considered downrange ejecta, it is notable that the Chesapeake Bay Crater produced rare probable uprange ejecta at Martha's Vineyard (Burns, Schnetzler, & Chase, 1961).

Poorly mixed MN-type layered impact glasses are therefore assumed to be derived from up to ~800 m depth, after (Artemieva, 2008). The implication of high ^{10}Be values at depth in the presence of poor mixing, is that there is a thick sequence of recent sediments at the impact site. Some ballpark calculations for the impact site stratigraphy can be made if the ^{10}Be iso-concentrations are interpreted to represent a ballistic equivalent of 'inverted' stratigraphy. Assuming the impact was pene-contemporaneous with sediment deposition, Antarctic, and South China Sea microtektites represent the first formed surficial ejecta, and tektites in Laos represent the last formed ejecta, a 2.28 to 2.97 Ma packet of sediment was sampled by AAT (early Pleistocene to Pliocene). Assuming ~800 m depth was sampled; an average sedimentation rate of 269 to 351 m/Ma

is derived. The calculations are crude owing to multiple variables, but the principal point is that acceptance of uprange tektite distribution demonstrates excavation from depth and by inference a thick sequence of recent, rapidly deposited, sediment was sampled by AAT. Even if the sediment column estimate was reduced in consideration of atmospheric drag, the same conclusions will apply. Material is not ejected uprange until later stages of impact as the circular crater forms.

To reset the Rb-Sr clock substantial exchange and homogenization of Sr with sea / formation water is required. Rapidly deposited sediments, especially in a deltaic, but even in open marine environments, may preserve previous Rb-Sr dates (Cordani et al., 2004) / an average of the provenance ages of the sedimentary constituents (Dickin, 2005).

A very fine, almost authigenic, claystone comprising minerals such as illite, free from detrital minerals, is optimal to reset the Rb-Sr clock (Dickin, 2005). A low percentage of illite might be taken as an indicator that the region is unsuitable for resetting the Rb-Sr clock, and as such may indicate viability as a source crater region (Fig. 19). In the YGH-SH Basin, clay mineral transformation, including illitization, typically occurs below 2,000 m sediment depth (Jiang, Xie, Chen, Wang, & Li, 2015). The uppermost 2,000 m of YGH-SH Basin sediment (deposited shortly before the impact and melted and ejected prior to illitization) would fulfil the ^{10}Be and Rb-Sr observations.

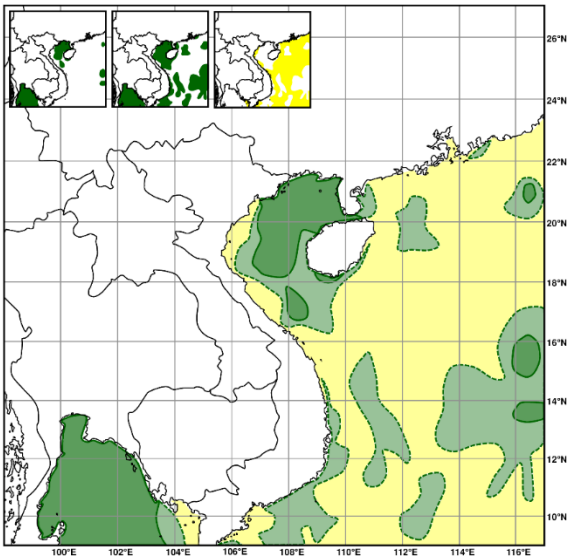

Fig. 19: Illite percentages in modern sediments after Liu et al. (2016). Solid lines with darker green shading represent under 20% illite. Dashed lines with lighter green shading represent under 30% illite. Yellow shaded regions yielded over 30% illite and represent lower probability regions. The Gulf of Tonkin region averages 27% illite. If it is assumed that the Rb-Sr clock was not reset, then areas of low illite concentrations represent plausible impact locations as these are the least suitable clay-rich rocks for obtaining a reset Rb-Sr age. Inset: Data used in map overlay. Green = Probable regions; Yellow = Less favorable regions for the AAT impact.

2.16 Pore Water / Sea Water Mixing Considerations: Tektites have very low water contents (Beran & Koeberl, 1997) due to the high formation temperatures that cause water to dissociate into H^+ and O^{2-} ions (Vickery & Browning, 1991). Ackerman, Skála, Křížová, Žák, & Magna (2019) believe that "volatile species derived from dissociated seawater and/or saline pore water" (p. 179) may aid the loss of Os in the form of Os oxides. According to Ackerman et al. (2019) "The low Os abundance in most of the analyzed Australasian tektites, combined with non-radiogenic ^{187}Os/^{188}Os far below average upper continental crust, may provide a direct test to distinguish continental versus seawater impact scenario" (p. 179). The presence of significant amounts of water is envisaged in the formation of AAT (Ackerman et al., 2019). This work followed K. T. Howard (2011) who had noted that where tektites are present, a water-rich surface layer can be inferred. The abundance and widespread distribution of AAT necessarily implicates a water-rich target.

A saline character of the pore water is supported by the elevated halogen content of AAT (Ackerman et al., 2019; Koeberl, 1992; Meisel, Langenauer, & Krähenbühl, 1992). AAT were noted to have relatively high B and Li abundances and δ^{11}B values of (-4.9 to +1.4‰) (Chaussidon & Koeberl, 1995). The B, Li, and δ^{11}B values were indicative of a source rock with a higher clay content and are consistent with marine pelagic and neritic sediments as well as river and deltaic sediments (Chaussidon & Koeberl, 1995). ^{10}Be, Rb-Sr and Sm-Nd values were indicative of a continental crustal source rock (Blum et al., 1992) and eliminated pelagic and deeper neritic sediments (Chaussidon & Koeberl, 1995). It was concluded that AAT were

derived from river and deltaic sediments with a higher clay content that have acquired B from the seawater (Chaussidon & Koeberl, 1995). Offshore Mekong River delta sediment was considered a potential source due to the rapid deposition rate of ^{10}Be-rich sediments (Chaussidon & Koeberl, 1995). A Mekong River source can now be eliminated by poorly compatible εNd values (Liu et al., 2007) and geographic position. The same conclusions, however, exceedingly accurately fit a Red River derived YGH-SH Basin source.

2.17 Sea Level in Source Region: The AAT impact occurred immediately prior to Termination IX, the transition from Marine Isotope Stage 19-20 (Mark et al., 2017). So, the impact occurred during a glacial stage when sea levels were low. Continental shelf regions, including the Gulf of Tonkin, would have been subaerially exposed, deltaic, or shallow shelf seas.

It is suggested that water-rich surface layers enhance, by orders of magnitude, the production of high velocity ejected melt (K. T. Howard, 2011). Recently deposited, uncompacted, siliciclastic sediments have a much higher pore water content compared to mature sedimentary rocks exposed at the surface and are therefore optimal for tektite production.

It was modelled that an impact into 300 m water depth, compared to dry land, will result in a greater distribution of tektites (Artemieva, 2013). A 300 m water depth, however, would significantly curtail the production of the highest velocity distal ejecta, by reference to Artemieva (2008), which are notably present in abundance. With greater water depth the lithologies become geochemically (^{10}Be, Rb-Sr) less suitable. A water depth of tens of meters (or less) corresponding to a glacial lowstand on the continental shelf is likely to be realistic (Fig. 20). The source region might be broadly envisaged within the realm of a river delta to shallow shelf sea containing poorly compacted, rapidly deposited sediments with saline pore waters.

2.18 Absence of Tsunamis Deposits: An impact on land or in a shallow sea would not be expected to produce significant tsunamis: resultant tsunamis would potentially be undifferentiable, in terms of magnitude, from tectonic tsunamis.

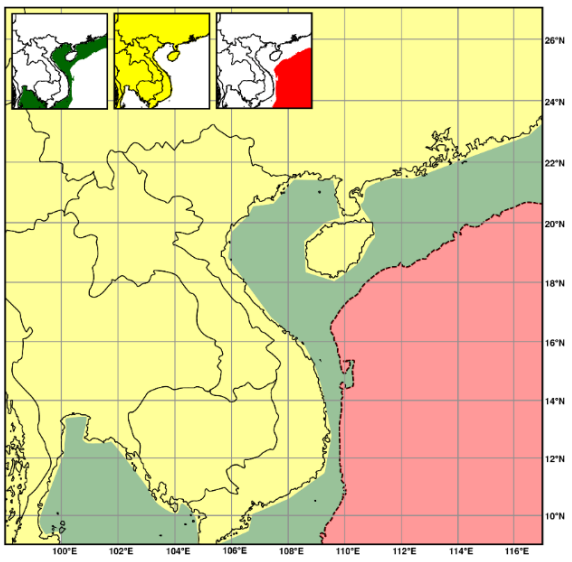

Fig. 20: The deeper seas in red cannot be considered as potential source areas as they could not produce the distal tektites. The areas in green are continental shelf regions (to 500 m below present sea level) (Liu et al., 2016). This shelf region is ideal for tektite production and some of this area would have been land during glacial lowstand. The area in yellow represents land areas which have a low probability of yielding the AAT source crater, simply because the crater would be evident and could not have been buried or eroded. Inset: Data used in map overlay. Green = Probable regions; Yellow = Less favorable regions; Red = Incompatible regions for the AAT impact.

Given the lower sea levels at the time of impact any evidence of tsunamis is likely below the current sea level.

2.19 Evidence of Cataclysmic Deposits: In northeastern Thailand tektite-bearing flood deposits have been reported from Ban Ta Chang (15.037° N, 102.291° E) and Chum Phuang (15.381° N, 102.728° E) (Bunopas et al., 1999). The presence of tektites and reversed polarities constrains the sediment to a period between the AAT impact event = 786 ± 2 ka (Mark et al., 2017) and the Brunhes / Matuyama polarity reversal = 783.4 ± 0.6 ka (Mark et al., 2017) (Haines, K. T. Howard, Ali, Burrett, & Bunopas, 2004; K. T. Howard, Haines, Burrett, Ali, & Bunopas, 2003). These catastrophic flood deposits are consistent with deposition shortly after the impact event. It is possible that these deposits are unrelated, but assuming that these deposits are related to the AAT impact event, it would suggest that the locations are within approximately 750 km of the impact site, after Collins,

Melosh, & Marcus (2005).

2.20 Absence of a Crater: A recent crater that is 43 ± 9 km in diameter (Glass & Koeberl, 2006) is sought. A structure on land should form a distinctive morphological scar, which in tropical regions would be expected to form of a lake. The 1.83 km diameter, 0.576 Ma (±0.047 Ma), Lonar Crater (Jourdan, Moynier, Koeberl, & Eroglu, 2011; Schmieder & Kring, 2020) contains a 1.2 km diameter lake. The 10.5 km, 1.13 Ma (±0.10 Ma) (Jourdan, 2012; Koeberl, Bottomley, Glass, & Storzer, 1997; Schmieder & Kring, 2020) Bosumtwi Crater in Ghana, again in a tropical region, contains an 8 km diameter lake. The only significant lake in Indochina, Tonle Sap, was suggested as a possible source crater by Hartung & Koeberl (1994). Tektite distribution patterns and geochemical regressions would indicate that this cannot be the AAT source crater.

Given the absence of a lake, if the crater were onshore, it would be impossible to erode anything more than the most surficial part of a relatively pervasive impact structure. Distinct pyroclastic-like lithologies should be observed. Igneous-like lithologies would have been observed with deeper, but implausible, erosion. Estimated denudation rates are 23 m to 393 m since the AAT impact crater formed (Carter, Roques, & Bristow, 2000; Jonell et al., 2017; Yan, Carter, Palk, Brichau, & Hu, 2011) with perhaps ± 75 m of erosion being a realistic average value to use.

Destruction of the crater by tectonic processes can be ruled out in the brief time since impact. Tectonic processes may, however, have enhanced sediment accommodation space, assisting burial. Newly formed craters are natural depocenters. Furthermore, post-impact, the crater floor would be expected to continue to sag, e.g., Ries Crater experienced 134 +23/-49m of crater floor subsidence lasting more than 600 ka (Arp et al., 2021). Burial of the crater appears to be the only viable option to hide a crater.

Burial by extensive flood basalts is a possibility but would require a thick and extensive area of ~1,450 km^2 or more of post-impact age lava flows to cover a ~43 km diameter crater. Bolaven Plateau (seen in southern Laos in Fig. 6) is the only plausible (although sub-optimally placed) volcanic center in the region of interest. Bolaven lacks suitably extensive flood basalts of a young post-impact age, allowing, at best, a 17 km diameter crater (Sieh et al., 2020), which is 7 times less energetic than predicted, after Collins et al. (2005), and more comparable with the Bosumtwi impact that produced the much smaller Ivory Coast Tektite strewn field. Geochemical considerations have already been discussed and raise objections for an AAT impact into a pre-existing volcanic center.

Burial by sediments appears to be the only plausible option to hide a crater. This could be by river sediments or within a basin, such as the YGH-SH Basin (Fig. 21). A river scenario is somewhat problematic due to the raised crater rim geometry that would more likely result in a lake and diverted river system. A basin scenario, with exceptionally high sedimentation rates, readily explains the absence of a crater and is entirely conceivable within the source region. Sedimentation rates in the YGH-SH Basin were estimated as 235 m/Ma in the late Miocene and 780 m/Ma in the Pliocene to Quaternary (Lei et al., 2011). High sedimentation rates prior to the impact readily explain the geochemical observations in tektites

2.21 Absence of an Ejecta Blanket: Whilst there have been reports of an ejecta blanket in and around the Bolaven Plateau (Sieh et al., 2020; Tada et al., 2019) (Fig. 22), no convincing evidence of a suevite deposits has been presented. The presence of high shock / high temperature tektites (Tada et al., 2019) in a low shock, un-melted, monomict breccia deposit suggests the crater is not nearby. The monolithologic, cobbly / boulder sandstone breccia (Sieh et al., 2020; Tada et al., 2019) is unlike a proximal suevite, which characteristically yields partial melts. Furthermore, the single represented lithology is a sandstone, which is unsuitable from a REE perspective to be the AAT source material. A localized mass transport or flash flood origin might be more plausible, either unrelated to the AAT impact or (to explain a widespread occurrence) related in terms of devegetation in the impact aftermath. An ejecta blanket from a 43 km diameter crater would be expected to be 100 m thick at 16 km, 20 m thick

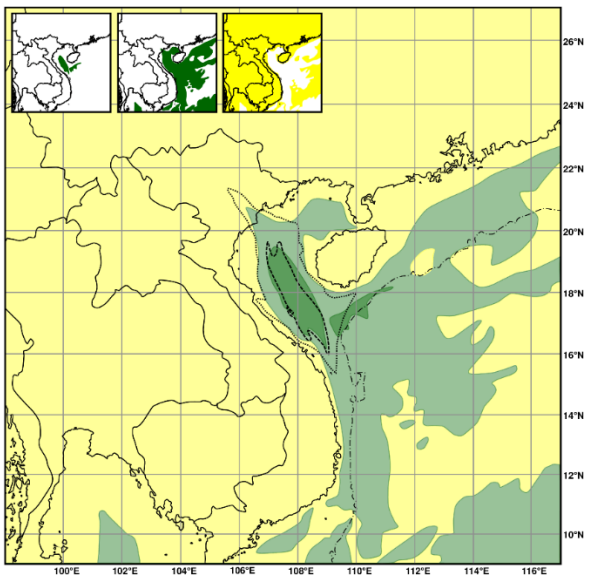

Fig. 21: Regions of moderate sedimentation rates (green) and high sedimentation rates (dark green), with a focus on Quaternary sedimentation (Métivier, Gaudemer, Tapponnier, & Klein, 1999). In terms of sedimentation, the dark green regions have, by far, the highest compatibility as a source region. Note that sedimentation rates and depocenters have varied considerably over time. The Yinggehai - Song Hong Basin is highlighted by a black dotted line with the depocenter marked by a black dashed line (Fan, 2018). The shelf break (500 m contour) is shown as a black dot-dashed line (Liu et al., 2016). Yellow shaded regions represent lower probability for the presence of the AAT impact crater. Inset: Data used in map overlay. Green = Probable regions; Yellow = Less favorable regions for the AAT impact.

at 43 km, 10 m thick at 60 km, 5 m thick at 81 km, and 1 m thick at 154 km from the rim of the post-impact crater. The described ejecta blanket is suggested to be 40-50 m thick (Sieh et al., 2020) based on the depth of incised stream valleys as opposed to direct observations. Tada et al. (2019) suggests an ejecta blanket ranging from under 1 m to a maximum of 9 m thickness. Sieh et al. (2020) models a much smaller impact of maximum 17 km diameter, which better fits with the proposed thinner ejecta blanket but fails to explain the widespread distribution and abundance of AAT. Finally, Sieh et al. (2020) elected not to perform a detailed study of planar deformation features in quartz grains, a diagnostic test (but not discounting reworking), instead relying on undiagnostic lithological observations of the deposit and the circular argument of proximity to an unproven crater. The proposed Bolaven ejecta blanket was not utilized in the map overlay, pending further evidence.

Tada et al. (2019) noted in their poster that the AAT proximal ejecta blanket has never conclusively been identified on land in Indochina. This observation remains true. Tada et al. (2019) went on to note that the ejecta deposit is important to constrain the impact location. Indeed, the absence of an ejecta blanket may be a constraining factor. It is difficult to envisage that all traces of an ejecta blanket have been eroded away. A more plausible explanation for the apparent absence of an ejecta blanket, is that the thick proximal ejecta deposit is located offshore (Fig. 22). If only a thin ejecta blanket was present onshore, then it is realistic that it could have been entirely eroded or reworked. The absence of an ejecta blanket suggests the point of impact is far from the current shoreline: probably at least 50 km (as conservatively depicted in Fig. 22), and more likely over 80 km (resulting in up to a 42 m and 10 m thick ejecta layer, respectively, on the current land surface, pre-erosion).

3. Conclusions

Multiple lines of independent data indicate that the AAT source crater will be found in the Gulf of Tonkin to central-eastern Indochinese region as opposed to ~800 km further north-northwest as would be implied if all tektites were downrange ejecta. Accepting a Gulf of Tonkin to central-eastern Indochina source region implies the existence of uprange tektites. The AAT impact was unarguably oblique and as such there should be a distinct uprange zone of avoidance in the early phase of impact (Gault & Wedekind, 1978; Schultz et al., 2009, 2007). Consequently, uprange tektites must be from a marginally later stage of impact. With reference to the calculated AAT crater diameter of 43 ± 9 km (Glass & Koeberl, 2006) and to ejection velocities in Artemieva (2008) it must be assumed that the uprange ejecta, for it to be present, must be deeply excavated. From the ^{10}Be content of these uprange tektites it must be concluded that a thick sequence of recent sedimentary rock has been sampled. This is indicative that the impact occurred in a pre-existing depocenter. The source crater location is thus largely restricted to the Yinggehai-Song Hong (YGH-SH) Basin. A YGH-SH Basin impact is not only in keeping with

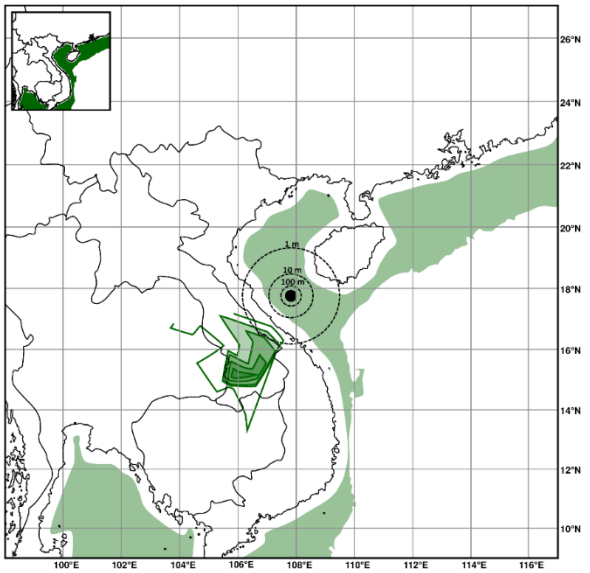

Fig. 22: Expected ejecta thickness from a 43 km diameter crater (black dashed lines). The crater position (Whymark, 2013) is for example only as the crater location is not established. In consideration of the absence of an ejecta layer onshore (either patchy or continuous), there is a higher probability that the impact was, conservatively, at least 50 km offshore from the current coastline (and likely more). A continental shelf region over 50 km from the current shoreline is depicted as a green shaded area. An unconfirmed ejecta layer was identified (Tada et al., 2019) (green lines centered on southern Laos). The breccia layer (Unit 2) reached a maximum thickness of 9 meters in the Bolaven Plateau. This unconfirmed ejecta layer was not utilized on composite overlay maps. Inset: Data used in map overlay. Green = Probable regions for the AAT impact.

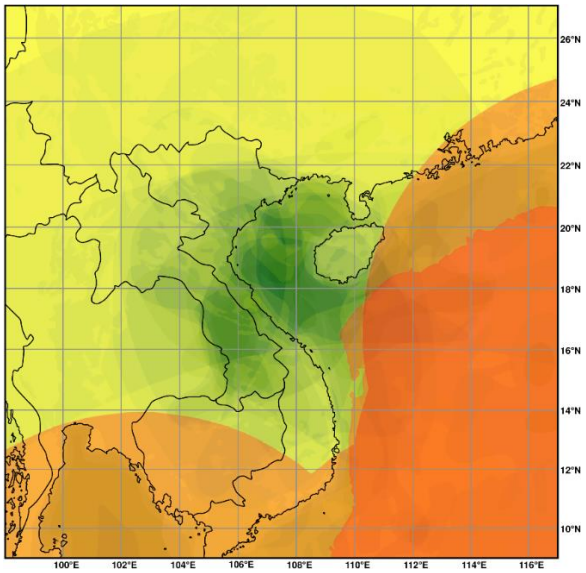

Fig. 23: Combined positive and negative data for source crater location. Greener areas = higher probability. Yellower areas = lower probability. Red / orange areas = no probability.

all available data, but the young, rapidly deposited, water saturated, siliciclastic sediment with saline formation water / sea water readily explain the abundance and geographic extent of the AAT. Furtherm ore, continued exceptionally high sedimentation rates in accommodation space created, in part, by the impact itself and subsequent sagging, would have resulted in rapid burial of the crater by hundreds of meters of sediment, thus explaining the apparent absence of the AAT source crater and its thick proximal ejecta blanket.

The principles of map overlay (McHarg, 1969) can be utilized to combine data and determine the most probable location of the AAT source crater. Some of the data presented and utilized is conflicting, e.g., the Jurassic versus recent (Rb/Sr versus ^{10}Be) age of the source rock. With perfect data sets all overlay map evidence will overlap on a central point. With more patchy or ambiguous data the overlap becomes partial or overlay elements become isolated, indicative that at least one of the lines of evidence is incorrect or insufficiently resolved. The nature of the partial data set for tektites, most critically for proximal tektites in the Gulf of Tonkin and South China Sea region, will result in error and a degree of skewness of the data. The use of multiple lines of evidence means that each observation only comprises a small percentage of the data set. Potentially misleading data should be overwhelmed by the weight of data, which, on average, should be correct.

An overlay map was constructed by placing maps of the same scale on top of one another. Fig. 23, constructed from all positive and negative data, utilized a total of 42 overlays (25 green, 15 yellow, and 2 red) taken from the insets in Figs. 1 - 6, 10, 12 - 17, & 19 - 22. White (no data) regions were transparent, green and yellow data regions were 90% transparent, whilst red data was weighted at 70% transparency. The green shaded areas = higher probability, yellow shaded areas = lower probability, and red / orange shaded areas = no probability for the crater being in the region. Fig. 24, utilized only negative data, using 17 overlays (15 yellow, and 2 red) taken from the insets in Figs. 1, 4 - 6, 10, 12 - 17, & 19 - 21. White (no data) regions were transparent, yellow data regions were 50% transparent and red data was

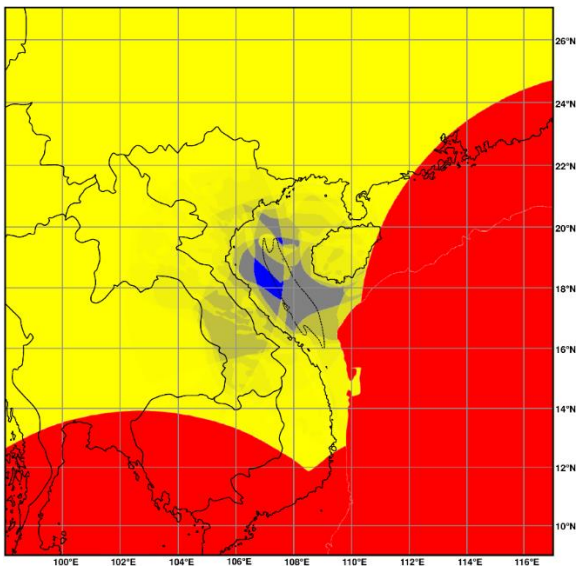

Fig. 24: Combined negative data for source crater location utilizing 50% transparency with a contrasting background color (blue). The dashed line represents the depocenter of the YGH-SH Basin. Blue areas = higher probability (no, or fewer objections). Yellow areas = lower probability. Red areas = no probability.

opaque. A blue background was added to highlight the most probable region of impact (blue). A region in the center or northwest segment of the Gulf of Tonkin had the least objections as an impact location, with a broader swathe encompassing the Gulf of Tonkin and central-eastern Indochina being plausible (Figs. 23 & 24). The most probable impact location, considering positive and negative data, is within ~100 km of E107.20°, N18.30°, but not (significantly) in a landward direction. The likelihood that the impact occurred in a depocenter with high sedimentation rates would indicate a basinward impact location (see Fig. 24 for the YGH-SH Basin depocenter).

A possible structure exists in the YGH-SH Basin at E107.85°, N17.78° (Whymark, 2013, 2018). This depocenter region is known as the 'Great Sag' (Clift & Sun, 2006). Evidence of the presence of a crater include a 43 km diameter annular gravity anomaly (Whymark, 2013, 2018). A circular region of shallow-rooted chaotic seismic from approximately the time of impact to the late Miocene (Gong & Li, 2004; Gong et al., 1997; Yan et al., 2011). A circular pattern of shale diapirs (Lei et al., 2011, 2015) which may relate to post-impact geothermal activity conducting fluids along lines of weakness. An outer elliptical pattern of shale diapirs, possibly indicating significant slumping of the suspected crater, as would be anticipated from an oblique impact crater with asymmetrical depth profile in a continental shelf setting. A high geothermal gradient (Lei et al., 2011) may record the residual heat from the impact event. Seismic line 0755 (Lei et al., 2015, Fig. 3) (supported by Figs. 1.3.2.6 & 1.3.2.7 in CCOP, 2008) is apparently consistent with an impact crater (onlap, rim fault, and chaotic seismic). Further seismic lines have been recorded over the potential crater (Lei et al., 2015; CCOP, 2008) but are of poor resolution or are not in the public domain. Overlay of YGH-SH Basin geophysical and well data would narrow the search for the AAT source crater. Efforts to locate the AAT source crater must shift from improbable and fruitless onshore regions to the highly probable YGH-SH Basin.

Acknowledgments

This project was self-funded. Thank you to Dr. J. Rimando for advice and to anonymous reviewers for constructive suggestions that enhanced this article.

Note

The author remains neutral regarding jurisdictional claims in maps and geographic nomenclature.

References

Ackerman, L., Skála, R., Křížová, Š., Žák, K., & Magna, T. (2019). The quest for an extraterrestrial component in Muong Nong-type and splash-form Australasian tektites from Laos using highly siderophile elements and Re-Os isotope systematics. *Geochimica et Cosmochimica Acta, 252*, 179–189. https://doi.org/10.1016/j.gca.2019.03.009.

Ackerman, L., Žák, K., Skála, R., Rejšek, J., Křížová, Š., Wimpenny, J., & Magna, T. (2020). Sr-Nd-Pb isotope systematics of Australasian tektites: Implications for the nature and composition of target materials and possible volatile loss of Pb. *Geochimica et Cosmochimica Acta, 276*, 135–150. https://doi.org/10.1016/j.gca.2020.02.025

Amare, K., & Koeberl, C. (2006). Variation of chemical composition in Australasian tektites from differrent localities in Vietnam. *Meteoritics & Planetary Science, 41*(1), 107–123.https://doi.org/10.1111/j.1945-5100.2006.tb00196.x

Arp, G., Dunkl, I., Jung, D., Karius, V., Lukács, R., Zeng, L., … Head III, J. W. (2021). A volcanic ash layer in the Nördlinger Ries impact structure (Miocene, Germany): Indication of crater fill geometry and origins of long-term crater floor sagging. *Journal of Geophysical Research: Planets*, e2020JE006764. https://doi.org/10.1029/2020JE006764

Artemieva, N. A. (2008, March 10–14). *Tektites: Model Versus Reality* [Abstract #1651]. Abstract submitted to the 39th Lunar and Planetary Science Conference, League City, Texas, United States of America. Retrieved from: https://www.lpi.usra.edu/meetings/lpsc2008/pdf/1651.pdf

Artemieva, N. A. (2013, March 18–22). *Numerical Modeling of the Australasian Tektite Strewn Field* [Abstract #1410]. Abstract submitted to the 44th Lunar and Planetary Science Conference, The Woodlands, Texas, United States of America. Retrieved from: https://www.lpi.usra.edu/meetings/lpsc2013/pdf/1410.pdf

Artemieva, N. A., & Pierazzo, E. (2003, February 7-9). *Oblique Impact and its Ejecta: Numerical Modeling* [Abstract #8022]. Abstract submitted to: Impact Cratering, Bridging the Gap Between Modeling and Observations, Houston, Texas, United States of America. Retrieved from: https://www.lpi.usra.edu/meetings/impact2003/pdf/8022.pdf

Beran, A., & Koeberl, C. (1997). Water in tektites and impact glasses by fourier-transformed infrared spectrometry. *Meteoritics & Planetary Science, 32*(2), 211–216. https://doi.org/10.1111/j.1945-5100.1997.tb01260.x

Blum, J. D., Papanastassiou, D. A., Koeberl, C., & Wasserburg, G. J. (1992). Neodymium and strontium isotopic study of Australasian tektites: New constraints on the provenance and age of target materials. *Geochimica et Cosmochimica Acta, 56*(1), 483–492. https://doi.org/10.1016/0016-7037(92)90146-A

Bunopas, S., Wasson, J. T., Vella, P., Fontaine, H., Hada, S., Burrett, C., … Khositanont, S. (1999). Early Quaternary global terrestrial impact of a whole comet in the Australasian tektite field, newest apparent evidences discovery from Thailand and East Asia. *Bull. Geol. Soc. Malaysia. Proceedings Geosea '98 Ninth Regional Congress on Geology, Mineral and Energy Resources of Southeast Asia., 43*, 555–575. https://doi.org/10.7186/bgsm43199956

Burns, C. A., Schnetzler, C. C., & Chase, J. N. (1961). Tektite from Martha's Vineyard, Massachusetts. *Geological Society of America Bulletin, 72*(2), 339. https://doi.org/10.1130/0016-7606(1961)72[339:TFMVM]2.0.CO;2

Čada, M., Houzar, S., Hrazdil, V., & Skála, R. (2002, September 23-26). *Field Trip Guidebook and Abstracts*. Presented at the 9th International Conference on Moldavites, impact glasses and impact processes, Františkovy Lázně, Czech Republic.

Cao, L., Jiang, T., Wang, Z., Zhang, Y., & Sun, H. (2015). Provenance of Upper Miocene sediments in the Yinggehai and Qiongdongnan basins, northwestern South China Sea: Evidence from REE, heavy minerals and zircon U–Pb ages. *Marine Geology, 361*, 136–146. https://doi.org/10.1016/j.margeo.2015.01.007

Carter, A., Roques, D., & Bristow, C. S. (2000). Denudation history of onshore central Vietnam: Constraints on the Cenozoic evolution of the western margin of the South China Sea. *Tectonophysics, 322*(3–4), 265–277. https://doi.org/10.1016/S0040-1951(00)00091-3

CCOP (2008). Capacity Building within Geoscience in East and Southeast Asia Project (ICB-CCOP 1). *Final Report (Volume I) (p. 250). Bangkok, Thailand: Coordinating Committee for Geoscience Programmes in East and Southeast Asia (CCOP)*. Retrieved from: http://library.dmr.go.th/Document/DMR_Technical_Reports/2008/22539.pdf

Chapman, D. R. (1964). On the unity and origin of the Australasian tektites. *Geochimica et Cosmochimica Acta, 28*(6), 841–880. https://doi.org/10.1016/0016-7037(64)90036-5

Chapman, D. R. (1971). Australasian tektite geographic pattern, crater and ray of origin, and theory of tektite events. *Journal of Geophysical Research, 76*(26), 6309–6338. https://doi.org/10.1029/JB076i026p06309

Chapman, D. R., & Scheiber, L. C. (1969). Chemical investigation of Australasian tektites. *Journal of Geophysical Research, 74*(27), 6737–6776. https://doi.org/10.1029/JB074i027p06737

Chaussidon, M., & Koeberl, C. (1995). Boron content and isotopic composition of tektites and impact glasses: Constraints on source regions. *Geochimica et Cosmochimica Acta, 59*(3), 613–624. https://doi.org/10.1016/0016-7037(94)00368-V

Chmeleff, J., Blanckenburg, F. von, Kossert, K., & Jakob, D. (2010). Determination of the ^{10}Be half-life by multicollector ICP-MS and liquid scintillation counting. *Nuclear Instruments and Methods in Physics Research Section B: Beam Interactions with Materials and Atoms, 268*(2), 192-199.https://doi.org/10.1016/j.nimb.2009.09.012

Clift, P. D., Long, H. V., Hinton, R., Ellam, R. M., Hannigan, R., Tan, M. T., … Duc, N. A. (2008). Evolving east Asian river systems reconstructed by trace element and Pb and Nd isotope variations in modern and ancient Red River-Song Hong sediments: Evolution of East Asian River Systems. *Geochemistry, Geophysics, Geosystems, 9*(4). https://doi.org/10.1029/2007GC001867

Clift, P. D., & Sun, Z. (2006). The sedimentary and tectonic evolution of the Yinggehai-Song Hong basin and the southern Hainan margin, South China Sea: Implications for Tibetan uplift and monsoon intensification: Evolution of Yinggehai-Song Hong Basin. *Journal of Geophysical Research: Solid*

Earth, *111*(B6), B06405. https://doi.org/10.1029/2005JB004048

Collins, G. S., Melosh, H. J., & Marcus, R. A. (2005). Earth impact effects program: A web-based computer program for calculating the regional environmental consequences of a meteoroid impact on Earth. *Meteoritics & Planetary Science*, *40*(6), 817–840. https://doi.org/10.1111/j.1945-5100.2005.tb00157.x

Collins, G. S., & Wünnemann, K. (2005). How big was the Chesapeake Bay impact? Insight from numerical modeling. *Geology*, *33*(12), 925–928. https://doi.org/10.1130/G21854.1

Condie, K. C. (1993). Chemical composition and evolution of the upper continental crust: Contrasting results from surface samples and shales. *Chemical Geology*, *104*(1–4), 1–37. https://doi.org/10.1016/0009-2541(93)90140-E

Cordani, U. G., Mizusaki, A. M., Kawashita, K., & Thomaz-Filho, A. (2004). Rb–Sr systematics of Holocene pelitic sediments and their bearing on whole-rock dating. *Geological Magazine*, *141*(2), 233–244. https://doi.org/10.1017/S0016756803008616

Dickin, A. P. (2005). *Radiogenic Isotope Geology* (2nd ed.), 492 p. Cambridge University Press. https://doi.org/10.1017/CBO9781139165150

Elkins-Tanton, L. T., Kelly, D. C., Bico, J., & Bush, J. W. M. (2002, March 11–15). *Microtektites as vapor condensates, and a possible new strewn field at 5 Ma* [Abstract #1622]. Abstract submitted to the 33rd Lunar and Planetary Science Conference, League City, Texas, United States of America. Retrieved from: https://www.lpi.usra.edu/meetings/lpsc2002/pdf/1622.pdf

Elliott, J. R., Huang, Y.-H., Minton, D. A., & Freed, A. M. (2018). The length of lunar crater rays explained using secondary crater scaling. *Icarus*, *312*, 231–246. https://doi.org/10.1016/j.icarus.2018.04.015

Fan, C. (2018). Tectonic deformation features and petroleum geological significance in Yinggehai large strike-slip basin, South China Sea. *Petroleum Exploration and Development*, *45*(2), 204–214. https://doi.org/10.1016/S1876-3804(18)30024-7

Feng, Y., Zhan, W., Chen, H., Jiang, T., Zhang, J., Osadczuk, A., … Zhang, W. (2018). Seismic characteristics and sedimentary record of the late Pleistocene delta offshore southwestern Hainan Island, northwestern South China Sea. *Interpretation*, *6*(4), SO31-SO43. https://doi.org/10.1190/INT-2018-0012.1

Fenner, C. (1935). Australites, part II. Numbers, forms, distribution and origin. *Transactions of the Royal Society of South Australia*, *59*, 125–140.

Fiske, P. S., Schnetzler, C. C., Mchone, J., Chanthavaichith, K. K., Homsombath, I., Phouthakayalat, T., … Xuan, P. T. (1999). Layered tektites of southeast Asia: Field studies in central Laos and Vietnam. *Meteoritics & Planetary Science*, *34*(5), 757–761. https://onlinelibrary.wiley.com/doi/abs/10.1111/j.1945-5100.1999.tb01388.x

Gault, D. E., & Wedekind, J. A. (1978, March 13-17). *Experimental studies of oblique impact*. In: Proceedings of the 9th Lunar and Planetary Science Conference (pp. 3843-3875), Houston, Texas, United States of America. Retrieved from:http://adsabs.harvard.edu/full/1978LPSC....9.3843G

Gentner, W. (1966). Auf der Suche nach Kratergläsern, Tektiten und Meteoriten in Afrika. *Naturwissenschaften*, *53*(12), 285–289. https://doi.org/10.1007/BF00712210

Glass, B. P. (2003, March 17–21). *Australasian microtektites in the South China Sea: Implications regarding the location and size of the source crater* [Abstract #1092]. Abstract submitted to the 34th Lunar and Planetary Science Conference, League City, Texas, United States of America. Retrieved from:https://www.lpi.usra.edu/meetings/lpsc2003/pdf/1092.pdf

Glass, B. P., & Barlow, R. A. (1979). Mineral inclusions in Muong Nong-type indochinites: Implications concerning parent material and process of formation. *Meteoritics*, *14*(1), 55–67. https://doi.org/10.1111/j.1945-5100.1979.tb00479.x

Glass, B. P., Huber, H., & Koeberl, C. (2004). Geochemistry of Cenozoic microtektites and clinopyroxene-bearing spherules. *Geochimica et Cosmochimica Acta*, *68*(19), 3971–4006. https://doi.org/10.1016/j.gca.2004.02.026

Glass, B. P., & Koeberl, C. (2006). Australasian microtektites and associated impact ejecta in the South China Sea and the Middle Pleistocene supereruption of Toba. *Meteoritics & Planetary Science*, *41*(2), 305–326. https://doi.org/10.1111/j.1945-5100.2006.tb00211.x

Glass, B. P., & Pizzuto, J. E. (1994). Geographic variation in Australasian microtektite concentrations: Implications concerning the location and size of the source crater. *Journal of Geophysical Research*, *99*(E9), 19075-19081. https://doi.org/10.1029/94JE01866

Glass, B. P., & Simonson, B. M. (2013). *Distal impact ejecta layers: A record of large impacts in sedimentary deposits*. 716 p. Heidelberg; New York: Springer. ISBN 978-3-540-88262-6

Gong, Z. S., & Li, S. T. (2004). *Dynamic research of oil and gas accumulation in northern marginal basins of South China Sea*. 339 p. Science in China Press, Beijing, (in Chinese with English abstract).

Gong, Z. S., Li, S. T., Xie, T. J., Zhang, Q. M., Xu, S. C., Xia, K. Y., … Liu, L. H. (1997). *Continental*

margin basin analysis and hydrocarbon accumulation of the northern South China Sea. 510 p. China Sci. Press, Beijing, (in Chinese with English abstract).

Haines, P. W., Howard, K. T., Ali, J. R., Burrett, C. F., & Bunopas, S. (2004). Flood deposits penecontemporaneous with ~0.8 Ma tektite fall in NE Thailand: Impact-induced environmental effects? *Earth and Planetary Science Letters, 225*(1–2), 19–28. https://doi.org/10.1016/j.epsl.2004.05.008

Hartung, J. B., & Koeberl, C. (1994). In search of the Australasian tektite source crater: The Tonle Sap hypothesis. *Meteoritics, 29*(3), 411–416.https://doi.org/10.1111/j.1945-5100.1994.tb00606.x

Hoang, N., Flower, M. F. J., & Carlson, R. W. (1996). Major, trace element, and isotopic compositions of Vietnamese basalts: Interaction of hydrous EM1-rich asthenosphere with thinned Eurasian lithosphere. *Geochimica et Cosmochimica Acta, 60*(22), 4329–4351. https://doi.org/10.1016/S0016-7037(96)00247-5

Hoang, N., Hauzenberger, C., Fukuyama, M., & Konzett, J. (2018, October 16-17). *Cenozoic volcanism in the Bolaven Plateau, southern Laos*. Abstract submitted to the Regional Congress on Geology, Minerals and Energy Resources of Southeast Asia (GEOSEA), Hanoi, Vietnam.

Howard, B. C. (2016). Australia Is Drifting So Fast GPS Can't Keep Up. *National Geographic*. [online]. [Cited 23 September 2016]. Retrieved from: https://www.nationalgeographic.com/news/2016/09/australia-moves-gps-coordinates-adjusted-continental-drift/

Howard, K. T. (2011). Volatile enhanced dispersal of high velocity impact melts and the origin of tektites. *Proceedings of the Geologists' Association, 122*(3), 363–382. https://doi.org/10.1016/j.pgeola.2010.11.006

Howard, K. T., Haines, P. W., Burrett, C. F., Ali, J. R., & Bunopas, S. (2003). Sedimentology of 0.8 Ma log-bearing flood deposits in northeast Thailand and mechanisms for pre-flood deforestation. *Proceedings, 8th International Congress on Pacific Neogene Stratigraphy, Chiang Mai, Thailand*, 49–67.

Huber, H. (2009). INAA of Muong-Nong type tektites and adjacent soil samples. *22nd Seminar Activation Analysis and Gamma-Spectroscopy. Program and Book of Abstracts*. 35.

Izokh, E. P., & An, L. D. (1983). Tektites of Vietnam. Tektites delivered by a comet: A hypothesis. *NASA Report No. NAS 1.7720103; NASA-TT-20103*. Transl. into English from *Meteoritika (Moscow), 42*, 158-170.

Javanaphet, C. (1969). *Geological Map of Thailand; Scale 1: 1,000,000 with Explanation*. Department of Mineral Resources, Bangkok, Thailand.

Jiang, T., Xie, X., Chen, H., Wang, Z., and Li, X. (2015) Geochemistry of pore water and associated diagenetic reactions in the diapiric area of Yinggehai Basin, northwestern South China Sea. *Journal of Earth Science, 26*(3), 306–316. https://doi.org/10.1007/s12583-015-0526-y

Jonell, T. N., Clift, P. D., Hoang, L. V., Hoang, T., Carter, A., Wittmann, H., … Rittenour, T. (2017). Controls on erosion patterns and sediment transport in a monsoonal, tectonically quiescent drainage, Song Gianh, central Vietnam. *Basin Research, 29*, 659–683. https://doi.org/10.1111/bre.12199

Jourdan, F. (2012). The $^{40}Ar/^{39}Ar$ dating technique applied to planetary sciences and terrestrial impacts. *Australian Journal of Earth Sciences, 59*(2), 199–224. https://doi.org/10.1080/08120099.2012.644404

Jourdan, F., Moynier, F., Koeberl, C., & Eroglu, S. (2011). $^{40}Ar/^{39}Ar$ age of the Lonar crater and consequence for the geochronology of planetary impacts. *Geology, 39*(7), 671–674. https://doi.org/10.1130/G31888.1

Jourdan, F., Nomade, S., Wingate, M. T. D., Eroglu, E., & Deino, A. (2019). Ultraprecise age and formation temperature of the Australasian tektites constrained by $^{40}Ar/^{39}Ar$ analyses. *Meteoritics & Planetary Science, 54*(10), 2573–2591. https://doi.org/10.1111/maps.13305

Kenkmann, T., Collins, G. S., Wittmann, A., Wünnemann, K., Reimold, W. U., & Melosh, H. J. (2009). A model for the formation of the Chesapeake Bay impact crater as revealed by drilling and numerical simulation. *Geological Society of America Special Papers, 458*, 571–585. https://doi.org/10.1130/2009.2458(25)

Koeberl, C. (1986). Muong Nong type tektites from the moldavite and North American strewn fields? *Journal of Geophysical Research: Solid Earth, 91*(B13), E253–E258. https://doi.org/10.1029/JB091iB13p0E253

Koeberl, C. (1992). Geochemistry and origin of Muong Nong-type tektites. *Geochimica et Cosmochimica Acta, 56*(3), 1033–1064. https://doi.org/10.1016/0016-7037(92)90046-L

Koeberl, C. (1994). Tektite origin by hypervelocity asteroidal or cometary impact: Target rocks, source craters, and mechanisms. *Geological Society of America Special Papers, 293*, 133–152. https://doi.org/10.1130/SPE293-p133

Koeberl, C., Bottomley, R., Glass, B. P., & Storzer, D. (1997). Geochemistry and age of Ivory Coast tektites and microtektites. *Geochimica et Cosmochi-mica Acta, 61*(8), 1745–1772. https://doi.org/10.1016/S0016-7037(97)00026-4

Koeberl, C., Kluger, F., & Kiesl, W. (1985). Rare earth elemental patterns in some impact glasses and tektites and potential parent materials. *Chemie Der Erde, 44*(2), 107–121.

Koeberl, C., Nishiizumi, K., Caffee, M. W., & Glass, B. P. (2015, July 27–31). *Beryllium-10 in Individual*

Australasian Microtektites and Origin of Tektites [Abstract #5187]. Abstract submitted to the 78th Annual Meeting of the Meteoritical Society, Berkeley, California, United States of America. Retrieved from: https://www.hou.usra.edu/meetings/metsoc2015/pdf/5187.pdf

Korschinek, G., Bergmaier, A., Faestermann, T., Gerstmann, U. C., Knie, K., Rugel, G., … Gostomski, C. L. von. (2010). A new value for the half-life of ^{10}Be by heavy-ion elastic recoil detection and liquid scintillation counting. *Nuclear Instruments and Methods in Physics Research Section B: Beam Interactions with Materials and Atoms*, *268*(2), 187–191. https://doi.org/10.1016/j.nimb.2009.09.020

Lei, C., Ren, J., Clift, P. D., Wang, Z., Li, X., & Tong, C. (2011). The structure and formation of diapirs in the Yinggehai–Song Hong Basin, South China Sea. *Marine and Petroleum Geology*, *28*(5), 980–991. https://doi.org/10.1016/j.marpetgeo.2011.01.001

Lei, C., Ren, J., Sternai, P., Fox, M., Willett, S., Xie, X., … Wang, Z. (2015). Structure and sediment budget of Yinggehai–Song Hong basin, South China Sea: Implications for Cenozoic tectonics and river basin reorganization in Southeast Asia. *Tectonophysics*, *655*, 177–190. https://doi.org/10.1016/j.tecto.2015.05.024

Liu, Z., Colin, C., Huang, W., Le, K. P., Tong, S., Chen, Z., & Trentesaux, A. (2007). Climatic and tectonic controls on weathering in south China and Indochina Peninsula: Clay mineralogical and geochemical investigations from the Pearl, Red, and Mekong drainage basins: controls on weatherings in S. China. *Geochemistry, Geophysics, Geosystems*, *8*(5). https://doi.org/10.1029/2006GC001490

Liu, Z., Zhao, Y., Colin, C., Stattegger, K., Wiesner, M. G., Huh, C. A., … Li, Y. (2016). Source-to-sink transport processes of fluvial sediments in the South China Sea. *Earth-Science Reviews*, *153*, 238–273. https://doi.org/10.1016/j.earscirev.2015.08.005

Lodders, K., & Fegley, B. (1998). *The Planetary Scientist's Companion*. 392 p. Oxford University Press on Demand. ISBN: 9780195116946

Ma, P., Aggrey, K., Tonzola, C., Schnabel, C., de Nicola, P., Herzog, G. F., … Klein, J. (2004). Beryllium-10 in Australasian tektites: Constraints on the location of the source crater. *Geochimica et Cosmochimica Acta*, *68*(19), 3883–3896. https://doi.org/10.1016/j.gca.2004.03.026

Mark, D. F., Renne, P. R., Dymock, R. C., Smith, V. C., Simon, J. I., Morgan, L. E., … Pearce, N. J. G. (2017). High-precision ^{40}Ar/^{39}Ar dating of Pleistocene tuffs and temporal anchoring of the Matu-yama-Brunhes boundary. *Quaternary Geochronology*, *39*, 1–23. https://doi.org/10.1016/j.quageo.2017.01.002

Matsuda, J., Maruoka, T., Pinti, D. L., & Koeberl, C. (1996). Noble gas study of a philippinite with an unusually large bubble. *Meteoritics & Planetary Science*, *31*(2), 273–277. https://doi.org/10.1111/j.1945-5100.1996.tb02023.x

McDonough, W. F., & Sun, S. S. (1995). The composition of the Earth. *Chemical Geology*, *120*(3–4), 223–253. https://doi.org/10.1016/0009-2541(94)00140-4

McHarg, I. L. (1969). *Design with Nature*. Garden City, N.Y.: Published for the American Museum of Natural History [by] the Natural History Press.

Meisel, T., Langenauer, M., & Krähenbühl, U. (1992). Halogens in tektites and impact glasses. *Meteoritics*, *27*(5), 576–579. https://doi.org/10.1111/j.1945-5100.1992.tb01079.x

Métivier, F., Gaudemer, Y., Tapponnier, P., & Klein, M. (1999). Mass accumulation rates in Asia during the Cenozoic. *Geophysical Journal International*, *137*(2), 280–318. https://doi.org/10.1046/j.1365-246X.1999.00802.x

Mizote, S., Matsumoto, T., Matsuda, J., & Koeberl, C. (2003). Noble gases in Muong Nong-type tektites and their implications. *Meteoritics & Planetary Science*, *38*(5), 747–758. https://doi.org/10.1111/j.1945-5100.2003.tb00039.x

O'Keefe, J. A. (1963). *Tektites*. 228 p. The University of Chicago Press.

Orbit 1.2 Software. (1998-2000). Published by Siltec Ltd. Retrieved (in 2011, no longer available) from: http://physics-animations.com/Physics/English/orbit.htm

Pierazzo, E., & Melosh, H. J. (2000). Melt Production in Oblique Impacts. *Icarus*, *145*(1), 252–261. https://doi.org/10.1006/icar.1999.6332

Povenmire, H. (2010, July 26–30). *The First Georgia--Area Tektite Found in South Carolina* [Abstract #5222]. Abstract submitted to the 73rd Annual Meeting of the Meteoritical Society, New York, United States of America. Retrieved from: https://www.lpi.usra.edu/meetings/metsoc2010/pdf/5222.pdf

Povenmire, H., & Strange, R. L. (2006, March 13–17). *The First Tektite from Dooly Crisp Counties, Georgia* [Abstract #1002]. Abstract submitted to the 37th Lunar and Planetary Science Conference, League City, Texas, United States of America. Retrieved from: https://www.lpi.usra.edu/meetings/lpsc2006/pdf/1002.pdf

Prasad, M. S., Mahale, V. P., & Kodagali, V. N. (2007). New sites of Australasian microtektites in the central Indian Ocean: Implications for the location and size of source crater. *Journal of Geophysical Research*, *112*(E6), E06007. https://doi.org/10.1029/2006JE002857

Rochette, P., Braucher, R., Folco, L., Horng, C. S., Aumaître, G., Bourlès, D. L., & Keddadouche, K.

(2018). ^{10}Be in Australasian microtektites compared to tektites: Size and geographic controls. *Geology*, *46*(9), 803–806. https://doi.org/10.1130/G45038.1

Schmieder, M., & Kring, D. A. (2020). Earth's Impact Events Through Geologic Time: A List of Recommended Ages for Terrestrial Impact Structures and Deposits. *Astrobiology*, *20*(1), 91–141. https://doi.org/10.1089/ast.2019.2085

Schmitt, S. R. (2004). Ballistic Trajectory (2-D) Calculator-Computes the maximum height, range, time to impact, and impact velocity of a ballistic projectile. [online]. [Cited 14 November 2020]. Retrieved from: http://www.convertalot.com/ballistic_trajectory_calculator.html

Schnetzler, C. C. (1992). Mechanism of Muong Nong-type tektite formation and speculation on the source of Australasian tektites. *Meteoritics*, *27*(2), 154–165. https://doi.org/10.1111/j.1945-5100.1992.tb00743.x

Schnetzler, C. C., & McHone, J. F. (1996). Source of Australasian tektites: Investigating possible impact sites in Laos. *Meteoritics & Planetary Science*, *31*(1), 73–76. https://doi.org/10.1111/j.1945-5100.1996.tb02055.x

Schnetzler, C. C., & Pinson Jr, W. H. (1963). The chemical composition of tektites. In: O'Keefe, J. A. (1963) *Tektites* (p. 95–129). The University of Chicago Press.

Schultz, P. H. (1992). Atmospheric effects on ejecta emplacement and crater formation on Venus from Magellan. *Journal of Geophysical Research: Planets*, *97*(E10), 16183–16248. https://doi.org/10.1029/92JE01508

Schultz, P. H., Anderson, J. B. L., & Hermalyn, B. (2009, March 23–27). *Origin and Significance of Uprange Ray Patterns* [Abstract #2496]. Abstract submitted to the 40th Lunar and Planetary Science Conference, The Woodlands, Texas, United States of America. Retrieved from: https://www.lpi.usra.edu/meetings/lpsc2009/pdf/2496.pdf

Schultz, P. H., Eberhardy, C. A., Ernst, C. M., A'Hearn, M. F., Sunshine, J. M., & Lisse, C. M. (2007). The Deep Impact oblique impact cratering experiment. *Icarus*, *191*(2), 84–122. https://doi.org/10.1016/j.icarus.2007.06.031

Shaw, H. F., & Wasserburg, G. J. (1982). Age and provenance of the target materials for tektites and possible impactites as inferred from Sm-Nd and Rb--Sr systematics. *Earth and Planetary Science Letters*, *60*(2), 155–177. https://doi.org/10.1016/0012-821X(82)90001-2

Shuvalov, V., & Dypvik, H. (2013). Distribution of ejecta from small impact craters. *Meteoritics & Planetary Science*, *48*(6), 1034–1042. https://doi.org/10.1111/maps.12127

Sieh, K., Herrin, J., Jicha, B., Schonwalder Angel, D., Moore, J. D. P., Banerjee, P., … Charusiri, P. (2020). Australasian impact crater buried under the Bolaven volcanic field, Southern Laos. *Proceedings of the National Academy of Sciences*, *117*(3), 1346–1353. https://doi.org/10.1073/pnas.1904368116

Stöffler, D., Gault, D. E., Wedekind, J. E., & Polkowski G. (1975). Experimental hypervelocity impact into quartz sand: Distribution and shock metamorphism of ejecta. *Journal of Geophysical Research*, *80*(29), 4062-4077. https://doi.org/10.1029/JB080i029p04062

Stöffler, D., Hamann, C., & Metzler, K. (2018). Shock metamorphism of planetary silicate rocks and sediments: Proposal for an updated classification system. *Meteoritics & Planetary Science*, *53*(1), 5–49. https://doi.org/10.1111/maps.12912

Tada, T., Carling, P. A., Tada, R., Songtham, W., Chang, Y., & Tajika, E. (2019, December 9-13). *Constraint on the Location of the Australasian Tektite Impact Event based on the Distribution of the Ejecta Deposits across the Eastern Indochina* [Abstract #NH51C-0786; Poster #0786]. American Geophysical Union Fall Meeting, San Francisco, United States of America. Abstract retrieved from: https://ui.adsabs.harvard.edu/abs/2019AGUFMNH51C0786T/abstract

Trnka, M. (2020, March 16–20). *Notes on Contents of 10Be Isotope in Tektites and Microtektites of the Australasian Strewn Field* [Abstract #1149]. Abstract submitted to the 51st Lunar and Planetary Science Conference, The Woodlands, Texas, United States of America. Retrieved from: https://www.hou.usra.edu/meetings/lpsc2020/pdf/1149.pdf

Trnka, M., & Houzar, S. (2002). Moldavites: A review. *Bulletin of the Czech Geological Survey*, *77*(4), 283–302. Retrieved from: http://www.geology.cz/bulletin/fulltext/04trnkafinal.pdf

Vickery, A. M. (1993). The theory of jetting: Application to the origin of tektites. *Icarus*, *105*(2), 441–453. https://doi.org/10.1006/icar.1993.1140

Vickery, A. M., & Browning, L. (1991, July 21-26). *Water depletion in tektites*. Abstract submitted to the 78th Annual Meeting of the Meteoritical Society, Monterey, California, United States of America. In: *Meteoritics*, 26, 403. Retrieved from: http://adsabs.harvard.edu/full/1991Metic..26Q.403V

Wasson, J. T. (2003). Large Aerial Bursts: An Important Class of Terrestrial Accretionary Events.*Astrobiology*, *3*(1), 163–179. https://doi.org/10.1089/153110703321632499

Wasson, J. T. (2017, March 20–24). *A Thermal-Plume Origin of Layered and Splash-Form Tektites and Libyan Desert Glass* [Abstract #2916]. Abstract submitted to the 48th Lunar and Planetary Science Conference, The Woodlands, Texas, United States of America. Retrieved from: https://www.hou.usra.edu/meetings/lpsc2017/pdf/2916.pdf

Wei, G., Liu, Y., Ma, J., Xie, L., Chen, J., Deng, W., & Tang, S. (2012). Nd, Sr isotopes and elemental

geochemistry of surface sediments from the South China Sea: Implications for Provenance Tracing. *Marine Geology*, *319–322*, 21–34. https://doi.org/10.1016/j.margeo.2012.05.007

Whymark, A. (2013, March 18–22). *Review of the Australasian tektite source crater location and candidate structure in the Song Hong-Yinggehai basin, Gulf of Tonkin* [Abstract #1077]. Abstract submitted to the 44th Lunar and Planetary Science Conference, The Woodlands, Texas, United States of America. Retrieved from: https://www.lpi.usra.edu/meetings/lpsc2013/pdf/1077.pdf

Whymark, A. (2018, March 19-23). *Further Geophysical Data in the Search for the Australasian Tektite Source Crater Location in the Song Hong--Yinggehai Basin, Gulf of Tonkin* [Abstract #1078]. Abstract submitted to the 49th Lunar and Planetary Science Conference, The Woodlands, Texas, United States of America. Retrieved from: https://www.hou.usra.edu/meetings/lpsc2018/pdf/1078.pdf

Whymark, A. (2020, August 5–7). *Newly Discovered Muong Nong-Type Layered Impact Glass / Tektites from Paracale, Philippines and Implications for Source Crater Location* [Abstract #2006]. Abstract submitted to the 11th Planetary Crater Consortium Meeting, Hawaii (Virtual), United States of America. Retrieved from: https://www.hou.usra.edu/meetings/crater2020/pdf/2006.pdf

Yan, Y., Carter, A., Palk, C., Brichau, S., and Hu, X. (2011). Understanding sedimentation in the Song Hong-Yinggehai Basin, South China Sea: Sedimentation in the Yinggehai Basin. *Geochemistry, Geophysics, Geosystems, 12*(6), https://doi.org/10.1029/2011GC003533

Zähringer, J., & Gentner, W. (1963). Radiogenic and atmospheric argon content of tektites. *Nature, 199*(4893), 583–583. https://doi.org/10.1038/199583a0

Thai Geoscience Journal 2(2), 2021, p. 30-37

ISSN-2730-2695; DOI-10.14456/tgj.2021.3

The 'new normal' for geoscience in a post-COVID world: connecting informed people with the Earth

Steven M. Hill*, Jane P. Thorne, Rachel Przeslawski, Rebecca Mouthaan, and Chris Lewis

Geoscience Australia, Canberra, Australia.
**Corresponding author: Steve.Hill@ga.gov.au*
Received 17 March 2021; Accepted 17 June 2021.

Abstract

We consider how our society can use data, information and knowledge of the Earth under a broad definition of geoscience to better connect with the Earth system. This is important in our changing world, in particular how geoscience contributes to our response to the societal impacts of the COVID-19 pandemic. Ultimately, informed decisions utilizing the best geoscience data and information provide key parts of our economic, environmental and cultural recovery from the pandemic. The connection to country and more widely connection to our planet and the greater Earth system that comes from personal experience has been especially challenged in 2020. Much of Australia's population have been encouraged to stay in our homes, first because of major fires and more recently in response to isolation from the COVID-19 pandemic. Although domestic travel became increasingly allowable, international travel has been restricted for much longer. This has increased the importance of trusted data and information initially from domestic locations and for more extended time between countries that are now less accessible. We discuss ways that geoscience governs our discovery and use of minerals, energy and groundwater resources and builds resilience and adaptation to environmental and cultural change. A broad definition of geoscience also includes positioning and location data and information, such as through integrated digital mapping, satellite data and real-time precise positioning. Important here is sharing, with two-way exchange of data, information and knowledge about the Earth, through outreach in geoscience education programs and interactions with communities across Australia, into neighboring countries in Asia and the Pacific, and across the world. An aspiration is for geoscience to inform social license through evidence-based decisions, such as for land and marine access, for a strong economy, resilient society and sustainable environment. At Geoscience Australia, we have developed a ten years strategic plan (Strategy 2028) that guides us to be a trusted source of information on Australia's geology and geography for government, industry and community decision making. This will contribute to a safer, more prosperous and well-informed Australia and its connection to neighbouring countries, such as in Asia, as well as people that are better connected to country and our planet.

Keywords: community education and outreach, earth system science, environment, geoscience, mapping, resources

1. Introduction

The importance of trusted, high-quality and relevant science to inform and advise governments and our communities is greater now than it ever has been. This is particularly the case for geoscience and its role to guide people's connection to the Earth as the place where we live and obtain the resources we need to live our lives. Our community's recognition of the value of geoscience ensures the future viability and evolution of geoscience and it's ability to contribute to informed impact in our nations, and our planet. This recognition, however, is not to be presumed (or assumed). The world changes and as such the roles and perceptions of geoscience need to evolve and adapt for its continued resilience and relevance.

This paper has three main parts:

1. It considers how geoscientists project and define themselves in society and suggests

that a broad definition of geoscience within a greater Earth system has greater value than more narrow, specialized foundations;

2. Demonstrations of how Geoscience Australia strategically supports and develops its science as part of the broad context of geoscience within an Earth system for maximum impact and value; and,

3. Consideration of how this approach is being developed in response to the post-COVID demands of our society and their connection to our planet.

2. Geoscience in the Earth System

Traditionally in Australia there has been an emphasis on the links between geology, geologists and our resources industry, particularly for mineral commodities such as iron ore, gold and base metals, but also energy commodities such as coal, oil, gas, and uranium. This largely reflects the importance of this industry for export earnings and our nation's prosperity. This has meant that the projection of the role of the geologist has not been challenged so much in the past as it is today. Rather than the vision of mining to express progress and prosperity there is now a greater call for the industry to be viewed on the basis of more trusted equitable and ethical criteria and the sustainable public value of the industry for not only the economy but also the environment and community. This includes assessment and visibility of the entire resources chain from investment, exploration, mining, and the destiny (such as uses, recycling or reuse) of the resources. This broader perspective calls for a broader context of our science of the Earth that extends beyond just rocks and resources but into the broader field of geoscience.

Geoscience embodies the science of the Earth. It especially includes but extends beyond geology to also include fields of geography, geodesy, Earth observation, marine science, pedology, geophysics, geochemistry, geohazards, and many parts of climatology, ecology, hydrology, space and planetary science and, environmental science. Geoscience investigates the past, measures the present and models the future behavior of the planet. It links closely with the biological, chemical and physical sciences as part of Earth system science (Steffen et al., 2020), to include a holistic view on interactions and dynamic processes between ice, rocks, water, air and life.

3. Geoscience Australia: role and science

At Geoscience Australia we embrace the broad perspective of geoscience, not just in our name, but in the strategic planning of our role, activities and our science. Geoscience Australia is Australia's national public-sector geoscience entity. We provide advice on the geology and geography of Australia to support progress, growth, and investment towards a safer, more prosperous and well-informed Australia. Our main stakeholders include government, industry and the community.

Our decadal strategy, *Strategy 2028*, sets out the impacts our work will have over the next decade under six key areas:

1. Building Australia's resource wealth. Australia has a rich and diverse mineral and energy endowment, which is a major contributor to the nation's wealth, economically and socially. The provision of high quality regional--scale geoscience data and information lowers the risks of exploration, advanced exploration, mining and processing technologies;

2. Supporting Australia's community safety. Providing disaster risk information to help Australians understand the consequences of hazard events, which contributes to more resilient communities now and in the future;

3. Securing Australia's water resources. Supporting the fair sharing of water resources by identifying the location, quantity and quality of groundwater resources to support sustainable water management in the driest inhabited continent;

4. Managing Australia's marine jurisdictions. Including baseline mapping, understanding of marine resources and assets, and the ability to measure change over time;

5. Creating a location-enabled Australia. Providing information on when and where

events and activities occur is essential to make decisions and improve economic, environmental and social outcomes. This includes delivery of real-time precise positioning, digital location information and Earth observation from satellite data platforms; and,

6. Enabling an informed Australia. Delivering world-class, trusted data and platforms and expertise to support high-impact geoscience, transparent evidence-based decisions and social licence to operate. This includes our education and science outreach programs.

To achieve these strategic impacts we need to be the best people and organization that we can as well as ensure that we have a strong foundation of excellent and relevant science. The Geoscience Australia Science Principles describe how we conduct science in both long--term planning and day-to-day operations. The six Science Principles are:

1. Relevant science to ensure that Geoscience Australia provides quality assured information to the right people in the right timeframe so they can make evidence-based decisions, particularly related to the Australian Government. This includes the provision of scientific advice to meet national and international obligations (e.g. *Paris Climate Agreement*, *Australia New Zealand Foundational Spatial Data Framework and United Nations Integrated Geospatial Information Network, Offshore Petroleum and Greenhouse Gas Storage Act 2006, and the United Nations - Global Geodetic Reference Frame Sustainable Development Goals, and Sendai Framework for Disaster Risk Reduction).*

2. Collaborative science to allow Geoscience Australia to meet emerging challenges that are more complex than any single individual, team or agency can achieve. This requires us to engage with not only the broader research and data community, but also non-scientific stake-holders who are more likely to use and value our information if they are involved in our work.

3. Quality science to maximise stakeholder confidence that the data and information we provide is accurate, results are repeatable, and any uncertainties are explained and accounted for. All of these mean our science reflects not just quality, but integrity. Data and information can then be used to inform current decisions and debate, and be re-used and re-purposed long after it is created. As both a government agency and a member of the Australian research community, we have key compliance requirements, including the Australian Code for the Responsible Conduct of Research.

4. Transparent science to demonstrate that our scientific activities are unbiased and reflect commitment to extend the role that science plays in the transparency of Australian Government processes (e.g. Principles on Open Public Sector Information, Declaration of Open Government). By openly sharing our work and abiding by the FAIR data principles (findable, accessible, inter-operable, reusable) we create a platform that supports further innovation in the tradition of scientific discovery.

5. Communicated science to ensure that Geoscience Australia's scientific data and information is accessible to and understandable by a variety of stakeholders. By tailoring the communication of scientific information to a particular audience and purpose, Geoscience Australia's scientific work can be valued by stakeholders. This also means communicating appropriate background knowledge to stake-holders and the public to increase their capability to understand complex ideas often associated with scientific research. Part of communication here also involves active listening, particularly to ensure that stake-holder's matters of concern and their needs are well understood.

6. Sustained science capability to undertake scientific activities that meet current and future strategic priorities. The type and level of science capability we retain in-house is inherently controlled by strategic demands and available budget. It is also dependent on technical and business capabilities such as information management, outreach and education, engineering, and communication.

Three examples of major projects from Geoscience Australia's work program are briefly outlined as well as their impact and value for our nation. These include:

i) Positioning Australia;
ii) Digital Earth Australia (DEA); and,

iii) Exploring for the Future (EFTF).

i. Positioning Australia

The Positioning Australia Program is developing a world-leading satellite positioning capability, which many refer to as GPS (Global Positioning System). The program will provide accurate, reliable, and real-time positioning across Australia. It will enable increased productivity, new and innovative technologies, and accelerate economic growth, particularly for regional Australia and businesses.

The program encompasses the National Positioning Infrastructure Capability (NPIC) and a Satellite Based Augmentation System (or SBAS) and is underpinned by the Australian Geospatial Reference System. Currently, we can know our position on the Earth within 5-10 metres of accuracy. By upgrading our existing ground stations, we will improve our positioning accuracy to within 3-5 centimetres. We are doing this by building the physical and data infrastructure and analytics capabilities to deliver 3 things:

1. 10 cm accuracy of positioning across Australia and its maritime zones through SBAS;
2. 3-5 cm accuracy of positioning for areas with mobile phone coverage, in particular regional and metropolitan areas, through NPIC; and,
3. Open-source tools and software to support use of positioning, navigation and timing services.

This work is vital for the next wave of innovation, from location-based automation or artificial intelligence, to augmented reality. Positioning Australia is fundamental in supporting the transformational technologies that will benefit our economy.

To trial this, we established 27 SBAS projects across 10 industry sectors including agriculture, aviation, construction, consumer, resources, road, rail, maritime, mining and water utilities. Based on the SBAS trial across 10 industry sectors, we have estimated the economic value of our positioning program. An independent report, which investigated the benefits of SBAS, found that it would create A$6.2 billion of value over 30 years; over A$200 million p/a economic benefit initially, with plenty of upside across a range of sectors. The benefits included:

- Improving the efficient spraying of = water on farms (by between 1 and 7%) by being able to spray exactly where water is needed;
- Finding injured patients to facilitate helicopter rescues more effectively;
- Enabling intelligent transport systems, to reduce road fatalities;
- Improving safety at mine sites; and,
- Supporting virtual fencing to manage livestock better.

It is also important to note that we expect there will be uses that we have not thought of yet, enabling innovation and new businesses to start and flourish

ii. Digital Earth Australia (DEA)

In the DEA program, we are transforming satellite imagery into insights about changes in Australia's natural and built environments. DEA provides access to high quality satellite imaging of the Earth's surface, to detect physical changes across Australia in unprecedented detail, including soil and coastal erosion, crop growth, water quality, and changes to cities and regions over time. It gives farmers, land managers, industry, and governments the information they need to make better decisions about how they optimise the use of their resources.

DEA will benefit users that need accurate and timely information on the health and productivity of Australia's landscape. It will support government and industry to better monitor change, to protect and enhance Australia's natural resources and enable more effective policy responses to natural resource management problems. Information extracted from satellite images of the Earth will assist emergency managers in real time during disasters like bushfires and floods. It will assist in more productive farming and enable informed decision making across governments.

iii. Exploring for the Future (EFTF)

Through the EFTF program, we are building a prospectus of mineral, energy, and groundwater resources for Australia. The program launched in 2016, and the first four years of work has focused on northern Australia, using innovative techniques to map the surface and image deep into the Earth, developing a much better understanding of Australia's resource potential.

The first phase of the EFTF program set out to address the strategic need for more geoscience information in northern Australia. Some 21 projects have delivered over 250 new datasets and technical reports, covering more than 3 million square kilometres of the continent, and creating images of the Earth's crust and upper mantle, down to 200 kilometres depth, assisting in identifying the regional--scale systems that result in the creation of ore deposits, oil and gas fields and groundwater resources.

All of these data are freely available through our digital catalogue and world-leading data discovery portal. The portal includes innovative 3D visualisation and analytical tools that can create maps to support analysis and decision--making. The portal can be visited at **eftf.ga.gov.au.**

The EFTF program has changed perceptions and behaviours in the minerals and petroleum industries, with the program's pre-competitive data and information translating into real impacts. For example, since 2018, 17 companies have acquired new exploration acreage in the region in between Tennant Creek and Mount Isa covering more than 100,000 square kilometres. This uptake of exploration tenements and the investment that follows, can be linked back to Geoscience Australia's program activities and outputs. Importantly, this new interest is in 'greenfield' areas—locations that have only seen limited exploration in the past. Nearby, the program has also stimulated work program commitments valued at close to $100 m in the South Nicholson Basin, an emerging petroleum play on the Queensland Northern Territory border. An independent analysis of the EFTF program's projected economic impacts indicates that the return on the government's investment will be substantial. The report considered three projects representing $40 million of investment under the program. The returns from the potential discovery and development of new mineral and energy resources were estimated by ACIL Allen to range from $446 million under the most conservative modelling to more than $2.5 billion under the most optimistic modelling.

The first phase of the program created hundreds of jobs, through more than 300 contracts worth $69.4 million. This included the creation of 11 jobs for Indigenous Australian trainees in Alice Springs, processing geological samples with the Centre for Appropriate Technology—a not-for-profit Aboriginal and Torres Strait Islander company. Any investments in mining and agricultural operations will also create further opportunities for employment in regional Australia, supporting economic recovery in regions where opportunities may otherwise be limited. Large mines can directly employ thousands of people and indirect employment can be several times that. Importantly, this brings with it the opportunity for significant levels of employment for Indigenous Australians in regional areas. These benefits further demonstrate the importance of the resources sectors as "engines" of the Australian economy – engines that are needed more than ever in the economic recovery from the COVID-19 pandemic.

The outcomes and impacts from the first phase of EFTF have inspired the extension of EFTF for a second phase. In June 2020, this program received a $125 million extension and expansion over the next four years. The emphasis of this phase is to take the program national. While the work will be extended into southern Australia, two corridors that extend north-south across the continent will ensure continued focus on prospective regions in northern Australia. This is a fantastic opportunity to continue our use of innovative geoscientific techniques to expand the national coverage of key datasets and to take more detailed looks into new regions to encourage further greenfield exploration. Through encouraging investment, the program will contribute towards the nation's post COVID-19 economic recovery, creating jobs where they are needed

in regional and remote communities both now and into the future.

4. Geoscience in response to change following COVID-19

COVID Change and Challenge

The COVID-19 pandemic has brought obvious illness and death to our world, but it has also brought challenges for our industries and economies, employment, travel and most particularly it has challenged the mental health of people and communities. For many it has created a new experience of uncertainty and loss of control of their lives, and as such has been a reminder that our society and the world changes. We live in interesting times and probably the most inevitable feature of our time is "change". Key here is going to be how we are resilient, how we adapt, but most of all how we adopt changes as opportunities.

One challenge that we still have to adapt to is how we will maintain and grow our "connection" within our community of scientists and extend that into our society. Most particularly how we best live and connect to our country and the nation and planet in which we live. In Australia, domestic travel within states and territories has flourished (particularly for tourism), however, interstate travel has had the risk of uncertainty due to border closures, while international travel has been extremely limited. With busy lives and then lockdowns and border closures and other pressures, maintaining and growing our connection to country and planet will challenge us. This leaves us open to risks of mis-information about regions and nations that we are now have less physical connection.

Indigenous Science

We have much to learn from indigenous people and their connection to country but also their traditions of respect and passing on skill and knowledge related to country. How many in our increasingly urban society understand where they live in relation to geology, geography and landscape? Despite the amount of landscaping and concreting, asphalt and artificial lawn that we cover the ground with, we still live as part of an active and changing Earth system.

Indigenous science incorporates traditional knowledge and perspectives that have built on thousands of years of observation and experimentation, and then may be combined with more conventional scientific methods. Indigenous science is typically expressed as observations, know-how, practices, skills and innovations. Previously it has been recognised in applications for agriculture, land management, ecology and medicine, although emerging potential exists in geoscience applications.

With much of this work being implemented in regional and remote areas we are also building opportunities to partner with indigenous communities, encouraging indigenous participation by sourcing goods and resources directly through local communities. Our motivation is to develop and sustain respectful and meaningful relationships, build local indigenous capacity and contribute to local economic development for mutual benefit.

Our best people and science to meet the challenge

To meet the challenges of a changing world, our science is more important than it has ever been, especially because of the risk of mis-information and poor decisions about country and places that we are less connected with. Skill and knowledge will be important here but so too how we make our data and information accessible as well as ensuring that we provide "fit-for-purpose" and relevant data and information for making efficient and connected decisions about our country.

Education and communication of our science will be important here. Geoscience Australia maintains an active and engaging geoscience education and outreach program with visiting school groups but also an increasing amount of online teaching materials and delivery. In 2019 our education centre hosted visits from over 11,300 students and 1050 teachers, and although the centre was closed for on-site visits for much of 2020, our online delivery into schools reached out to

many more than this. We are also making our national collection of minerals and fossils more accessible via online "galleries" and associated information. One example of this is our online Google Arts and Culture exhibit of "Minerals in ModernTechnology" (https://artsandculture.google.com/story/RQXxTbNbs585MQ).

This also is reflected in the respectful way that we access land and marine areas to conduct our science, and as part of this, Geoscience Australia has recently established a Land and Marine Access team (LAMA) to lead us on a best practice approach in this area. It is increasingly important that this access is legally compliant but also prevents harm and includes timely and accountable record keeping, such as access agreements. A key component here is that access is purposeful, transparent, effective and inclusive. This means that all stakeholders interested in, or affected by field activities will be engaged using the most appropriate communication channels and language. Communication will be open and honest, seeking to build trust and credibility. Engagement will occur early in the planning process and will continue throughout the project life cycle, providing opportunities for stakeholders to ask questions, seek clarification and to contribute their own experiences and information. The field access cycle will be closed by all data obtained by field activities being delivered back to those communities that have been impacted by data acquisition.

Whilst communication and education are important pursuits we also need to bring our best ears and actively listen to the community and their matters of concern that we are trying to engage with (e.g. Stewart & Lewis, 2017). We must continue to nurture an inclusive culture in our geoscience community, to ensure that all of us feel we can belong, that we are valued for who we are as well as our knowledge, skills and experience. This includes providing equal opportunities to participate, contribute and progress. To maximise our opportunities for success we need to tap into the full breadth and diversity of expertise, people and talent that we possess across our geoscience community and our science partners. This not only makes us better people and provides a better place to work but also improves scientific outcomes and innovations, such as through contributions from our cognitive diversity and the novel questions, new discoveries, and greater networks and connections that come from that (Medin & Lee et al., 2012; Dutt, 2019; Handley et al., 2020; Hanson, Woden, & Lerback, 2020).

5. Conclusions

We hope that it has given you some new insights and perspectives on how a definition of ourselves as ***geoscientists*** within the context of a broader Earth system can bring higher impact and value to our nation, neighboring countries, such as in Asia, and across the world. Let's bring our best and most connected person to achieve better geoscience!

Acknowledgements

This paper has been published with permission of the Chief Executive Officer of Geoscience Australia. The authors acknowledge the insights and benefits from discussions with other staff at Geoscience Australia. We also thank the organizers of the CCOP Thematic Session (56th CCOP Annual Session) for providing the opportunity to present this orally and now as a written manuscript. Feedback and discussion with delegates of CCOP conference following the oral presentation have also been valuable and inspirational.

We acknowledge the owners and communities, including aboriginal communities whose land and sea country that we have worked on to conduct our geoscience. Our collaboration with Australia's state and territory governments have also been important for enabling our geoscience to have its value, impact and connection.

References

Dutt, K. (2019). Race and racism in geosciences. *Nature Geoscience*, *13*, 2-3. https://doi.org/10.1038/s41561-019-0519-z

Handley, H.K., Hillman, J., Finch, M., Ubide, T., Kachovich, S., McLaren, S, Petts, A., Purandare, J., Foote, A. & Tiddy, C. (2020). In Australasia, gender is still on the agenda in geosciences. *Advances in Geoscience*, *53*, 205-226. https://doi.org/10.5194/adgeo-53-205-2020

Hanson, B., Woden, P. & Lerback, J. (2020). Age, gender and international author networks in the Earth and space sciences: implications for addressing implicit bias. *Earth and Space Science, 7(5).* https://doi.org/10.1029/2019EA000930

Medin, D.L. & Lee, C.D. (2012, April). Diversity makes better science. *Association for Psychological Science Observer, 25(5).* Retrieved from https://www.psycho-logicalscience.org/observer/diversity-makes-better-science

Steffen, W., Richardson, K., Rockstrom, J., Schellnhuber, H.J., Dube, O.P., Dutreuil, S., Lenton, T.M. & Lubchenco, J. (2020). The emergence and evolution of Earth System Science. *Nature Reviews Earth & Environment, 1*, 54-63. https://doi.org/10.1038/s43017-019-0005-6

Stewart, I.S. & Lewis, D. (2017). Communicating contested geoscience to the public: moving from 'matters of fact' to 'matters of concern', *Earth-Science Reviews, 174*, 122-133. https://doi.org/10.1016/j.earscirev.2017.09.003

Thai Geoscience Journal 2(2), 2021, p. 38-42

ISSN-2730-2695; DOI-10.14456/tgj.2021.4

3D geological mapping of central Tokyo

Susumu Nonogaki* and Tsutomu Nakazawa
Geological Survey of Japan, AIST, Tsukuba, Japan
*Corresponding author: s-nonogaki@aist.go.jp
Received 17 March 2021; Accepted 29 June 2021.

Abstract

The Geological Survey of Japan (GSJ) carried out 3D geological mapping of central Tokyo. In this project, we performed surface-based geological modeling using borehole logs created by GSJ and also those provided by local governments as well as the development of the Web system for sharing 3D geoinformation. The 3D geological map of central Tokyo will be released on the "Urban Geological Map" website in a year. In this paper, we describe the current progress of this project.

Keywords: borehole logs, geotechnical properties, Tokyo, voxel model, 3D geological map.

1. Introduction

Recently there is growing demand for subsurface information to contribute to the evaluation of geological risk, such as liquefaction and amplification of ground motion, in urban areas in Japan due to frequent disasters caused by large-scale earthquakes. To meet this demand, GSJ has carried out a 3D geological mapping project since 2013. In the project, we create 3D geo-information based on detailed stratigraphic studies and on computer modeling of subsurface geological structures and make it open to the public on the Internet. To date, we have created a 3D geological map of the northern Chiba area, eastern part of Tokyo metropolitan area (Naya et al., 2018), and released it on the "Urban Geological Map" website (https://gbank.gsj.jp/urbangeol/index_en.html). As the next stage of this work, we are carrying out 3D geological mapping of central Tokyo, cooperating with the Civil Engineering & Training Center (CETC) of the Tokyo Metropolitan Government. In this paper, we describe an outline of the 3D geological mapping method and summarize the current progress of the work.

2. Methodology

The study area comprises the special wards of Tokyo, Japan (Fig. 1). This area geologically consists of three parts: upland with Pleistocene deposits, lowland with Holocene deposits, and reclaimed land along the coast. In this area, there are more than 60,000 borehole logs created for public construction works. The borehole logs are accumulated as XML files by CETC. Most of them have simple lithofacies descriptions and Standard Penetration Test results (SPT *N*--values). In our project, we utilize these borehole logs to assess the subsurface geology.

Fig. 2 shows a flow diagram of the 3D geological mapping. In the mapping, we perform (1) establishment of a standard stratigraphic framework, (2) stratal correlation using borehole logs, (3) surface-based geological modeling, and (4) release of the map on the Internet. The details of each process are described below.

2.1 Establishment of standard stratigraphic framework

A standard stratigraphic framework beneath central Tokyo is established based on high--quality stratigraphic data obtained from drilling surveys and laboratory work by GSJ. The stratigraphic data includes detailed core descriptions such as sedimentary facies, tephra marker layers, and fossils, ^{14}C age measurement, and PS velocity and density logging.

2.2 Stratal correlation using borehole logs

Stratal correlation between borehole logs obtained from past construction work is carried out by adopting the standard stratigraphic frame work. In order to increase the efficiency of the stratal correlation process, voxel models of geotechnical properties, such as lithofacies and SPT *N*-values, are constructed from a large number of borehole logs based on Nonogaki et al. (2020) and are used

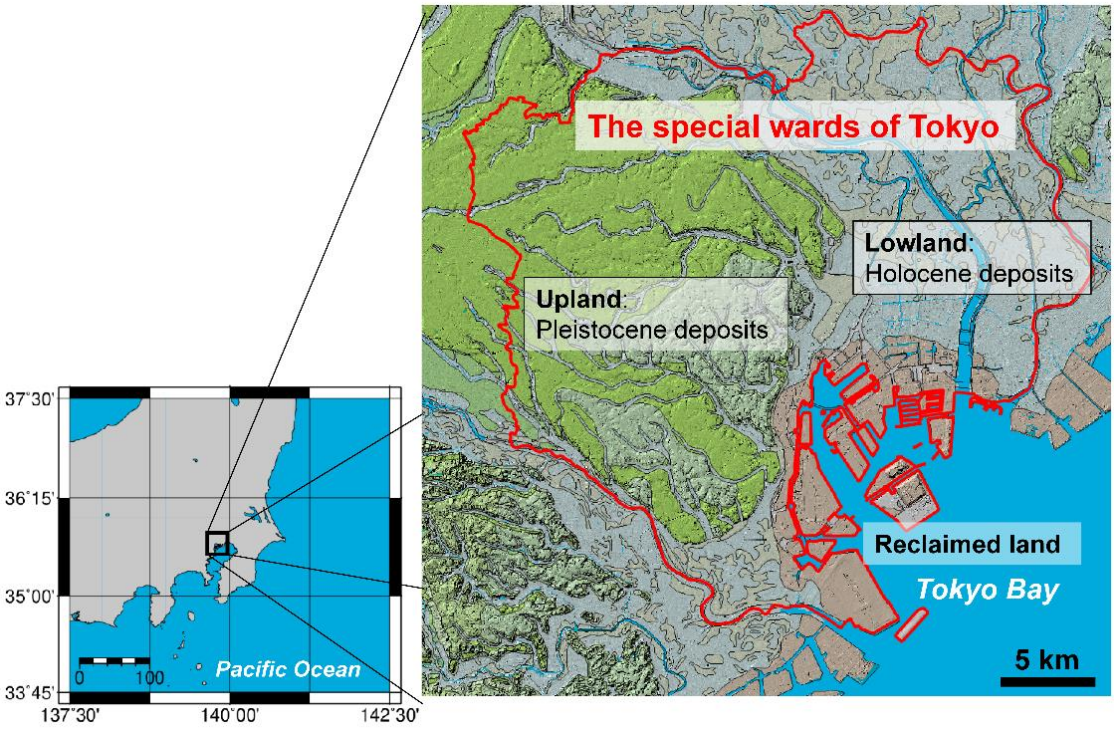

Fig. 1: Study area. Solid red lines indicate the special wards of Tokyo, Japan. Base map is based on the Fundamental Geospatial Data (DEM 5-m-mesh Elevation) (Geospatial Information Authority of Japan, 2019) and the Seamless Digital Geological Map of Japan 1:200,000 (Geological Survey of Japan, AIST, 2020).

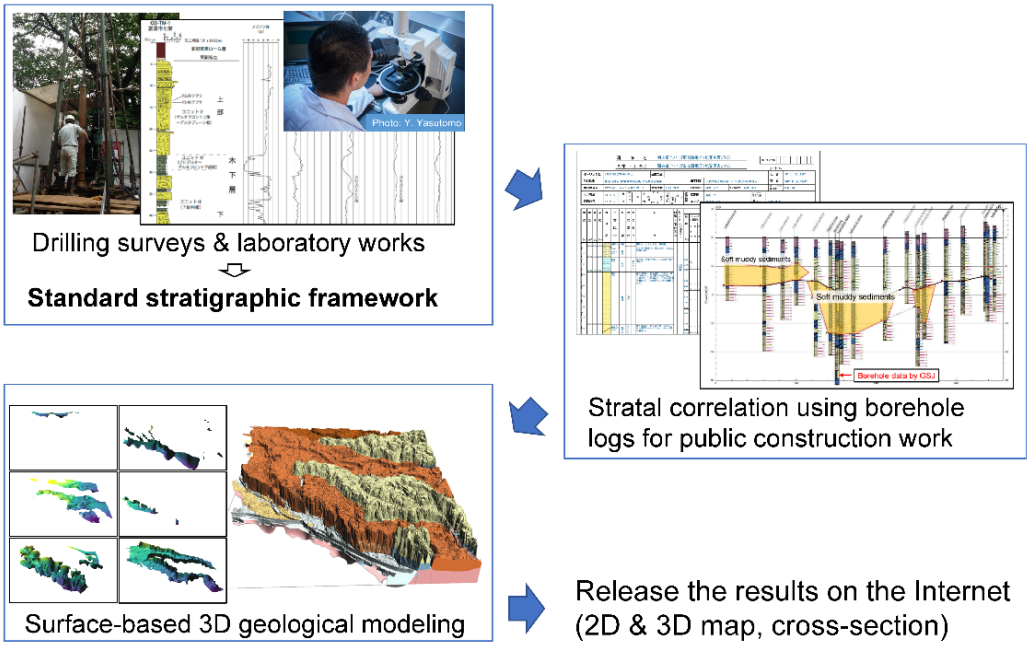

Fig. 2: Flow diagram of 3D geological mapping.

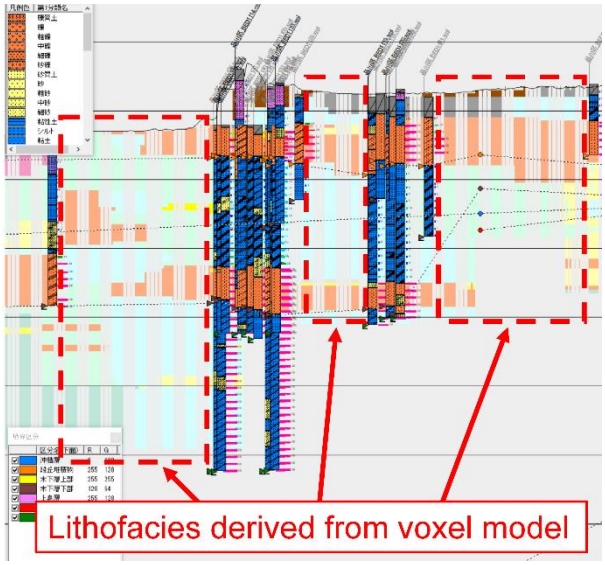

Fig. 3: Example of stratal correlation with voxel model of geotechnical properties. Lithofacies derived from voxel model is displayed in broken red line frames.

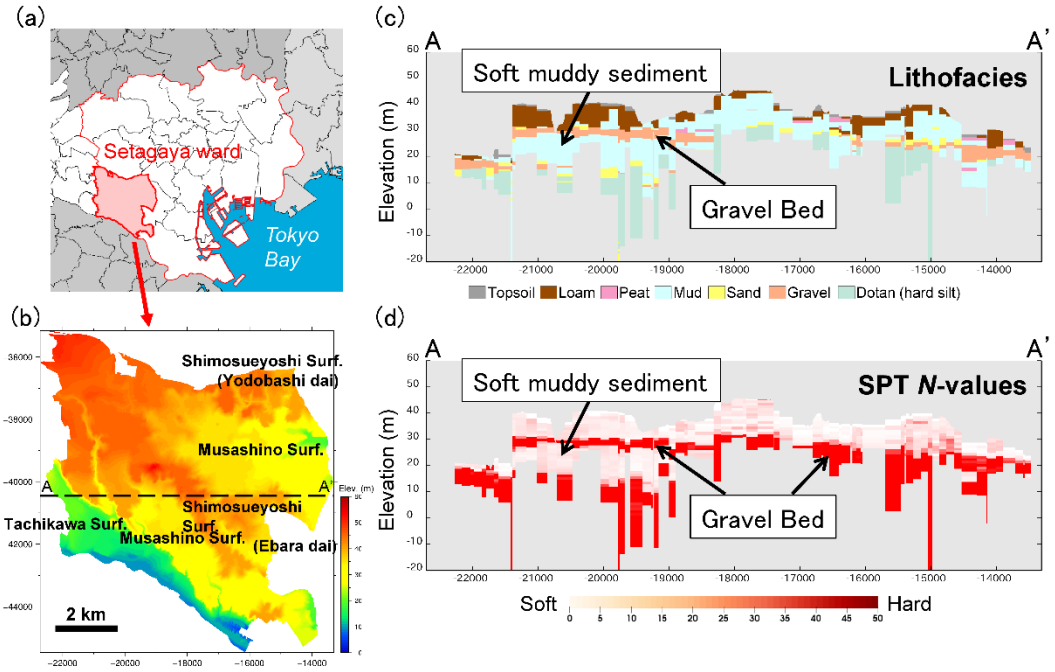

Fig. 4: Example of vertical cross-section images of geotechnical properties in the upland area. (a) index map showing Setagaya wards, Tokyo, (b) topographical map, (c) cross-section image of voxel model of lithofacies, and (d) cross-section image of voxel model of SPT N-values. (a) was based on the National Land Numerical Information (administrative boundary) (Geospatial Information Authority of Japan, 2020). (b) was based on the Fundamental Geospatial Data (DEM 5-m-mesh Elevation) (Geospatial Information Authority of Japan, 2019).

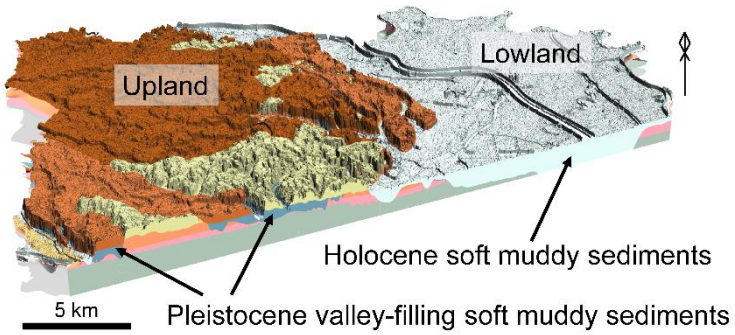

Fig. 5: Provisional 3D geological model of central Tokyo.

as auxiliary data for the data for the correlation process (Fig. 3).

2.3 Surface-based geological modeling

The Digital Elevation Models (DEMs) of the geological boundary surfaces are generated by the spline fitting method (Nonogaki, Masumoto & Shiono, 2012) using the results of stratal correlation. Additionally, based on Shiono, Masumoto & Sakamoto (1998), a surface-based 3D geological model is constructed by combining the DEMs with a consideration of the geological history.

2.4 Release on the Internet

The 3D geological model is available to the public on the "Urban Geological Map" website. On the website, the user can browse 2D and 3D geological map and borehole logs used for mapping as well as being able to create geological cross-sections along arbitrary lines.

3. Current progress

We constructed voxel models of lithofacies and SPT *N*-values to a depth of several tens of meters in the study area and finished stratal correlation of about 50,000 borehole logs. Moreover, we generated the DEMs of nine geological boundary surfaces using the result of stratal correlation and constructed a provisional 3D geological model of central Tokyo comprised of ten geological layers. The spatial resolution (grid size) of each DEM is five meters. Fig. 4 shows the vertical cross-sections of the voxel models in Setagaya ward. The cross-sections reveal that soft muddy sediments, which have high risk of amplifying earthquake ground motion, underlay hard gravel bed in the upland area. Fig. 5 shows aprovisional 3D geological model of central Tokyo. The geological model also clearly shows the distribution pattern of some geological layers which have a risk of natural disasters.

4. Conclusions

The 3D geological map of central Tokyo is expected to contribute to increasing the accuracy of geological risk evaluation. Furthermore, it is also helpful for planning urban infrastructure, analyses of groundwater flow, and for the real estate business. The 3D geological map of central Tokyo will be released in 2021.

References

Geological Survey of Japan, AIST (2020). Seamless Digital Geological Map of Japan 1:200,000, January 2020 version [online] (in Japanese). [Cited 20 January 2021]. https://gbank.gsj.jp/seamless/.

Geospatial Information Authority of Japan (2019). Fundamental Geospatial Data (DEM 5-m-mesh Elevation), July 2019 version [online] (in Japanese). [Cited 20 January 2021]. https://fgd.gsi.go.jp/download/menu.php.

Geospatial Information Authority of Japan (2020). National Land Numerical Information (Administrative boundary), October 2020 version [online] (in Japanese). [Cited 20 January 2021]. https://nlftp.mlit.go.jp/ksj/.

Naya T., Nonogaki S., Komatsubara J., Miyachi Y., Nakazawa T., Kazaoka O., … Nakazato H. (2018). *Explanatory text of the Urban Geological Map of the northern area of Chiba Prefecture*, 55p. Tsukuba, Japan: Geological Survey of Japan, AIST (in Japanese with English abstract).

Nonogaki S., Masumoto S., & Shiono K. (2012). Gridding of geological surfaces based on equality--inequality constraints from elevation data and trend

data. *International Journal of Geoinformatics, 8*, 49-–60.

Nonogaki S., Masumoto S., Nemoto T., Nakazawa T., & Nakayama T. (2020). Voxel modeling of lithofacies using Voronoi diagram based on locations of a large number of borehole data. *Geoinformatics*, *31*, 3–10 (in Japanese with English abstract). doi: 10.6010/ geoinformatics.31.1_3

Shiono K., Masumoto S., & Sakamoto M. (1998). Characterization of 3D distribution of sedimentary layers and geomapping algorithm—Logical model of geologic structure. *Geoinformatics*, *9*, 121–134 (in Japanese with English abstract). doi: 10.6010/geo informatics1990.9.3_121

Thai Geoscience Journal 2(2), 2021, p. 43-60

ISSN-2730-2695; DOI-10.14456/tgj.2021.5

REE and Th potential from placer deposits: a reconnaissance study of monazite and xenotime from Jerai pluton, Kedah, Malaysia

Fakhruddin Afif Fauzi[1*], Arda Anasha Jamil[2], Abdul Hadi Abdul Rahman[3], Mahat Hj. Sibon[3], Mohamad Sari Hasan[4], Muhammad Falah Zahri[5], Hamdan Ariffin[1], Abdullah Sulaiman[1]

[1]*Department of Mineral and Geoscience Kedah / Perlis / Pulau Pinang, Alor Setar, Malaysia*
[2]*Department of Mineral and Geoscience Johor, Johor Bahru, Malaysia*
[3]*Department of Mineral and Geoscience Selangor / W.P., Shah Alam, Malaysia*
[4]*Department of Mineral and Geoscience Pahang, Kuantan, Malaysia*
[5]*Technical Service Division, Department of Mineral and Geoscience, Ipoh, Malaysia*
*Corresponding author: afif@jmg.gov.my
Received 17 March 2021; Accepted 29 June 2021.

Abstract

Thorium (Th), rare earth elements (REE), yttrium (Y) and scandium (Sc) are among crucial elements in minerals that have a very high worldwide demand for green energy generation and high technology manufacturing industries. The current principal ore minerals for these elements are monazite, bastnäsite and xenotime. A reconnaissance study on monazite and xenotime minerals was conducted in southern part of Jerai peak area, which consists of mostly pegmatites and granite bedrocks and alluvial plains. Heavy mineral concentrate samples were obtained from various origins including gravelly layer from stream banks, flowing stream beds and seasonal stream beds for recent fluvial environment. Samples were also taken from weathered bedrocks of pegmatites and granites and different subsurface profiles from 12 pits dug in the alluvial plain area. Monazite and xenotime contents from stream bed samples are higher (8.43% and 6.05%) compared to other origins in recent fluvial environment and higher in weathered pegmatites (13.70% and 1.45%) compared to weathered granites. The monazite and xenotime content are also higher in eastern side of the alluvial plain, up to 3.16% and 2.91% respectively, but lower than samples from recent fluvial environment. The Th, REE and Y contents are very high up to 1,530 ppm, 21,031 ppm and 7,604 ppm respectively in samples containing monazite and/or xenotime. The Sc content, however, is very low which is up to 87.8 ppm in all samples although it shows positive correlation with monazite and/or xenotime contents. Both REE containing minerals could be economically potential if mined as placer suites together with garnet, tourmaline and other industrially beneficial minerals.

Keywords: Jerai, Kedah, monazite, REE, thorium, xenotime

1. Introduction

1.1 Background

The importance of rare earth elements (REE), thorium (Th), yttrium (Y) and scandium (Sc) has become worldwide emergence in electronics and high technology industries. REE, Y and Sc are crucial for production of magnets in computer drives and defence applications, metal alloys including batteries and superalloys, phosphors such as LED and optical sensors, additive in ceramics and glass polishing and also used as catalyst in various chemical processes (Jha, 2014). Th, as ThO_2 is well-known for better energy generating purpose than uranium (U) as the former does not easily oxidized and resistant to ionic radiation (IAEA, 2005).

REE is defined as a set of 17 chemical elements in the periodic table, comprising 15 lanthanides which are cerium (Ce), dysprosium (Dy), erbium (Er), europium (Eu), gadolinium (Gd), holmium (Ho), lanthanum (La), lutetium (Lu), neodymium (Nd), praseodymium (Pr), promethium (Pm), samarium (Sm), terbium (Tb), thulium (Tm) and ytterbium (Yb), as well as yttrium (Y) and scandium (Sc) (Connelly and Damhus, 2005).

The history of REE dated back in 1788 when Johan Gadolin discovered a rare pitch--black rock in Ytterby, Sweden. The rock

samples were taken across European countries where their scientists competed to distinguish elements that exist as well as to complete the Lanthanide Series of Periodic Table of Elements. In fact, the names of yttrium, erbium, terbium and ytterbium derived from the origin of the sample. Th, on the other hand, was discovered by Jöns Jacob Berzelius, a Swedish scientist in 1828.

Placers are defined as mineral deposits formed by the mechanical concentration of minerals from weathered debris, such as beaches and streams, by which the economic mineral deposits have high density but are very resistant to chemical and physical breakdown (Sengupta and Van Gosen, 2016). Among these minerals are monazite, xenotime, bastnäsite and loparite which are considered as the most important placer rare earth minerals (REM) in the world (Zhou et al., 2017). The former 2 minerals are common by-products of alluvial tin mining in Malay Peninsular since early 1900s (Willbourn, 1925). The placer REM are practically mined together with other minerals including garnet, zircon, cassiterite, and Ti-bearing minerals like rutile and ilmenite as mineral suite or co-products before separation processes (Sengupta and Van Gosen, 2016).

Placer REM currently represent the third most important global REE source of production after Bayan Obo carbonate rocks in inner Mongolia and Mountain Pass carbonatites in California, which come from the monazite and xenotime dispersed in Neogene to Quaternary beach sand in Australia (McLennan and Taylor, 2012). In comparison, current and previous productive placer deposits contain 6% to 7% of heavy minerals including REM as reported in Eneabba district, Australia and Xun Jiang district, China (Shepherd, 1990; Jackson and Christiansen, 1993).

In 1980s, the xenotime-bearing alluvial placer deposits in Malaysia were once the largest source of Y in the world (Castor and Hendrick, 2006). JMG (2019) stated that the production of both monazite and xenotime in Malaysia increased from 25 tonnes in 2009 to 1,654 tonnes in 2018, which were obtained from alluvial tailings in Ipoh, Perak. USGS (2019) estimated that Malaysia has 30,000 tonnes of rare earth oxides (REO) in 2018.

Monazite is a phosphate mineral consisting REE (Ce, La, Nd), Th and U. Monazite is a common accessory mineral in peraluminous granites, syenitic and granitic pegmatites, quartz veins and carbonatites but lesser in charnockites, migmatites and paragneisses (Rapp and Watson, 1986). In peraluminous granites, monazite constitutes a major host of LREE, excluding Eu, Th and U, with minor amount of Y and HREE (Hinton and Paterson, 1994; Bea et al., 1994; Bea, 1996). The monazite stability in silicate melts depends on SiO_2, CaO and P_2O_5, including oxygen fugacity, peraluminous content and content ratios of lanthanides and actinides (Cuney and Friedrich, 1987; Casilas et al., 1995). Felsic differentiation towards granite plutons strongly depletes LREE and Th due to monazite fractionation (Ward et al., 1992; Wark and Miller, 1993; Zhao and Cooper, 1993). According to Che Zainol Bahri et al. (2018), the Th content in Malaysian monazite ranges between 2,525 ppm to 40,868 ppm while Willbourn (1925) mentioned that the mineral contains 3.5% to 8.38% of ThO_2. *Atomic Energy Licencing Act 1984* stated that if radionuclide of Naturally Occurring Radioactive Materials (NORM) of Th-232 exceeds 1 Bq/g, it is considered as radioactive. 1 Bq/g of Th-232 is equivalent to 246 ppm, assuming the chain is in equilibrium.

Xenotime is also a phosphate mineral but abundant particularly in Ca-poor peraluminous granites, which accounts for huge fraction of Y and HREE contents and variable portion of substituted U (Wark and Miller, 1993; Bea, 1996). In xenotime-bearing peraluminous granites, the Y and HREE fractions contained in xenotime vary from 30% to 50%, that is closely related to xenotime-apatite-zircon concomitance during plutonic facies differentiation (Bea, 1996; Wark and Miller, 1993; Förster and Tischendorf, 1994). Xenotime also contains minor amounts of Th and LREE, particularly Nd and Sm (Förster, 1998b).

Hence, this conducted study is to determine the potential of Th and REE based on monazite and xenotime distributions in placer environments within Jerai Pluton area.

1.2 Previous studies

Studies on the occurrences of monazite and xenotime in Malaysia were commenced as parts of regional mapping and regional geochemical surveys by Geological Survey of Malaysia since 1925, continued by Department of Mineral and Geoscience Malaysia (JMG) from 2000 until present.

The Malaysian monazite generally has moderately well-rounded discrete or as some parts with colour varies from clear, deep canary yellow through cream coloured with resinous lustre due to progressive oxidation of REE (Flinter et al., 1963; Wan Hassan, 1989). The Jerai monazite, however, has unusual elongated rolled grains of flattened form with deep green colour (Wan Hassan, 1989; Flinter et al., 1963). Wan Hassan (1989) distinguished the xenotime crystal habit to have squat tetragonal bipyramid in Malaysian Tin Belt and prism with double pyramidal terminations in Malaysian Eastern Belt.

Studies on radioactive minerals on Malaysian Central Belt then were conducted in 1993 to 1995 (Mohd Hasan et al. 1993, 1995; Zakaria et al. 1994). Academy of Sciences Malaysia (ASM) later initiated a study on REE associated with ion adsorption clay in 2013 (ASM, 2014).

In 2018, JMG conducted a reconnaissance study on REE, Th and Sc potentials in Malaysia. The preliminary study comprised their potential in clayey horizons in weathered granites and placer deposits, including Jerai Pluton (Abdul Rahman et al. 2018a, b). Hence, this paper is aimed to deliver the outcomes of the study commenced in the pluton area.

1.3 Study area

The study area is situated at the south of Mount Jerai, west of Kedah state with a total of 40 km2. The area is mostly covered with paddy fields with freshwater for drainage sourced from streams flowing from the peak. The study area lies in the National Jerai Geopark (Fig.1).

2. Geological Setting

2.1 Regional geology

The Jerai Pluton lies within the western tin granites of Peninsular which is part of the Southeast Asian Magmatic Arc that was triggered during Late Permian to Triassic subduction-collision event due to the closure of Palaeo-Tethyan Ocean beneath the Southeast Asian crust (Robb, 2019) (Fig.1).

The tin granites of western Peninsular Malaysia have been considered as products of partial melting of the metamorphic basement during the collision of Sibumasu and East Malaya blocks (Liu et al., 2020; Ng et al., 2015), based on their ilmenite-series, peraluminous character (Ishihara et al., 1979), and characteristic of S-type granites (Chappell and White, 2001). More recently, the genetic link between the tin mineralization and the granites has been constrained, by which the age of tin ores and their granitic hosted rocks in the western Peninsular Malaysia is within the range of the 230 to 210 Ma (Yang et al., 2020).

2.2 Local geology

The study area consists of granitic bedrock, metasedimentary bedrocks and unconsolidated deposits.

The granitic bedrock covered the northern part of the study area. It is from the Jerai Pluton that intruded during Late Triassic and shaped the mountain (Fig.1). Jamil et al. (2006) divided the pluton into 3 facies according to mineralogical criteria, which are biotite – muscovite granite, tourmaline granite and pegmatite. The pegmatite facies which occurred as veins ranging from few centimetres to several meters, are the primary source of tin associated with Nb-Ta (Bradford, 1972). Khoo (1977) proposed that the pegmatites also occurred as sync-plutonic dykes that filled the ductile cracks in granites during intrusion. Apart of tourmalines, garnets, particularly pinkish variety, are the common accessory minerals in Jerai Granite found in this study.

The metasedimentary facies within the study area are quartzites and schists from Cambrian Jerai Formation. Both facies are mineralized with magnetite and/or hematite (Bean and Hill, 1969; Bradford, 1972) and regarded as source of iron ores since 535 B.C. (Mokhtar and Saidin, 2018).

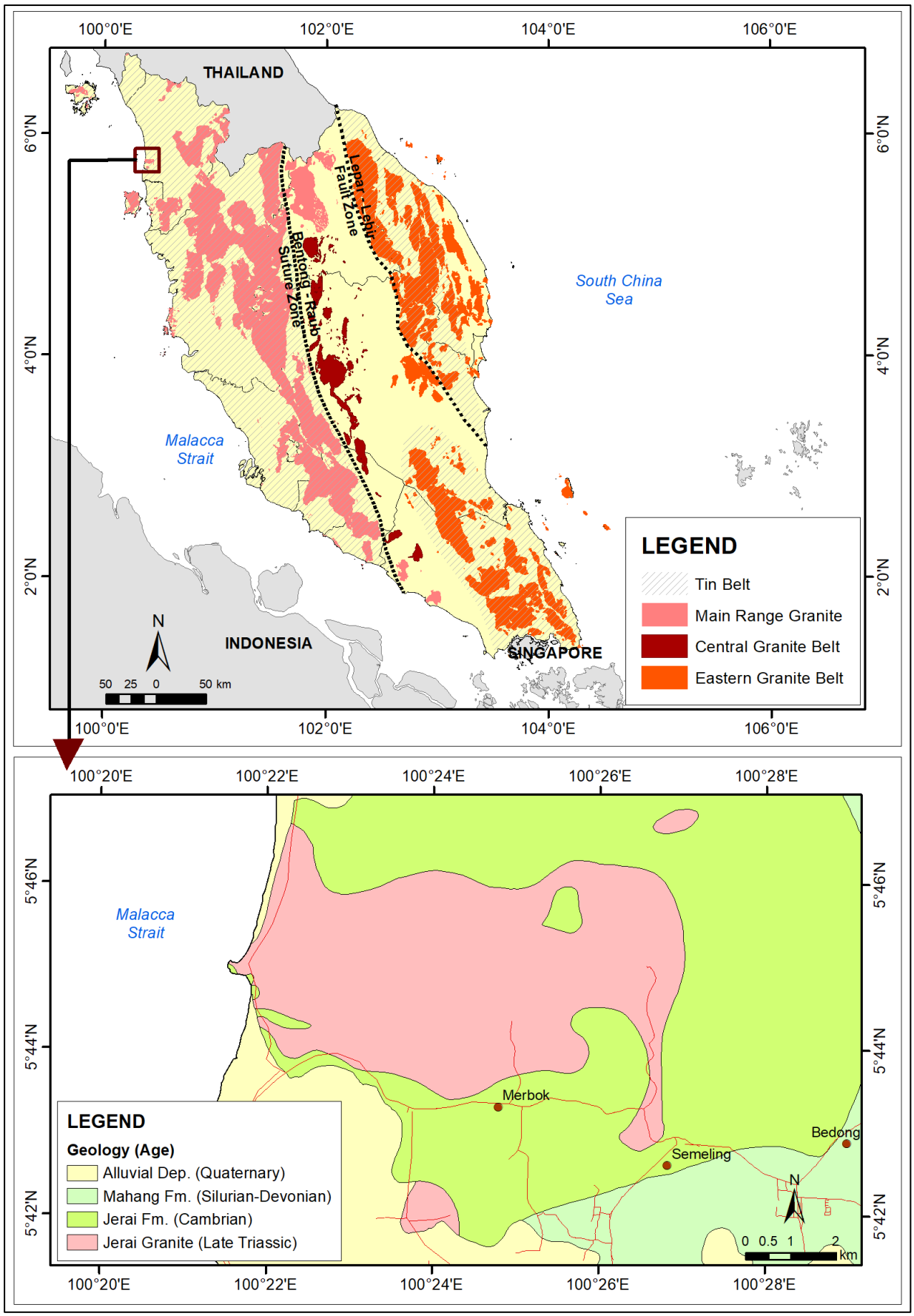

Fig. 1: Maps showing the Granite Belts and tin belts in Peninsular Malaysia (above, after Hosking, 1973) and the general geology of study area (below, after JMG, 2014).

The unconsolidated deposits cover the southern part of the study area. They mostly consist of clay, mud and silt originated from marine influence during Quaternary period (JMG, 2014).

3. Materials and Methodology

Heavy concentrate samples were collected from current and seasonal stream beds, stream banks and gravelly layers on stream banks; weathered granites and pegmatites (Figs. 1, 2, 3, 4 & 5) and distinguishable layers from dug pits with depth between 3.2 metres up to 4.0 metres (Figs. 6 & 7) All sampling locations are shown in Fig. 8.

The samples were obtained through panning using 5 litre sized wooden pan. All samples then underwent removal of light minerals (i.e. SG ≤ 2.85) including quartz using Bromoform solution before thoroughly rinsed with spirit methyl, followed by distilled water. Once dried, the samples were weighted and magnetically separated using hand magnet and Frantz Isodynamic Magnetic Separator Model L-1 into 4 different magnetism; 0.4 Ampere, 0.7 Ampere, 1.0 Ampere and non-magnetic.

Samples of different magnetism were then taken for quantitative mineral estimation (QME) analysis under stereo microscope aided by mineral lists according to magnetism (Table 1) and descriptions by Wan Hassan (1989) and Devismes (1978).

Selected concentrate samples were analysed through LA-ICP-MS method in Laboratory Branch, JMG Technical Service Division in order to determine their REE, Th, Y and Sc contents. The U content is also analysed for all selected samples. Apart from individual content, the REE results are also calculated according to total light REE (TLREE), total heavy REE (THREE) and total REE (TREE).

4. Results

A total of 43 samples including 3 samples from weathered bedrocks and 28 samples from pits were successfully obtained in this study.

4.1 QME analysis

The monazite content in samples from recent fluvial environment (Table 2) is from none to 8.43% and the xenotime content in samples from the same environment is from none to 6.05%. Sample KC56 which originated from stream bed contains the most monazite and xenotime. Samples KC41 and KC59 also contain monazite more than 4% and sample KC41 has xenotime content more than 4%. Garnet, particularly pinkish variety is common in all samples while allanite and zircon exist in few samples. Other minerals identified include mostly magnetite, hematite and tourmaline (Figs. 9 & 10). The average content of monazite and xenotime in recent fluvial environment samples is 5.14% and 2.82% respectively, with an average sum of 7.96%.

While for weathered bedrock samples, the highest monazite and xenotime content is in pegmatite, which is 13.70% and 1.45% respectively, compared to weathered granite.

In general, sandy layers in pits have considerably greater amount of heavy concentrate minerals compared to silty and clayey layers. The monazite and xenotime content in samples from pits (Table 3) is ranging from none to 3.16% and none to 2.91%, respectively. The highest content of both monazite and xenotime originated from pit C but in different layers, by which the deeper layer (KCC003) has higher content of monazite 3.16% while shallower layer (KCC001) has greater content of xenotime (3.91%). Similar to samples from recent fluvial environments, pinkish garnet is also common in all samples while allanite and zircon appear in few samples. Other minerals identified are magnetite, hematite, tourmaline and ilmenite. No mineral concentrates exist from upper layer of pit I (KIC001) and pit K as these pits mainly consist of greyish mud – clay with organic materials. The average content of monazite and xenotime in Quaternary deposit environment samples is only 1.66% and 1.10% respectively, with an average sum of 2.76%.

4.2 LA-ICP-MS analysis

A total of 10 concentrate samples from recent fluvial environment were analysed by LA-ICP-MS (Table 4). The Th content of the

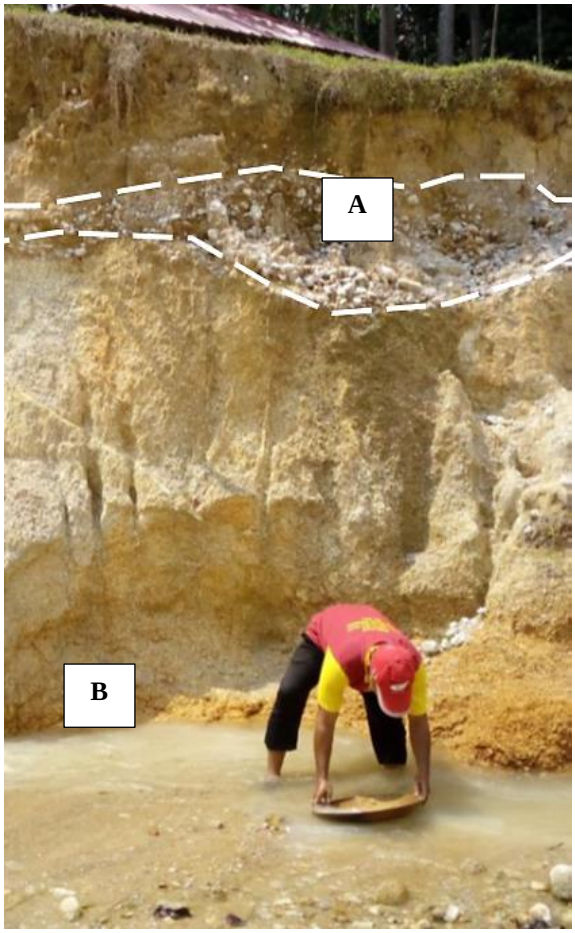

Fig. 2: Origins of the samples in recent fluvial environment include gravelly layer (A) and stream bed (B).

Fig. 3: The occurrence of eluvial bed near S. Batu Pahat.

Fig. 4: Sampling of weathered bedrock.

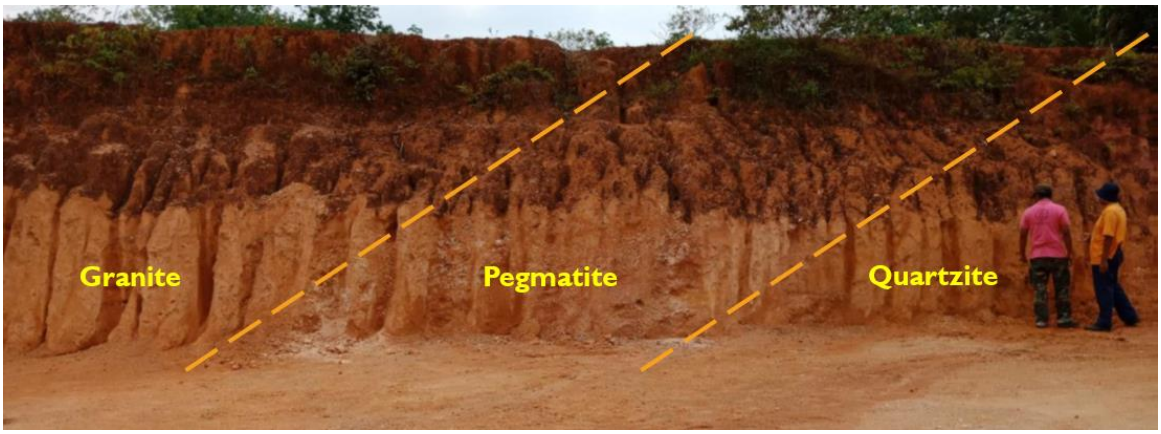

Fig. 5: Outcrops of weathered granite and pegmatite bedrocks from Jerai Pluton in contact with quartzite of Jerai Formation.

Fig. 6: Pit is dug using JCB excavator.

Fig. 7: One of the dug pits.

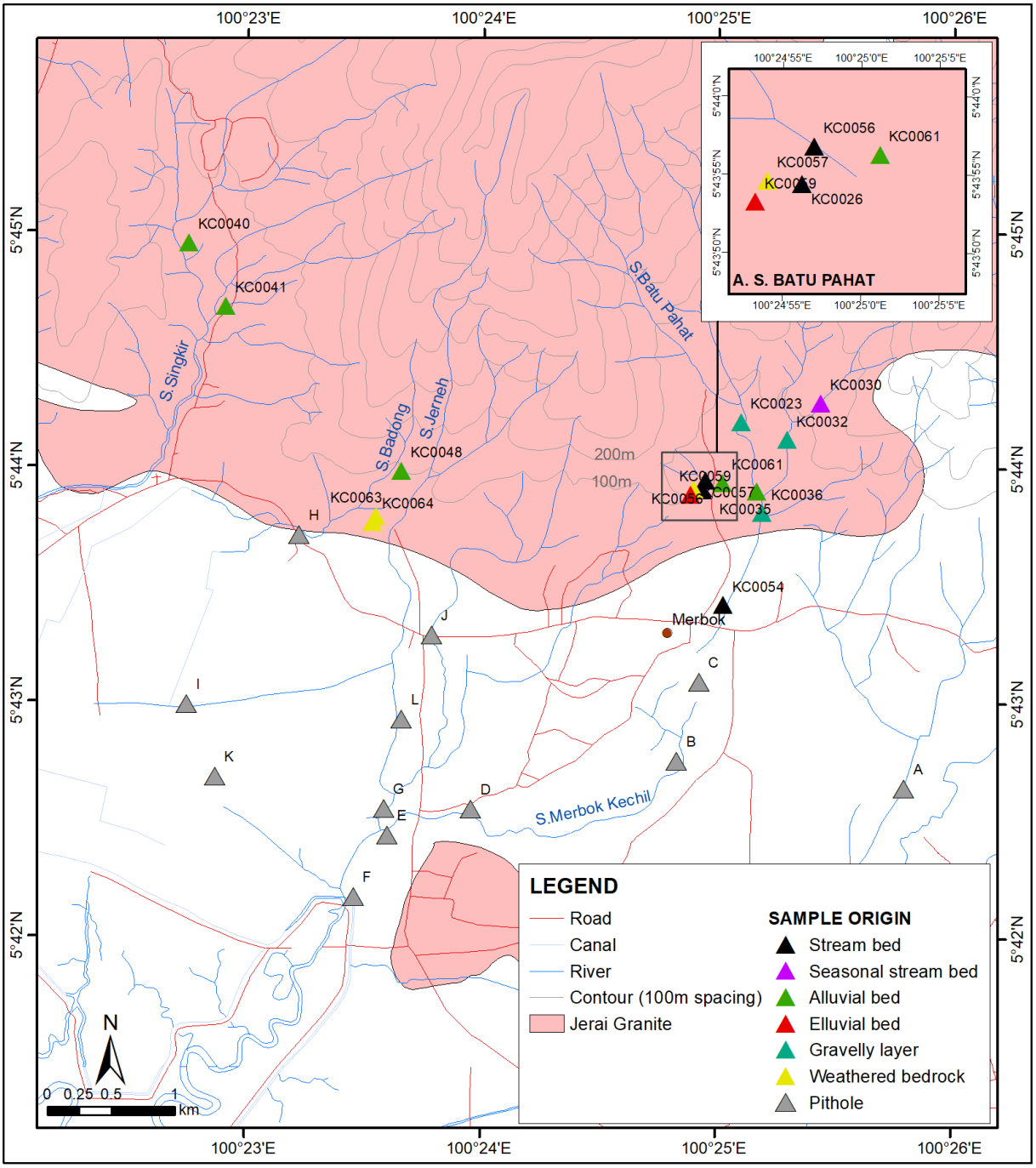

Fig. 8: Sampling locations in the study area.

samples ranges from 74.6 ppm to 1,530.0 ppm. The U content ranges from 48.5 ppm to 1,553.0 ppm. The Sc content ranges from 16.5 ppm to 87.8 ppm while the Y content ranges from 266.0 ppm to 7,604.0 ppm.

The TREE content ranges from 928 ppm to21,031 ppm. The THREE content ranges from 411 ppm to 11,435 while ther TLREE content ranges from 517 ppm to 9,596 ppm All samples have higher TLREE than THREE content except KC56 and KC59.

Sample KC56 has the highest content of U, Y, La, Pr, Nd, Sm, Gd, Tb, Dy, Ho, Er, Tm, Yb and Lu and also TREE, HREE and LREE. Sample KC41 has the greatest content of Th and Ce while sample KC59 has the greatest content of Sc. Sample KC23 has the lowest content of Th, U, Y, TREE, THREE and TLREE.

4.3 Statistical relationships

Comparisons of QME and LA-ICP-MS results

Table 1: List of common minerals separated using Bromoform, hand magnet and magnetic separator according to magnetism (Che Harun et al. 2009).

Light minerals (separated with Bromoform)	Magnetic (hand magnet)	Magnetic Separator (Frantz Isodynamic Model L-1			
		0.4 Ampere	0.7 Ampere	1.0 Ampere	Non-Magnetic
Quartz	Magnetite	Ilmenite	Ilmenite	Tourmaline	Pyrite
	Hematite	Iron Oxide	Tourmaline	Hydroilmenite	Quartz
	Iron Oxide	Garnet	Staurolite	Monazite	Cassiterite
	Pyrrhotite	Siderite	Pyrite	Pyrite	Rutile
			Epidote	Quartz	Leucoxene
			Garnet	Epidote	Corundum
			Hydroilmenite	Staurolite	Tourmaline
			Xenotime	Allanite	Topaz
			Seiderite	Columbite	Zircon
			Allanite	Garnet	Gold
			Columbite	Xenotime	Anatase
			Rutile	Rutile	
			Wolframite	Struverite	

are presented as crossplots of selected elements and minerals in Fig. 11. They show no perfect linear relationship (R2 > 0.95) between the element and mineral content. However, Th and REE have generally strong, positive relationship with monazite. Similar positive histogram patterns for Ce-Nd-La vs monazite are observed. The Sm vs monazite histogram pattern is similar to the REE vs monazite histogram pattern.

The Y element has strong, positive relationship with both monazite and xenotime. Similar pattern of Y vs xenotime histogram is shown by the Yb vs xenotime histogram.

The Sc element, however, has better positive relationship with monazite compared to garnet while U has strong relationship with monazite.

5. Discussions

5.1 Monazite and xenotime magnetism

In this study, the Jerai monazite is not only observed in 0.7-Amp fraction but also appeared but less in 1.0-Amp fraction. This is acceptable as monazite mineral is always slightly magnetised compared to quartz but very much weaker than hematite (Willbourn, 1925; Abaka-Wood et al., 2016).

The xenotime mineral observed in both 0.4- and 0.7-Amp fractions are in concordance with the mineral magnetism guide (Table 1) and the fact that it has slightly higher magnetism than ilmenites (Kim and Jeong, 2019).

5.2 Monazite and xenotime distribution

The higher content of monazite and xenotime in weathered pegmatite compared to weathered granites indicates that pegmatite facies in Jerai Pluton is the primary source of both rare earth minerals.

The humid, tropical climate with high precipitation allows granitic bedrock to decompose to kaolinite and lateritic soils. This permits highly resistant minerals including monazite and xenotime to be transported and deposited either into eluvial environments and nearby river systems before reaching alluvial plain further downstream to become placer deposits (Ghani et al., 2019). The occurrences of pegmatites close or at the upstream of sampling points in recent fluvial environment could be the main factor of different content of the minerals regardless of the sample origin. This is shown by the fact that samples KC56 and KC41, which were taken from stream bed and alluvial bed respectively, have relatively higher monazite and xenotime contents as both sampling points are in the same S. Batu Pahat basin while pegmatite dykes occurred at the upstream of the river basin (Bradford, 1972). Sample KC30 which also contains considerable amount of monazite and xenotime could have pegmatite bedrock at

Table 2: Mineral contents (%) in samples obtained from recent fluvial environment. The symbol '-' denotes not detected and 'TR' denotes trace.

Sample No.	K023	KC30	KC32	KC36	KC40	KC41	KC54	KC56	KC59	KC57	KC63	KC64
Origin	Gravelly layer	Seasonal stream	Gravelly layer	Gravelly layer	Alluvial bed	Alluvial bed	Stream bed	Stream bed	Eluvial bed	Weathered pegmatite	Weathered pegmatite	Weathered granite
Allanite	TR	TR	TR	-	-	-	1.38	-	-	-	-	-
Garnet	32.52	6.18	25.25	39.37	23.75	6.83	47.59	40.56	17.06	0.76	5.61	0.06
Monazite	TR	3.30	-	0.96	-	4.34	0.81	8.43	4.82	4.72	13.70	-
Xenotime	-	3.10	-	TR	TR	4.41	TR	6.05	1.76	0.17	1.45	TR
Zircon	-	4.59	0.27	-	-	0.72	TR	-	0.33	-	0.31	TR
Other Minerals	67.48	82.82	74.49	59.67	76.25	83.69	50.22	44.97	76.02	94.36	78.93	99.94
Total Weight Analyzed (g)	4.53	5.66	2.83	2.76	2.92	2.21	2.53	2.87	2.55	2.11	2.89	2.34

Table 3: Mineral contents (%) in samples obtained from Quaternary alluvial environment. The symbol '-' denotes not detected and 'TR' denotes trace.

Pit	A			B				C			D		
Sample No.	**KAC 001**	**KAC 002**	**KAC 003**	**KBC 002**	**KBC 003**	**KBC 004**	**KBC 005**	**KCC 001**	**KCC 002**	**KCC 003**	**KDC 001**	**KDC 002**	**KDC 003**
Depth (m)	1.2 – 2.1	2.1 – 2.8	2.8 – 3.6	0.4 – 1.0	1.0 – 1.8	1.8 – 2.8	2.8 – 3.6	0.5 – 0.6	1.2 – 2.3	2.7 – 2.7	0.7 – 1.2	1.2 – 2.4	2.5 – 3.4
Allanite	-	-	0.63	TR	-	-	-	-	-	-	-	-	-
Garnet	7.08	5.34	8.61	11.01	7.64	4.85	8.63	61.28	52.14	59.28	4.05	11.57	4.39
Monazite	-	1.35	-	TR	-	TR	TR	1.47	TR	3.16	-	-	TR
Xenotime	-	-	-	-	TR	-	-	2.91	-	0.79	TR	TR	0.83
Zircon	2.67	0.22	1.42	TR	0.27	0.13	-	TR	0.42	-	0.24	-	0.33
Other Minerals	90.25	93.10	89.34	88.99	92.09	95.02	91.37	34.33	47.44	36.78	95.71	88.43	94.45
Total Weight Analysed (g)	3.05	2.97	3.02	2.98	2.75	2.97	3.06	2.78	2.85	3.04	2.96	3.72	3.01

Table 3 (cont.): Mineral contents (%) in samples obtained from Quaternary alluvial environment. The symbol '-' denotes not detected and 'TR' denotes trace.

Pit	E			F		G		H			I	
Sample No.	**KEC 001**	**KEC 002**	**KEC 003**	**KFC 001**	**KFC 002**	**KGC 001**	**KGC 002**	**KHC 001**	**KHC 002**	**KHC 003**	**KIC 001**	**KIC 002**
Depth (m)	0.7 – 1.6	1.7 – 2.4	2.5 – 3.2	1.0 – 1.2	2.7 – 3.2	0.6 – 1.6	1.6 – 3.2	0.6 – 1.0	3.0 – 3.2	3.2 – 3.7	1.6 – 2.5	2.8 – 3.6
Allanite	-	-	-	-	-	-	-	-	-	-	(no concentrate exists)	-
Garnet	3.25	1.36	3.79	9.90	3.09	5.95	9.20	6.00	2.20	6.20		10.08
Monazite	TR	-	0.75	TR	1.62	TR	TR	TR	-	-		TR
Xenotime	1.54	TR	0.75	0.00	TR	-	-	1.14	-	-		0.86
Zircon	0.32	0.36	-	-	-	-	0.71	-	0.43	TR		0.65
Other Minerals	94.88	98.28	94.71	90.10	95.29	94.05	90.08	92.86	97.36	93.80		88.40
Total Weight Analysed (g)	2.95	2.64	3.06	3.09	3.11	2.69	3.08	2.80	2.54	3.03		2.38

Table 3 (cont.): Mineral contents (%) in samples obtained from Quaternary alluvial environment. The symbol '-' denotes not detected and 'TR' denotes trace.

Pit	J		K		L	
Sample No.	**KJC 001**	**KJC 002**	**KKC 001**	**KKC 002**	**KLC 001**	**KLC 002**
Depth (m)	0.7 – 2.1	3.1 – 3.6	(no concentrate obtained)	(no concentrate obtainde)	0.7 – 2.0	2.0 – 3.3
Allanite	-	-			-	-
Garnet	5.97	9.90			5.76	1.06
Monazite	TR	TR			1.61	TR
Xenotime	-	-			TR	TR
Zircon	0.51	-			0.64	0.15
Other Minerals	93.52	90.10			92.00	98.80
Total Weight Analysed (g)	2.84	3.09			2.18	3.03

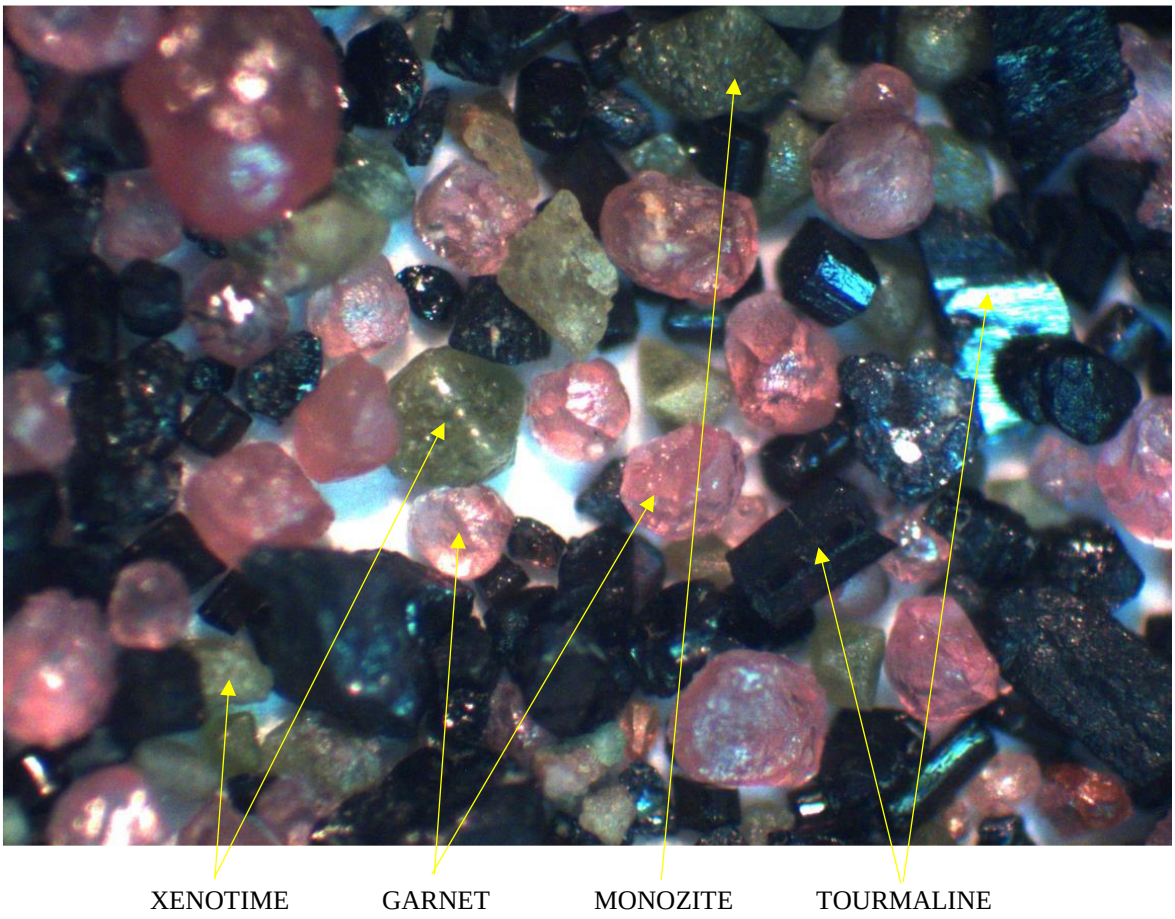

Fig. 9: Minerals observed in 0.7 Amp sample fraction of KC56 under stereo microscope. Total magnification is 40x.

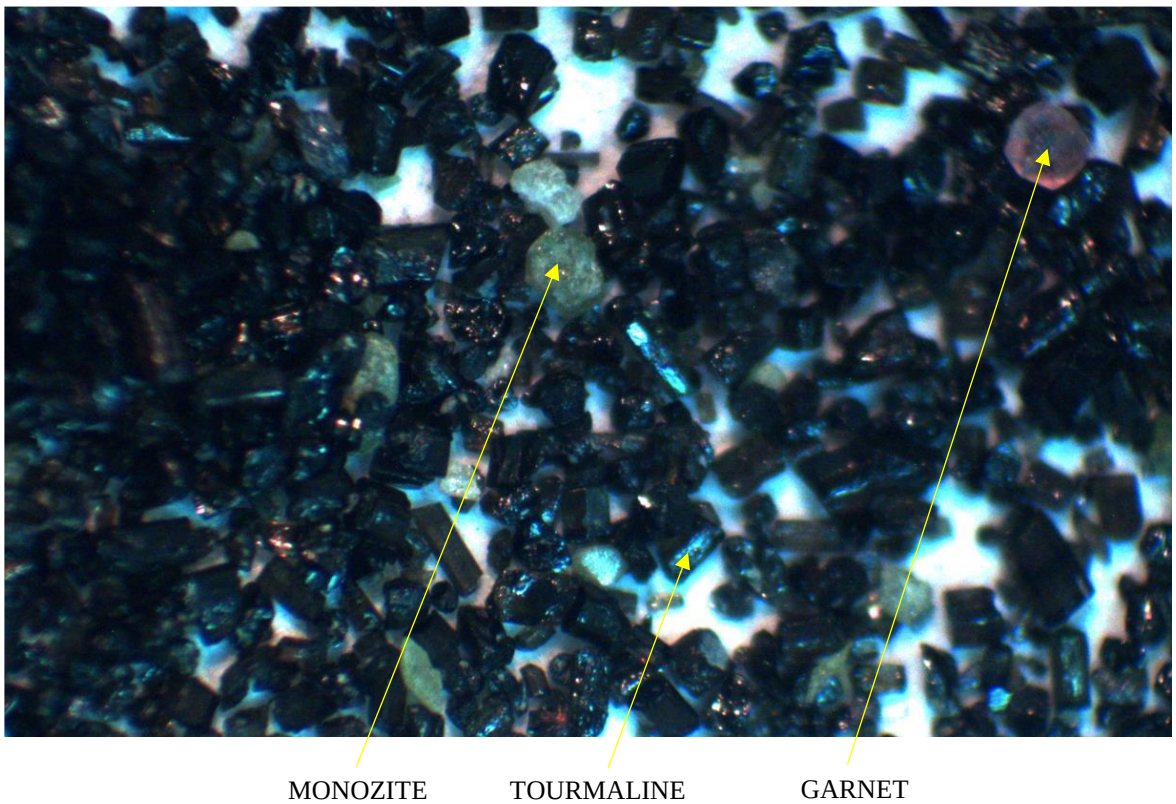

Fig. 10: Minerals observed in 1.0 Amp sample fraction of KCC003 under stereo microscope. Total magnification is 35x.

Table 4: Th, U, Sc, Y and REE content (in ppm) in selected concentrate samples.

Sample No.	Th	U	Sc	Y	LREE							HREE							TREE +Y	THREE +Y	TLREE
					La	Ce	Pr	Nd	Sm	Eu	Gd	Tb	Dy	Ho	Er	Tm	Yb	Lu			
KC23	74.6	48.5	22.5	266.0	114.0	255.0	25.6	98.8	23.6	0.3	20.5	4.6	32.9	6.9	23.3	5.2	44.4	7.2	928.4	411.0	517.3
KC30	198.0	255.0	35.2	750.0	312.0	752.0	83.7	297.0	94.1	0.2	81.4	18.1	107.0	19.5	60.0	12.5	102.0	16.5	2706.0	1167.0	1539.0
KC32	210.0	272.0	44.2	1088.0	317.0	750.0	82.0	301.0	97.6	0.8	96.4	23.3	149.0	27.8	83.5	17.8	145.0	23.0	3202.2	1653.8	1548.4
KC36	319.0	201.0	35.7	825.0	441.0	1013.0	112.0	395.0	104.0	2.0	88.1	18.0	112.0	21.8	66.7	13.5	110.0	17.3	3339.5	1272.4	2067.1
KC40	168.0	104.0	16.5	372.0	249.0	565.0	58.9	207.0	47.2	1.0	37.7	7.6	49.3	9.8	30.4	6.2	49.4	7.6	1698.0	569.9	1128.1
KC41	1530.0	639.0	48.9	3650.0	1979.0	4537.0	494.0	1769.0	438.0	10.8	390.0	77.6	482.0	94.8	288.0	55.6	405.0	61.5	14732.3	5504.5	9227.8
KC54	252.0	290.0	48.2	951.0	405.0	905.0	101.0	359.0	99.0	1.9	89.3	20.2	129.0	24.7	76.1	16.5	133.0	20.7	3331.4	1460.5	1870.9
KC56	1383.0	1553.0	70.1	7604.0	2011.0	4531.0	529.0	1911.0	608.0	6.3	644.0	154.0	1014.0	196.0	590.0	124.0	962.0	147.0	21031.3	11435.0	9596.3
KC57	312.0	414.0	36.4	1546.0	497.0	1174.0	133.0	472.0	156.0	0.4	154.0	35.1	221.0	40.3	121.0	24.9	203.0	31.4	4809.1	2376.7	2432.4
KC59	704.0	1097.0	87.8	5214.0	1071.0	2550.0	300.0	1077.0	390.0	1.7	445.0	110.0	717.0	135.0	402.0	85.7	684.0	107.0	13289.4	7899.7	5389.7
Min.	74.6	48.5	16.5	266.0	114.0	255.0	25.6	98.8	23.6	0.2	20.5	4.6	32.9	6.9	23.3	5.2	44.4	7.2	928.4	411.0	517.3
Max.	1530.0	1553.0	87.8	7604.0	2011.0	4537.0	529.0	1911.0	608.0	10.8	644.0	154.0	1014.0	196.0	590.0	124.0	962.0	147.0	21031.3	11435.0	9596.3
Ave.	515.1	487.4	47.7	2226.6	739.6	1703.2	191.9	688.7	205.8	2.5	204.6	46.9	301.3	57.7	174.1	36.2	283.8	43.9	6906.8	3375.1	3531.7

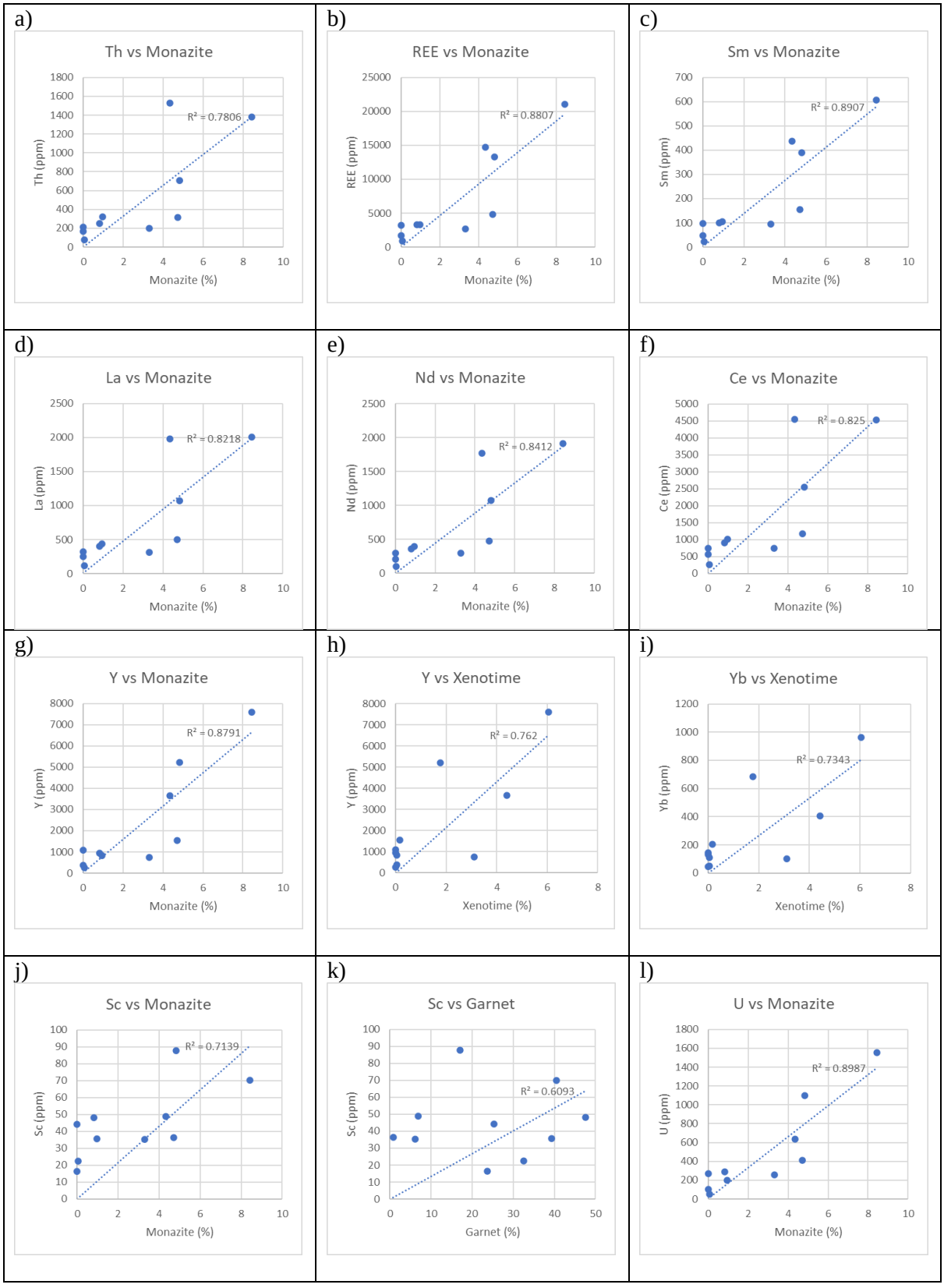

Fig. 11: Plots of selected elements vs minerals with goodness-of-fit values (R^2).

upstream while sample KC54, although collected from stream bed of S.Ayer Jerneh, contains only traces of both minerals. This is due to fact that pegmatites do not occur much at its upstream (Bradford, 1972).

The gravelly layers at recent stream banks are regarded as the paleo stream beds of high energy water flow (Harraz, 2013). However, very low monazite and xenotime content in the layers is either due to dispersion of the minerals during deposition by high energy stream flow or the parent rocks did not completely weather yet to permit both minerals to deposit. In the alluvial plain, the lower content of monazite and xenotime than in the recent fluvial environment is expected as heavy minerals, including both rare earth minerals were widespread when reaching the relatively flat plain area under lower energy regime (Gupta and Krishnamurthy, 2005).

In comparison, the monazite and xenotime contents between sampling points in the alluvial plains show relatively higher at eastern side (downstream S. Batu Pahat) compared to western side (downstream S. Jerneh and S. Badong). The main factor of different distribution pattern is the influence of marine sedimentation during Pleistocene period at the western plain area (Khoo, 1996; Allen, 2000). This is also supported by the occurrence of clayey or muddy layers in pits in that area, suggestive of Gula Formation which were deposited in paleo tidal flat or swamp environment during following Holocene period (Hassan, 1990) (Fig. 12).

5.3 Elements and mineral relationships

A positive relationship is shown by Th and monazite, indicating that monazite is the chief mineral containing the radioactive element. This is also shown by strong relationship between U and monazite. Monazite is one of the minerals searched for its Th content, although the Th content is lower than in thorianite (ThO_2) and thorite ($(Th,U)SiO_4$) (Voncken, 2016). The U occurs as U^{4+} only as accessory in selected minerals like apatite, zircon and monazite that is concentrated into residual melts (Robb, 2005). However, thorianite, thorite and apatite are not observed during QME analysis while zircon occurs in very lesser amount compared to monazite but low Th and U content may also be contributed by dark Nb-Ta minerals that could exist in placer deposits (Bradford, 1972; Zhang et al., 2002).

Apart from radioactive elements, the monazite also has strong relationships with REE, Y and Sc, indicating that the Jerai monazite contains many elements in its crystal lattices. Monazite generally contains higher amount of HREE while xenotime tends to contain higher amount of LREE (Förster, 1998a, b). All samples in this study, excluding KC41, KC564 and KC57, fit the different LREE-HREE concentrations.

The similarities of La, Ce and Nd vs monazite plots could represent uniform concentration ratios of these element in one monazite mineral. In fact, the highest content of Ce compared to La and Nd would suggest the monazite-Ce species occurs the most in Jerai area (Mindat.org, 2021).

The Y content has stronger relationship with monazite compared to xenotime. Although Y is the main element in xenotime, Flinter et al. (1963) studied that the Jerai monazite also contains considerably high amount of Y with value ranges 2.5% to 5.9%. The variation of Y content could also be the main factor of samples containing higher monazite than xenotime, but has higher HREE concentration because Y is considered as HREE in this study.

Similarities of Y and Yb plots are due to fact that both HREE also have uniform concentration ratios and tend to occur together (Förster, 1998b).

Sc is likely contributed by monazite compared to garnet, although its content is considerably very low. Sc is more common as trace amounts in iron and magnesium rich rocks (Gupta and Krishnamurthy, 2005).

5.4 Mining potential

The maximum total content of monazite and xenotime per sample is 14.48% in stream bed of S. Batu Pahat (KC56) for recent fluvial environment and 4.38% in Quaternary alluvial plain environment KCC001 (KCC001). These contents

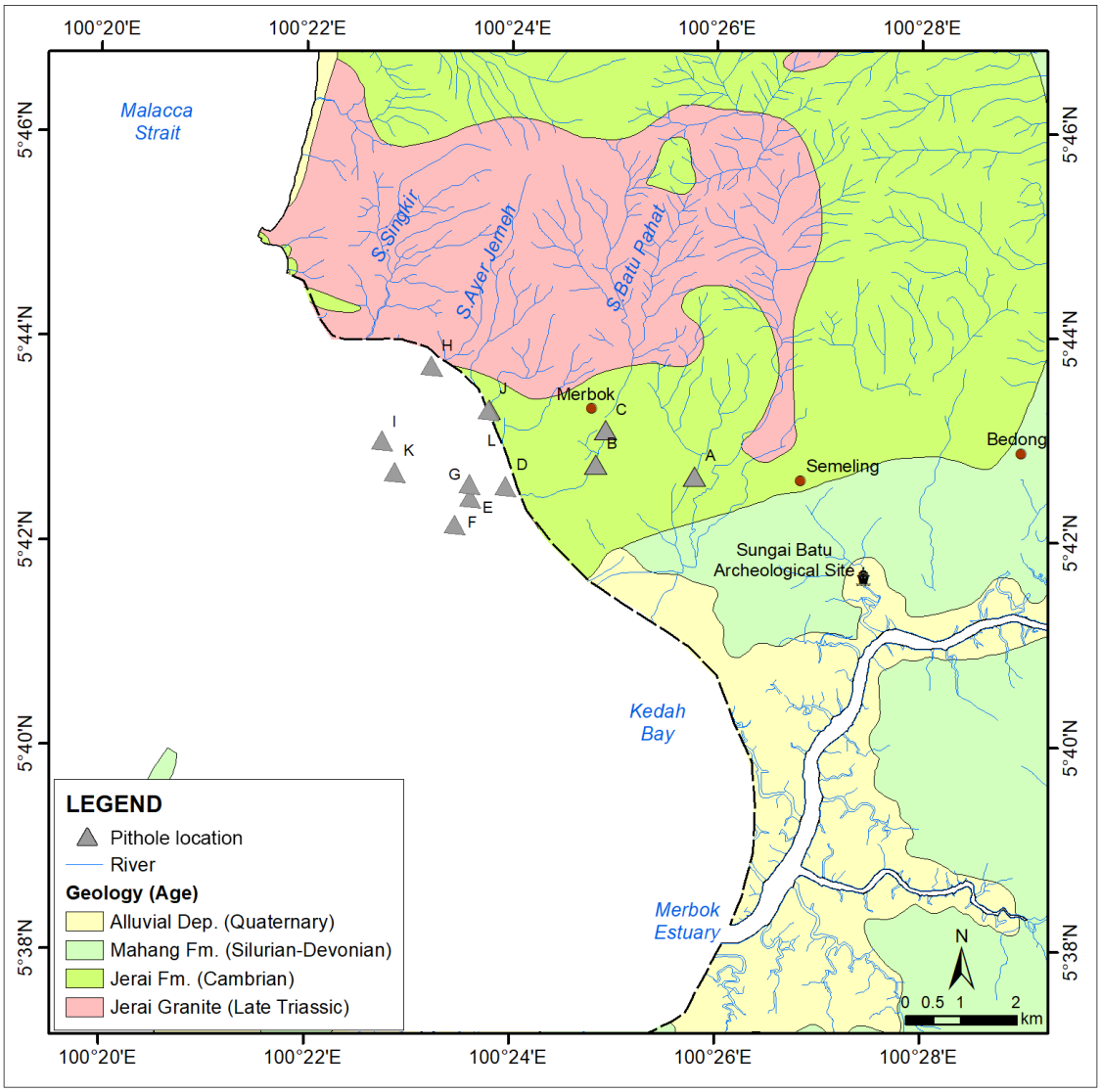

Fig. 12: Simplified geological map showing the studied pithole locations with respect to Kedah Bay and Merbok Estuary area and coastal line before 15th Century (modified from Khoo, 1996). The sea level may be higher during that time according to the discovery of ancient jetty near Sungai Batu Archaeological Site (Zakaria et al., 2011).

are exceptionally higher than those in productive placer deposits in Eneabba (Australia) and Xun Jiang (China) districts (Shepherd, 1990; Jackson and Christiansen, 1993). In comparison of sum average of both minerals, fluvial deposit has relatively more potential.

Rather than mining the REM alone, exploiting all existing heavy mineral suits could be more potential yet economic to practice. Garnets are the most occurring minerals in all samples for both fluvial and alluvial environments. Garnets are used to make abrasives to clean compacted mud and silt from well casings in petroleum industry and to polish optical lenses and metal (Rock&Gem, 2019). Tourmaline, particularly black, schorl species are also abundant in all samples. It is widely used based on its pyroelectricity and emission of far infrared radiation (Lameiras et al., 2010). Other minerals that exist abundantly in placer deposits in Jerai area include hematite, magnetite, Nb-Ta minerals and lesser cassiterite (Bradford, 1972) still has industrial demands.

6. Conclusion and recommendation

The monazite and xenotime contents are relatively higher in recent fluvial deposits than Quaternary alluvial deposits. Higher content of

both minerals was shown in both fluvial and downstream, alluvial plains of S. Batu Pahat basin. The occurrences of pegmatite as chief host rock for monazite and xenotime at upstream could be the factor of higher content of the minerals in S. Batu Pahat than S. Ayer Jerneh and S. Singkir. The lower content of mineral samples including monazite and xenotime in western side of Quaternary plain is due to influence of marine sedimentation during Quaternary period. The higher Th and LREE content are contributed by monazite while Y and HREE are chiefly contributed by xenotime. The Sc content is also contributed by monazite although it is considerably low.

The monazite and xenotime in Jerai area are economically potential as placer deposits if mining method considers of harvesting other minerals like garnet, tourmaline, iron ores and Nb-Ta minerals which could be industrially beneficial. Other analysis techniques such as XRD, FESEM and EPMA are also recommended to be done in order to detail the mineral contents in the placer deposits.

Acknowledgements

The authors would like to thank The Director General of JMG Malaysia for giving the opportunity for this study to be published and JMG REE Team for ideas and supports given during this study. Also special thanks to Ms. Brendawati Ismail, JMG Chief Editor and Mr. Ledyhernando Taniou for proofread.

References

Abaka-Wood, G.B., Addai-Mensah, J., & Skinner, W. (2016). Magnetic separation of monazite from mixed minerals. Chemeca.

Abdul Rahman, A.H., Sibon, M., & Hasan, M.S. (2018a). Reconnaissance study on thorium element from monazite source in southern Kedah. Putrajaya, Malaysia: Department of Mineral and Geoscience Malaysia.

Abdul Rahman, A.H., Sibon, M., & Hasan, M.S. (2018b). Reconnaissance study on rare earth elements in southern Kedah. Putrajaya, Malaysia: Department of Mineral and Geoscience Malaysia.

Allen, J. (2000). In support of trade: Coastal site location and environmental transformation in early historical period Malaysia and Thailand. *Bulletin Indo Pacific Prehistory Association, 20*, 62–78.

ASM (2014). Blueprint for the establishment of rare earth-based industries in Malaysia: summary for policy maker. Kuala Lumpur, Malaysia: Akademi Sains Malaysia.

Bea, F. (1996). Residence of REE, Y, Th and U in granites and crustal protoliths; Implications for the chemistry of crustal melts. *Journal of Petrology, 37(3)*, 521–552. doi: 10.1093/petrology/37.6.1601.

Bea, F., Pereira, M.D., Corretge, L.G., & Fershtater, G.B. (1994). Differentiation of strongly peraluminous, perphosphorous granites: The Pedrobernardo pluton, central Spain. *Geochimica et Cosmochimica Acta, 58*(12), 2609– 2627. doi: 10.1016/0016-7037(94)90132-5.

Bean, J.H., & Hill, J.H. (1969). The iron-ore deposits of West Malaysia, Vol.2. Kuala Lumpur, Malaysia: Geological Survey of Malaysia.

Bradford, E.F. (1972). The geology and mineral resources of the Gunung Jerai area, Kedah. District Memoir 13. Kuala Lumpur, Malaysia: Geological Survey of Malaysia.

Casillas, R., Nagy, G., Panto´, G., Bra¨ndle, J., & Fo´rizs, I. (1995). Occurrence of Th, U, Y, Zr, and REE- bearing accessory minerals in late Variscan granitic rocks from the Sierra de Guadarrama (Spain). *European Journal of Mineralogy, 7*(4), 989–1006.

Castor, S.B., & Hedrick, J.B. (2006). Rare earth elements. In J.E. Kogel, N.C. Trivedi, J.M. Barker, and S.T. Krukowski (Ed.), Industrial minerals and rocks—commodities, markets, and uses (pp.769-792). Colorado, USA: Society for Mining, Metallurgy, and Exploration, Inc.

Chappell, B.W., & White, A.J.R. (2001). Two contrasting granite types: 25 years later. *Australian Journal of Earth Science, 48*(4), 489–499. doi: 10.1046/j.1440-0952.2001.00882.x.

Che Harun, H., Ismail, A., Che Wan, R., Sulaiman, Z.A., Ash'ari, M.A., Husin, Z., Abdul Ghani, M.Z., Che Kasim, M.Z., Ismail, Y., Abu Hasan, M., Daril, K., Md Slar, K., Hamzah, A.B., & Zakri, H. (Ed.) (2009). Placer tin exploration guidelines (in Malay). JMG.GP.03. Kuala Lumpur, Malaysia: Department of Mineral and Geoscience Malaysia.

Che Zainol Bahri, C.N.A., Ismail, A.F., Ab Majid, A., Mohd Ruf, M.I.F., & Al-Areqi, W.M. (2018). Extraction and purification of thorium oxide from monazite mineral. *Sains Malaysiana, 47*(8), 1873–1882. doi: 10.17576/jsm-2018-4708-28.

Connelly, N.G., & Damhus, T. (2005). Nomenclature of inorganic chemistry: IUPAC recommendations (p. 51). London, England: RSC Publishing.

Cuney, M., & Friedrich, M. (1987). Physicochemical and crystal-chemical controls on accessory mineral paragenesis in granitoids: Implications for uranium

metallogenesis. *Bulletin Mine´ralogie, 110*, 235–247.

Devismes, P. (1978). Atlas photographique des mineraux d'alluvions. Paris, France: *Mem. Bur. Rech. Geol. Minières.*

Flinter, B.H., Butler, J.R., & Harral, G.M. (1963). A study of alluvial monazite from Malaya. *The American Mineralogist, 48*, 1210–1226.

Förster, H-J. (1998a). The chemical composition of REE-Y-Th-U-rich accessory minerals in peraluminous granites of the Erzgebirge-Fichtelgebirge region, Germany. Part I: the monazite-(Ce)-brabantite solid solution series. *American Mineralogist, 83*, 259–272.

Förster, H-J. (1998b). The chemical composition of REE-Y-Th-U-rich accessory minerals in peraluminous granites of the Erzgebirge-Fichtelgebirge region, Germany. Part II: Xenotime. American Mineralogist, 83, 1302–1315.

Förster, H.-J., & Tischendorf, G. (1994). The western Erzgebirge-Vogtland granites: implications to the Hercynian magmatism in the Erzgebirge-Fichtelgebirge anticlinorium. In R. Seltmann, H. Ka¨mpf, and P. Mo¨ller (Ed.), Metallogeny of collisional orogens (pp. 35-48). Prague, Czech Republic: Czech Geological Survey.

Ghani, A.A., Shahjamal, M., Ng, T.F., Ismail, N.E.H., Mohamad Zulkifley, M.T., Islami, N., Quek, L.Z., Abu Bakar, A.F., Amir Hassan, M.H., Abdul Aziz, J.H., & Masor, A.F. (2019). Ce anomaly in I-type granitic soil from Kuantan, Peninsular Malaysia: Retention of zircon in the weathering product. *Sains Malaysiana, 482)*, 309–315. doi: 10.17576/jsm-2019-4802-06.

Gupta C.K., & Krishnamurthy, N. (2005). Extractive metallurgy of the rare earths (p. 484). Florida, USA: CRC Press.

Hassan, K. (1990). A summary of the Quaternary geology investigations in Seberang Prai, Pulau Pinang and Kuala Kurau. *Geol. Soc. Malaysia Bulletin, 26*, 47–53.

Harraz, H.Z. (2013). Topic 7: Placer mineral deposits. A short series lectures, Tanta University.

Hinton, R.W., & Paterson, B.A. (1994). Crystallisation history of granitic magma: Evidence from trace element zoning. *Mineralogical Magazine, 58A*, 416–417.

Hosking, K.F.G. (1973). The primary tin mineralization patterns of West Malaysia. *Geol. Soc. Malaysia Bulletin, 6*, 297–308.

IAEA (2005). Thorium fuel cycle – potential benefits and challenges. Report no. IAEA-TECDOC-1450 (p. 90) Vienna, Austria: Author.

Ishihara, S., Sawata, H., Arpornsuwan, S., Busaracome, P., & Bungbrakearti, P. (1979). The magnetite-series and ilmenite-series granitoids and their bearing on tin mineralization, particularly of the Malay Peninsula region. *Geol. Soc. Malaysia Bulletin, 11*, 103–110.

Jackson, W.D., & Christiansen, G. (1993). International strategic minerals inventory summary report—rare-earth oxides: USGS Circular 930-N (p. 68p). Virginia, USA: USGS.

Jamil, A., Ghani, Azman A., Zaw, K., Osman, S., & Quek, L.X. (2016). Origin and tectonic implications of the ~200 Ma, collision-related Jerai Pluton of the Western Granite Belt, Peninsular Malaysia. *Journal of Asian Earth Sciences, 127*(2016), 32–46. doi: 10.1016/j.jseaes.2016.06.004.

Jha, A.R. (2014). Rare earth materials: Properties and applications. Florida, USA: CRC Press.

JMG (2014). Geological map of Kedah. Kuala Lumpur, Malaysia: Author.

JMG (2019). Mining industries in Malaysia 2018. Putrajaya, Malaysia: Author.

Kim, K., & Jeong, S. (2019). Separation of monazite from placer deposit by magnetic separation. *Minerals, 2019*(9), 149–160. doi: 10.3390/min9030149.

Khoo, T.T. (1977). Occurrence and implication of syncplutonic pegmatite dykes in the Gunung Jerai granite, Kedah. *Geol. Soc. Malaysia Bulletin*, 8, 117–120.

Khoo T.T. (1996). Geomorphological evolution of the Merbok estuary area and its impact on the early state of Kedah, northwest Peninsular Malaysia. *J. SE Asian Earth Sci, 13*(3-5), 347–371. doi: 10.1016/0743-9547(96)00042-6.

Lameiras, F.S., Nunes, E.H.M., & Maria-Leal, J. (2010). Backgrounds for the industrial use of black tourmaline based on Its crystal structure characteristics. *Ferroelectrics, 377*(1), 107–119. doi: 10.1080/00150190802523719.

Liu, L., Hu, R., Zhong, H., Yang, J., Kang, L., Zhang, X., Fu, Y., Mao, W., & Tang, Y. (2020). Petrogenesis of multistage S-type granite from the Malay Peninsula in the Southeast Asian tin belt and their relationship to Tethyan evolution. *Gondwana Research, 84*, 20–37. doi: 10.1016/j.gr.2020.02.013.

Atomic Energy Licensing Act 1984 (Malaysia).

McLennan, S.M., & Taylor, S.R. (2012). Geology, geochemistry and natural abundances of the rare earth elements. In A.D. Atwood (Ed), The rare earth elements: fundamentals and applications (p. 8). West Sussex, United Kingdom: Wiley.

Mindat (2011). Monazite-(Ce). https://www.mindat.org/min-2751.html. Accessed 20 January 2021.

Mohd Hasan, M.Z., Zakaria, M.R., Lee, A.K., & Chong, F.S. (1993). Transect 2 radioactive mineral exploration, Peninsular Malaysia. Kuala Lumpur, Malaysia: Geological Survey of Malaysia.

Mohd Hasan, M.Z., Zakaria, M.R., & Ong, W.S. (1995). Transect 1 radioactive mineral exploration, Peninsular Malaysia. Kuala Lumpur, Malaysia: Geological Survey of Malaysia.

Mohd Mokhtar, N.A., & Saidin, M. (2018). The contributions of Lembah Bujang to the iron industry in Malaysia (in Malay). Melayu: *Jurnal Antara-bangsa Dunia Melayu, 11*(2), 182–199.

Ng, S.W.P., Chung, S.L., Robb, L.J., Searle, M.P., Ghani A.A., Whitehouse, M.J., Oliver, G.J.H., Sone, M., Gardiner, N.J., & Roselee, M.H. (2015). Petrogenesis of Malaysian granitoids in the Southeast Asian tin belt: Part 2. U-Pb zircon geochronology and tectonic model. *Geological Society of America Bulletin, 127*, 1238–1258. doi:10.1130/B31214.1.

Rapp, R.P., & Watson, E.B. (1986). Monazite solubility and dissolution kinetics: Implications for the thorium and light rare earth chemistry of felsic magmas. *Contr. to Mineral. and Petrol., 94*, 304-316. doi:10.1007/BF00371439.

Robb, L. (2005). Introduction to ore-forming processes. New Jersey, USA: Blackwell Science Ltd.

Robb, L.J. (2019). The geology of tin deposits with special reference to tin mineralisation in Peninsular Malaysia. Proceedings of the National Tin Conference 2019. Kuala Lumpur: Malaysia: Tin Board.

Rock & Gem (2019). Rietreved from https://www.rockngem.com/garnet-an-industrial-commodity/#:~:text=Garnet%20Applied%20Benefits&text=The%20petroleum%20industry%20uses%20huge,for%20water%20and%20industrial%20liquids.

Sengupta, D., & Van Gosen, B.S. (2016). Chapter 4: Placer-type rare earth element deposits. In P.L. Verplanck, & M.W. Hitzman (Ed.), Rare earth and critical elements in ore deposits. Reviews in Economic Geology (pp. 81–100). Virginia, USA: SEG.

Shepherd, M.S. (1990). Eneabba heavy mineral sand placers. In F.E. Hughes, (Ed.), Geology and mineral deposits of Australia and Papua New Guinea (p.1591). London, United Kingdom: Institute of Mining and Metallurgy.

USGS (2019). Mineral commodity summary 2019. Virginia, USA: Author.

Voncken, J.H.L. (2016). The rare earth elements: An introduction. London, United Kingdom: Springer Nature.

Wan Hassan, W.F. (1989). Some characteristics of the heavy detrital minerals from Peninsular Malaysia. *Geology Society of Malaysia Bulletin, 24*, 1–12.

Ward, C.D., McArthur, J.M., & Walsh, J.N. (1992). Rare earth element behaviour during evolution and alteration of the Dartmoor granite, SW England. *Journal of Petrology, 33*(4), 785–815. doi:10.1093/petrology/33.4.785.

Wark, D.A., & Miller, C.F. (1993). Accessory mineral behaviour during differentiation of a granite suite: Monazite, xenotime, and zircon in the Sweetwater wash pluton, southeastern California, U.S.A. *Chemical Geology, 110*(3), 49–67. doi: 0009-2541(93)90247-G.

Willbourn, E.S. (1925). A list of minerals found in British Malaya together with a description of their properties, composition, occurrences and uses. *Journal of the Malayan Branch of the Royal Asiatic Society, 3*(3), 57–100.

Yang, J., Zhou, M., Zhong, H., Williams-Jones, A.E., Liu, L., Zhang, X., Fu, Y., & Mao, W. (2020). Granite-related tin metallogenic events and key controlling factors in Peninsular Malaysia, Southeast Asia: New insights from cassiterite U-Pb dating and zircon geochemistry. *Economic Geology, 115*(3), 581–601. doi:10.5382/econgeo.4736.

Zakaria, I. I., Saidin, M., & Abdullah, J. (2011). Ancient jetty at Sungai Batu Complex, Bujang Valley, Kedah. Postgraduate Student Forum. Retrieved from http:// www.cuhk.edu.hk/ant/PostgraduateForum2011/Arch/IklilIzzatiZAKARIA.pdf.

Zakaria, M.R., Mohd Hasan, M.Z., Lee, A.K., Ong, W.S., & Teoh, L.H. (1994). Transect 3 radioactive mineral exploration, Peninsular Malaysia. Kuala Lumpur, Malaysia: Geological Survey of Malaysia.

Zhang, P., Tao, K., Yang, Z., Yang, X., & Song, R. (2002). Rare earths, niobium and tantalum minerals in Bayan Obo ore deposit and discussion on their genesis. *Journal of Rare Earths, 20*(2), 81–86.

Zhao, J.-X., & Cooper, J.A. (1993). Fractionation of monazite in the development of V-shaped REE patterns in leucogranite systems: Evidence from a muscovite leucogranite body in central Australia. *Lithos, 30*(1), 23–32. doi: 10.1016/0024-4937(93)90003-U.

Zhou, B., Li, Z., & Chen, C. (2017). Global potential of rare earth resources and rare earth demand from clean technologies. *Minerals, 2017*(7), 203–217. doi:10.3390/min7110203.

Thai Geoscience Journal 2(2), 2021, p. 61-71

ISSN-2730-2695; DOI-10.14456/tgj.2021.6

Geology, occurrence and gemmology of Khamti amber from Sagaing region, Myanmar

Thet Tin Nyunt[1*], Cho Cho[2], Naing Bo Bo Kyaw[3], Murali Krishnaswamy[4], Loke Hui Ying[5], Tay Thye Sun[5], Chutimun Chanmuang N[6].

[1] Department of Geological Survey and Mineral Exploration, Ministry of Natural Resources and Environmental Conservation, 15011 Nay Pyi Taw, Myanmar
[2] School of Earth Sciences, China University of Geosciences (Wuhan); Myanma Gems Enterprise, 15011 Nay Pyi Taw, Myanmar
[3] Myanma Gems Enterprise, 15011 Nay Pyi Taw, Myanmar
[4] Department of Chemistry, NUS High School of Mathematics and Science, 20 Clementi Ave. 1, Singapore 129957
[5] Far East Gemological Laboratory, 12 Arumugam Road #04-02, LTC Building B, Singapore 409958
[6] Institut für Mineralogie und Kristallographie, Universität Wien, Althanstraße 14, 1090, Vienna, Austria
**Corresponding author: thettinnyunt@gmail.com*
Received 17 March 2021; Accepted 4 June 2021

Abstract

A large quantity of Burmite (or Myanmar amber) is produced at Tanai in the Hukaung valley in Kachin State and at Hti Lin (Tilin) in the Magway Region. Another occurrence of amber is found in Pat-tar bum (also called Pat-ta bum) which is located near the Nampilin stream, about 40 km southeast of Khamti (Hkamti), Khamti Township, Sagaing Region. The present mining sites in Pat-ta bum are Laychun (Lachun) Maw (most productive), Kyat Maw, Shan Maw, Gyar Maw, Kyauk Tan Maw and Nameindra Maw. Low grade metamorphic rocks, Kanpetlet schists and similar schists to the Naga Hills are exposed in the eastern part which include glaucophane schist, graphite schist, and epidote schist. Sedimentary units of Miocene age of the Upper Pegu Group are widely exposed in the western, middle and northeastern part. Amber is found in *Orbitolina* (mid-Cretaceous) bearing limestone which ranges from a few centimetres to up to two metres in thickness. This limestone is intercalated with sandstone and carbonaceous shaley limestone and sometimes together with carbonaceous materials. The bedding dips vary from 20˚ to 35˚ and amber production follows the bedding plane. Amber is also found in sandstone and carbonaceous shale. The primary amber mining is carried out by blasting the amber-bearing limestone, sandstone and carbonaceous shaley limestone along their bedding planes and aditing. The colour of Pat-tar bum (Khamti) amber varies from yellow, greenish-yellow, orangy-yellow, golden yellow, brownish-yellow and brown. Gemmologically, it is transparent to opaque and the refractive index ranges from 1.53 to 1.54 (spot reading), and the specific gravity ranges from 1.03 to 1.09. Ultraviolet radiation analyses show that very strong chalky yellowish-blue under long wave and weak chalky yellowish-blue or greenish weak chalky yellowish-blue or greenish under short wave. Some of the deep brownish material displays weak chalky blue or yellow under long wave ultraviolet light and inert under short wave ultraviolet light. Inclusions that identified in amber samples in the present study are flattened gas bubbles, flow marks, some brownish organic debris and various organic inclusions (spiders, flies, feather-like and plant-like inclusions and other organic materials). Eleven analysed specimens of Pat-tar bum amber were quite similar to one another and the IR features are dominated by a group of absorption bands at around 2800–3000 cm^{-1}, relatively narrow bands in the range of 950–1750 cm^{-1} overlaying a broad hump at 800–1400 cm^{-1}, and a weak broad band at around 3420 cm^{-1}. Pat-tar bum amber does not show the characteristic IR and Raman bands of young copal (which lie in the 1050–1250 cm^{-1} region and at 1764 cm^{-1}), which provides the confirmation for the older age of the amber i.e., mid--Cretaceous as confirmed by *Orbitolina* sp. in the host limestone.

Keywords: amber, FTIR and Raman spectra, Khamti, *Orbitolina* sp., Pat-tar bum

1. Introduction

Major production of Burmite (Myanmar amber) in Myanmar is from Tanai, Hukaung valley in Kachin State and Hti Lin (Tilin), Magway Region. Another occurrence of amber is found in Pat-tar bum (also called Pat-ta bum) which is located near the Nampilin stream, about 40 km southeast of Khamti (Hkamti), Khamti Township, Sagaing Region and about 112 km southwest of Tanai (Fig. 1). The present mining sites in Pat-tar bum are Laychun (also spelled Lachun or Lachon) Maw (most productive), Kyat Maw, Shan Maw, Gyar Maw, Kyauk Tan Maw and Nameindra Maw ("Maw" means "mine" in Myanmar) (Thet Tin Nyunt et al., 2019, 2020).

2. Geology

Paleocene to Eocene molasse-type sedimentary units of the Paunggyi Formation and the Cretaceous units are locally exposed including limestone in the study area (Fig. 2). Ultramafic and mafic intrusions of mostly Jurassic age also occurred (Soe Thura Tun et al., 2014). These intrusions include peridotite and serpentinite which are the important source for jadeitite near Nansibon (Cho Cho, 2016 ; Kyu Kyu Thin, 2016). Low grade metamorphic rocks, Kanpetlet schists and similar schists to those of the Naga Hills are exposed in the eastern part which include glaucophane schist, graphite schist, and epidote schist. *Orbitolina* sp. bearing limestone (mid--Cretaceous, Albian?) intercalated with sandstone, shaley limestone and carbonaceous limestones are exposed in the Pat-tar bum area. Sedimentary units of Upper Pegu Group of Miocene age are widely exposed in the western, middle and northeastern part.

3. Occurrence of Amber

Amber from Pat-tar bum is found in *Orbitolina* sp. (mid-Cretaceous, Albian?) bearing limestone (Fig. 3). The fossils that present in the amber bearing limestone can only identify that these fossils ranges from Lower Aptian to Albian. So more thin sections are necessary for further identification of this important fossils (Tian Jiang, pers. comm.). The thickness of amber bearing limestone is ranges from a few centimetres to up to two metres. This limestone are intercalated with sandstone and carbonaceous shaley limestone and sometimes together with carbonaceous materials (Thet Tin Nyunt, et al., 2019, 2020).

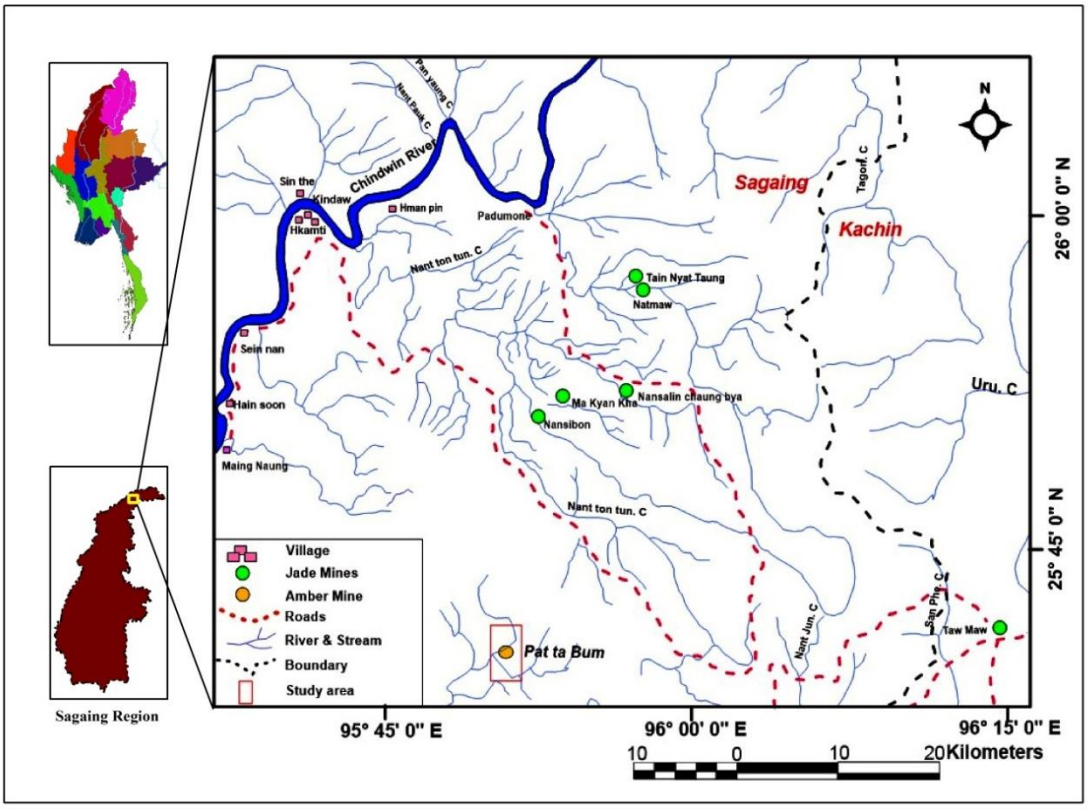

Fig 1: Location map of the Pat-tar bum amber mine in Sagaing Region.

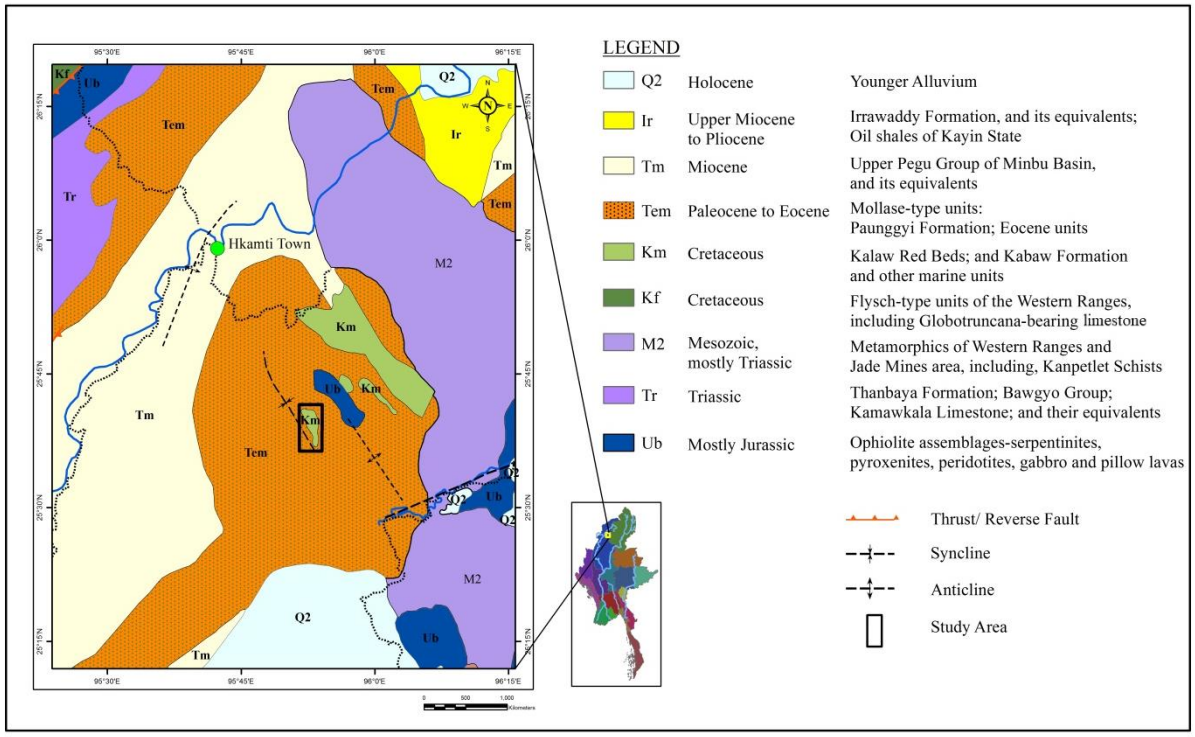

Fig 2: Regional geological map of the Pat-tar bum area (after Soe Thura Tun et al., 2014).

Fig 3: *Orbitolina* sp. in amber bearing mid-Cretaceous (Albian?) limestone (10×, cross-polarised transmitted light). (photos by Cho Cho)

4. Amber Production

Five major production sites including 13 blocks where the mining operation has been operated by Sea-Sun-Star Co. Ltd. are: Laychun (Lachun) Maw, Kyat Maw, Shan Maw, Gyar Maw and Kyauk Tan Maw (Fig. 4). Nameindra Maw is now under suspension. Among them, the Laychun Maw is currently the most productive. The dips of the bedding vary from 20˚ to 35˚ and amber production is carried out along the bedding plane by adits. The primary amber mining is carried out by blasting the amber-bearing limestone, sand-stone and carbonaceous shaley limestone along their bedding plane and aditing into the limestone. Excavated amber-bearing limestone were sorted by manpower outside of the adit (Figs. 5, 6 & 7).

5. Gemmology

The colour of Pat-tar bum (Khamti) amber varies from yellow, greenish-yellow, orangy--yellow, golden yellow, brownish-yellow, brown and reddish brown (Fig. 8). Clarity is from transparent to opaque, the refractive index ranges from 1.53 to 1.54 (spot reading), and specific gravity (SG) ranges from 1.03 to 1.09. These ranges are typical of amber (O'Donoghue, 2008) where the higher SG is due to the attachment of calcite matrix. Ultraviolet radiation analyses show that very strong chalky yellowish-blue under long wave and weak chalky yellowish-blue or greenish

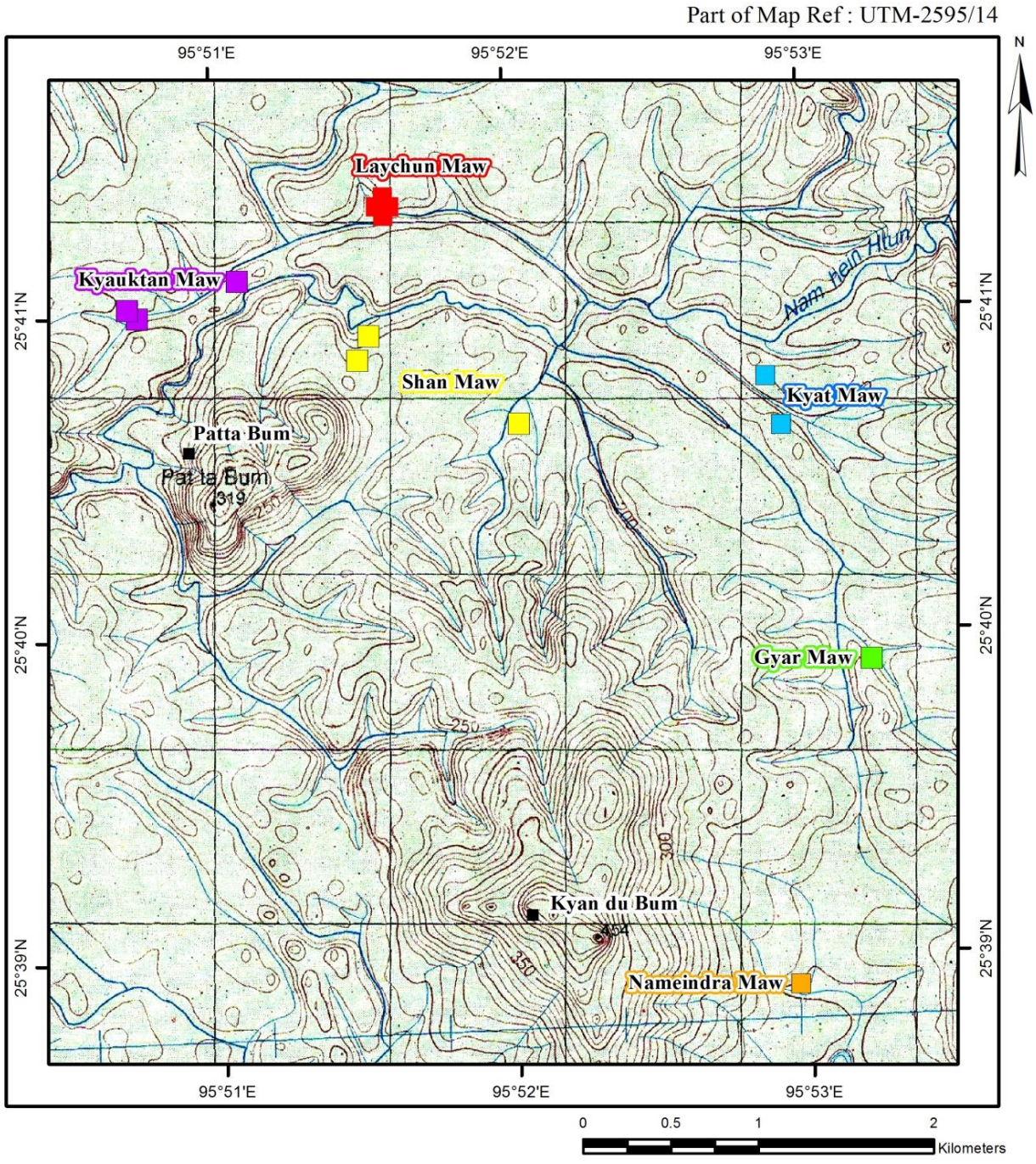

Fig 4: Location map of the Pat-tar bum amber mines.

Fig 5: Amber excavation at Laychun Maw: (a) Manual extraction of amber by manpower outside of the adit; (b) amber with carbonaceous materials in limestone; (c) extracted amber and (d) yellowish brown honey colour amber from Laychun Maw. (photos by Thet Tin Nyunt)

weak chalky yellowish-blue or greenish under short wave (Kocsis et al., 2020). Some of the deep brownish material displays weak chalky blue or yellow under long wave ultraviolet light and inert under short wave ultraviolet light.

6. Inclusions in Amber

Inclusions that are contained in amber samples collected the present study are flattened gas bubbles, flow marks, some brownish organic debris and various animal inclusions (spiders, flies, feathers-like and plant-like inclusions, and organic materials) (Figs. 9 & 10).

7. FTIR and Raman analyses

In the present study, eleven samples of Pat--tar bum amber were analyses by FTIR (Fourier--transform infrared) and Raman analyses. Fig. 11 presents a pair of infrared absorption [recorded in ATR (attenuated total reflection) mode] and Raman spectra obtained from amber sample KT21, which is representative of all samples analysed herein. The IR spectrum is dominated by a group of absorption bands at around 2800-3000 cm^{-1}, relatively narrow bands in the range 950-1750 cm^{-1} overlaying a broad hump at 800-1400 cm^{-1}, and a weak broad band at around 3420 cm^{-1} (Fig. 11, top; for details see Thet Tin Nyunt et al., 2020). The positions and relative intensities of bands in the IR spectrum of Khamti amber are similar to those seen in the IR spectra of Myanmar amber from Tanai and Hti Lin regions reported by various authors (e.g. Tay et al., 2015; Liu, 2018; Chen et al., 2019; Jiang et al., 2020; see Fig. 12), with the exception of a broad band at around ~3420 cm^{-1} (present study) or ~3500 cm^{-1} (Thet Tin Nyunt et. al., 2019), respectively, in the spectra of Khamti amber. The absence of bands at 3048, 1642 and 887 cm^{-1} in the Raman spectrum (Fig. 11, bottom) as well as in the IR spectrum confirms that the Khamti material is amber and

Fig. 6: Nature of amber bearing limestone and amber production at Laychun Maw: (a-b) Entrance for adit of the amber bearing limestone along the bedding plane where the amber is obtained; (c) The amber from amber bearing limestone is transported by a pulley system (yellow bucket with rope and pulley); (d) Intercalation of amber bearing limestone and carbonaceous materials, sometimes with sandstone. (photos by Thet Tin Nyunt)

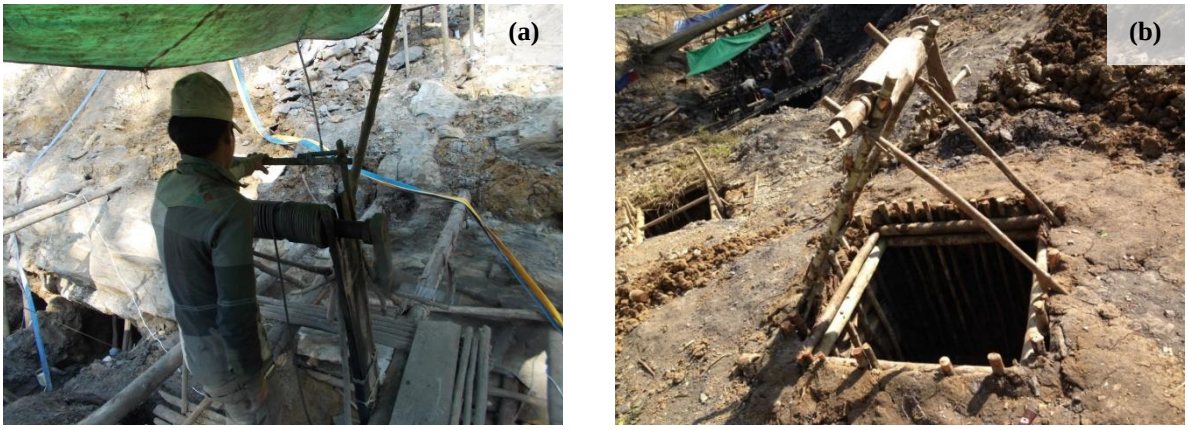

Fig. 7: (a-b) Vertical shafts (1.2 m across, locally called Laybin) are also used to reach the amber bearing limestone at Kyat Maw. (photos by Thet Tin Nyunt)

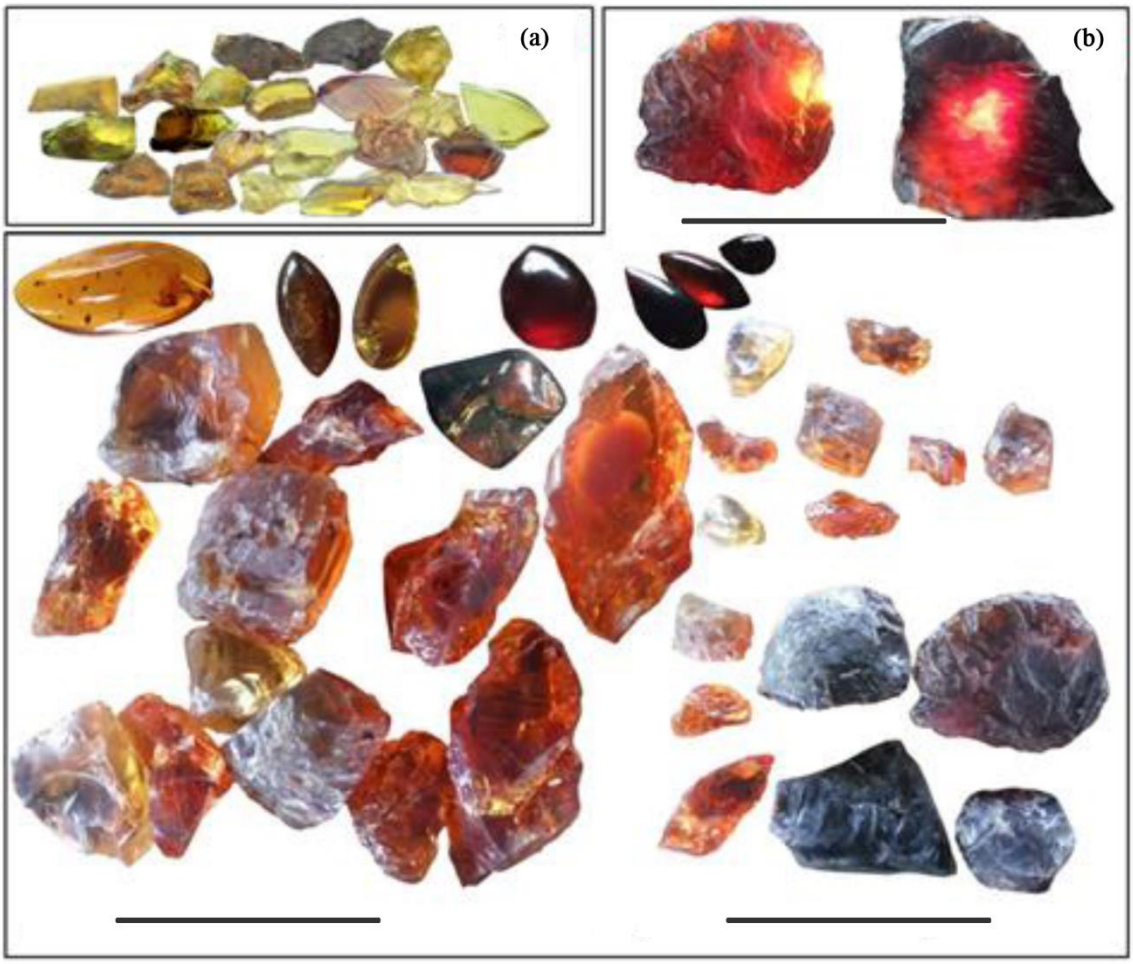

Fig. 8: (a) Twenty one analysed samples of amber for this research range from 0.45 ct (small brownish piece at the left) to 2.49 ct (yellow sample at the centre). (photo by Tay Thye Sun); (b) Khamti ambers with different colour varieties. (photos by Thet Tin Nyunt)(scale bars are 10 cm in length).

not copal (Brody et al., 2001; Wang et al., 2015; compare also Liu, 2018).

8. Discussion and Conclusion

Gemmological properties of Khamti amber, such as refractive index, specific gravity and bright luminescence under LWUV illumination, are quite similar to ambers from the Tanai and Hti Lin regions. A difference consists in the broad, O-H stretching related IR absorption band around 3500 cm^{-1} (3420 cm^{-1} in our samples) in the spectra of Khamti amber. This band is not found in amber from Tanai and Hti Lin, and it can be attributed to O-H stretching. In our previous study (Tay et al., 2015), the analysis of Tanai and Hti Lin amber was carried out with only five samples each and the IR work was focused at the range 3000 cm^{-1}.

Thus, following the discovery of 3500 cm^{-1} absorption in Khamti amber, a preliminary analysis of the Tanai and Hti Lin samples around 3500 cm^{-1} found that some samples appeared to have a peak at 3500 cm^{-1} which we need to do further analysis to confirm it. Therefore, considering the presence of carbonyl groups, this hydroxyl can be assigned to carboxylic acid, rather than molecular water in Khamti amber. The characteristic FTIR and Raman spectra of young copal have not been observed from the Khamti amber which provides confirmation for the older age of the amber i.e., mid-Cretaceous (Albian) or older age as confirmed by the *Orbitolina* sp. in the host limestone. Moreover, it appears likely that Khamti amber was captured and buried earlier or during the formation of the mid-Cretaceous (Albian) limestone.

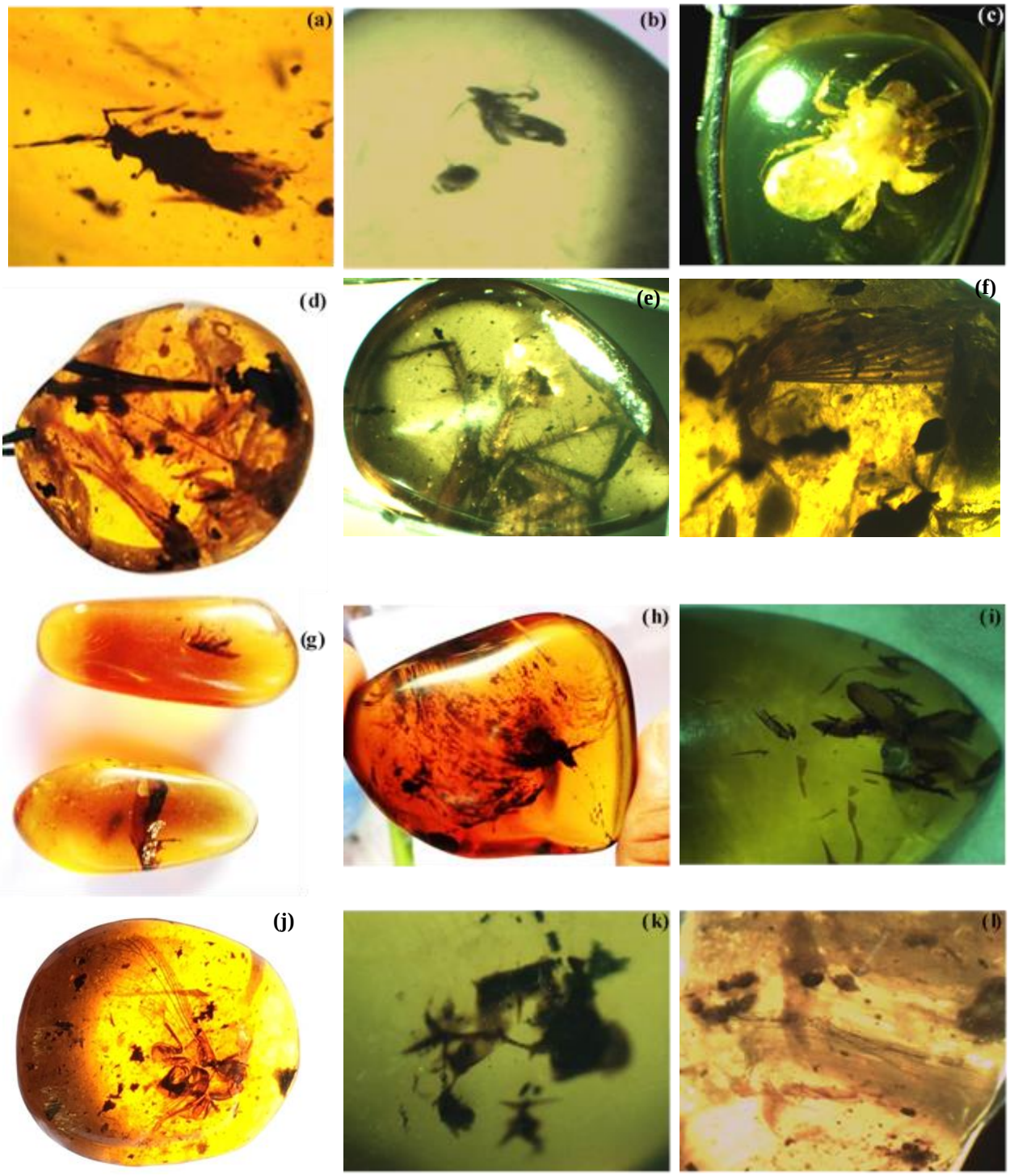

Fig. 9: Inclusions in Khamti amber: (a) Fly; (b) Mosquitoes?; (c) Spider; (d) Bird-Feather; (e) Spider; (f) Insect wings and organic debris; (g) Mosquito; (h) Organic debris; (i) Parts of insects (j) Dragon fly? (k) Some parts of insects and organic debris and (l) Ants and organic materials. (photomicrographs by Thet Tin Nyunt; dark field, 40×)

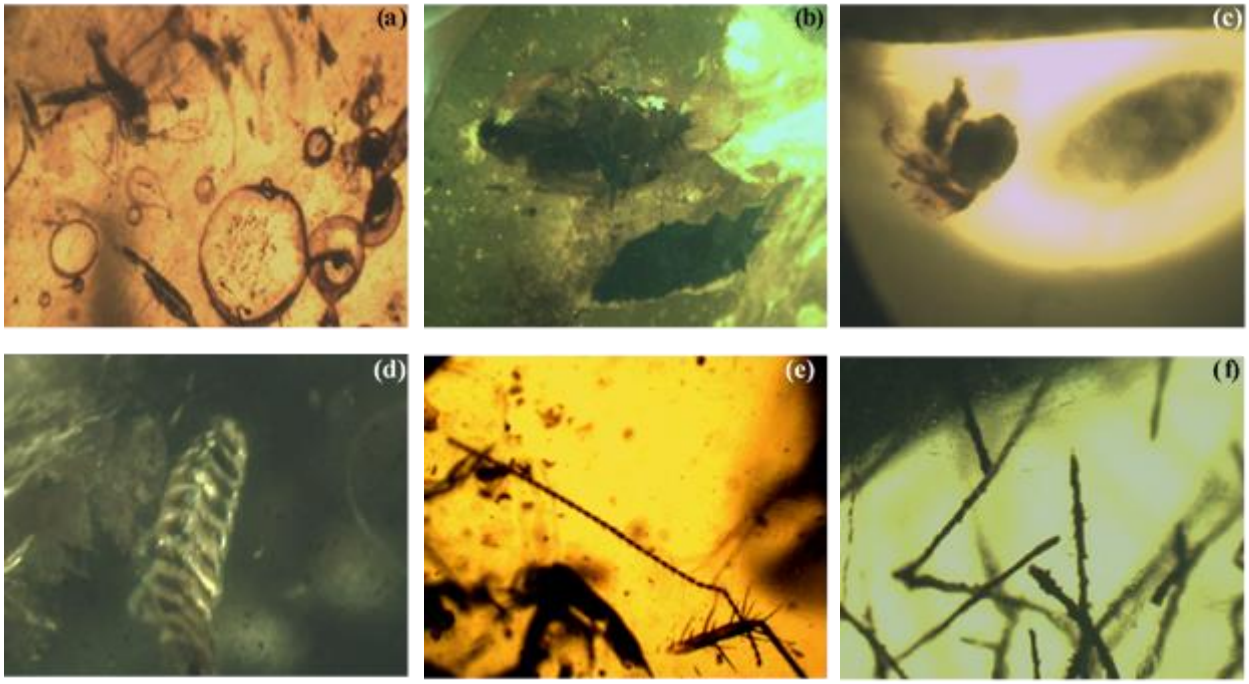

Fig. 10: (a) Organic debris and gas bubbles; (b) Insect inclusions; (c) Organic debris; (d) Insect inclusion; (e-f) Plants, other organic debris and gas bubbles in Khamti amber. (photomicrographs by Thet Tin Nyunt; dark field, 40×)

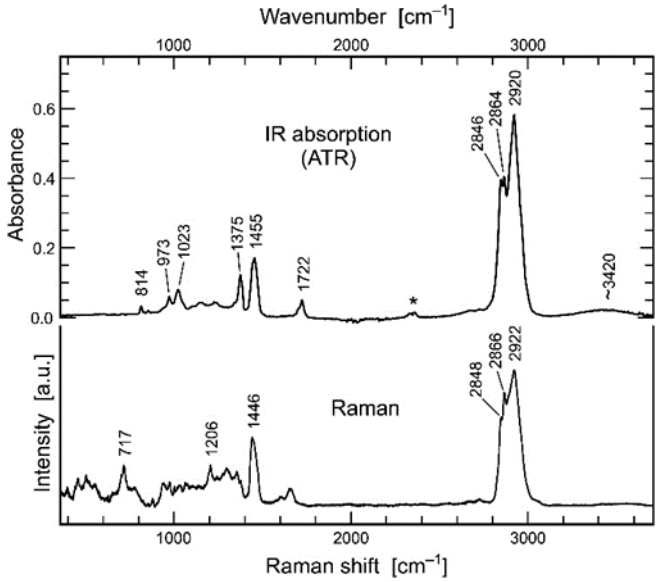

Fig. 11: Representative of IR absorption spectrum (top) and Raman spectrum (bottom) of Khamti amber (modified after Thet Tin Nyunt et al., 2020). The asterisk in the IR spectrum marks an analytical artefact (absorption by CO_2 in the air). The Raman spectrum has been corrected for strong broad-band background luminescence.

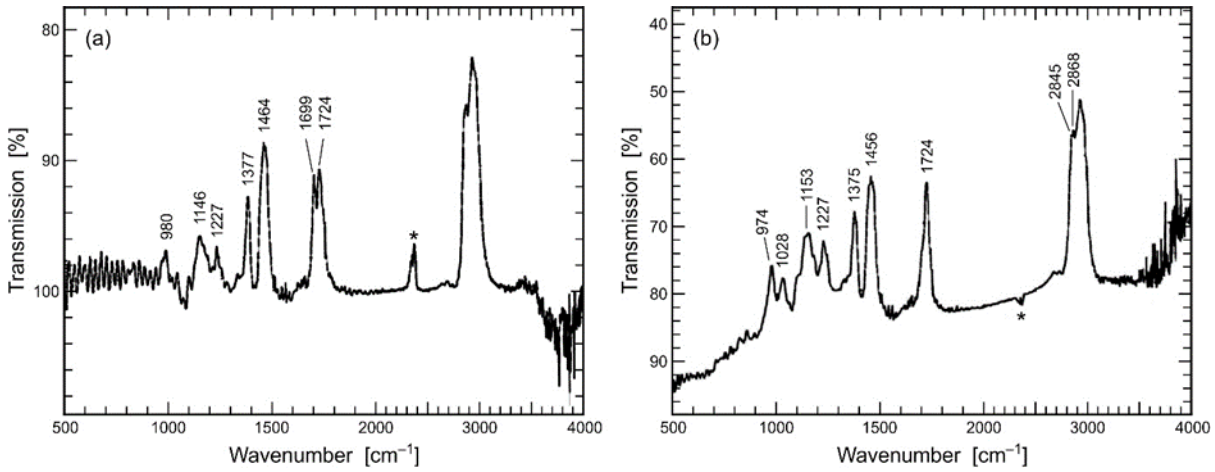

Fig. 12: (a) Infrared spectrum of Hti Lin amber with a double band at 1724 and 1699 cm^{-1}; (b) Infrared spectrum of amber from Tanai shows a single band at 1724 cm^{-1} (redrawn from Tay et al., 2015). Asterisk mark an analytical artefact (absorption by CO_2 in the air).

Acknowledgements

We are very thankful to the CCOP Technical Committee for allowing us to present this article in the CCOP 56th Annual Meeting Thematic Session 2020. Sincere thanks are due to Khaing Nan Shwe Gems & Jewellery Co. Ltd. for their generous support. U Tin Kyaw Than (Principal, Gemmological Science Centre, Myanmar) is thanked for his advice during the present research. We thank Andreas Wagner for sample preparation, Dr. Eugen Libowitzky for help with the FTIR–ATR analyses, and Prof. Dr. Lutz Nasdala for help with Raman analyses. Much appreciation to Daw Gjam, U Aung Naing, Dr. Ko Hein and also the Yangon Gems and Jewellery Entrepreneur Association (YGJEA) for providing financial support that enabled lead author Dr. Thet Tin Nyunt to present the results of this study at the at the poster session of the 36th International Gemmological Conference (IGC, 2019) in Nantes, France. Thanks, are also contribute to Prof. Dr. Bo Wang, Director, Nanjing Institute of Geology and Paleontology and Dr. Jiang Tian, China University of Geosciences (Beijing) for identification and discussion on fossils. Last, but not least, the assistance of Ko Min Thiha, Daw Yi Yi Win (DGSE) and Daw Thuzar Tun (Yangon University) in figure arrangements is gratefully acknowledge.

References

Brody, R.H., Edwards, H.G.M. and Pollard, A.M., 2001. A study of amber and copal samples using FT-Raman spectroscopy. *Spectrochimica Acta Part A: Molecular and Biomolecular Spectroscopy*, *57*(6), 1325–1338, https://doi.org/10.1016/s1386-1425(01)00387-0.

Chen D., Zeng Q., Yuan Y., Cui B. and Luo W., 2019. Baltic amber or Burmese amber: FTIR studies on amber artifacts of Eastern Han Dynasty unearthed from Nanyang. *Spectrochimica Acta A: Molecular and Biomolecular Spectroscopy*, *222*, 117270, https://doi.org/10.1016/j.saa.2019.117270.

Cho Cho, 2016. Mineralogy and occurrences of jadeite jade and associated rocks from Natmaw area, Hkamti Township, Sagaing Region, Unpublished M.Sc. (Thesis), Department of Geology, Yangon University, 101 p.

Jiang, X., Zhang, Z., Wang, Y. and Kong, F., 2020. Gemmological and spectroscopic characteristics of different varieties of amber from the Hukawng Valley, Myanmar. *Journal of Gemmology*, *37*(2), 144-162, http://doi.org/10.15506/jog.2020.37.2.144.

Kocsis L., Usman A., Jourdan A.-L., Hassan S.H., Jumat N., Daud D., Briguglio A., Slik F., Rinyu L. and Futó I., 2019. The Bruneian record of "Borneo Amber": A regional review of fossil tree resins in the Indo-Australian Archipelago. *Earth-Science Reviews*, https://doi.org/10.1016/j.earscirev.2019.103005.

Kyu Kyu Thin, 2016. Mineralogy and occurrences of jadeite jade from Nansibon Area, Hkamti Township, Sagaing Region, Unpublished MSc. (Thesis), Department of Geology, Yangon University, 94 pp.

Liu S.I., 2018. Burmese amber from Khamti, Sagaing Region. *Journal of Gemmology*, *36*(2), 107–110.

O'Donoghue M., 2008. *Gems*, 6th edn. Elsevier, Oxford, 904 pp. ISBN: 978–0–719803413.

Soe Thura Tun, Maung Thein, Nyunt Htay and Kyaing Sein, 2014. Geological Map of Myanmar 1:2,250,000. Myanmar Geosciences Society, Yangon, Myanmar.

Tay T.S., Kleismantas A., Thet Tin Nyunt, Zheng M.R, Krishanswamy M. and Loke H.Y., 2015. Burmese amber from Hti Lin. *Journal of Gemmology*, *34*(7), 606–615, http://dx.doi.org/10.15506/JoG.2015.34.7.606.

Thet Tin Nyunt, Tay Thye Sun, Cho Cho, Naing Bo Bo Kyaw and Wai Yang Lai Aung, 2019. Amber from Khamti, Sagaing Region, Myanmar. *International Gemmological Conference, Nantes, France*, 27–31 August, 219–221.

Thet Tin Nyunt, Tay, T. S., Loke, H.Y., Krishnaswamy, M., Cho, Cho, Naing Bo Bo Kyaw, Wai Yan Lai Aung and Chutimun Chanmuang N., 2020. Amber from Khamti, Sagaing Region, Myanmar, *Journal of Gemmology*, 37(3), 314-322.DOI:10.15506/JoG.2020.37.3.314.

Wang, Y., Shi, G., Shi, W. and Wu, R., 2015. Infrared spectral characteristics of ambers from three main sources (Baltic, Dominica and Myanmar). *Spectroscopy and Spectral Analysis, 35*(8), 2164–2169, https://doi.org/10.3964/j.issn.1000-0593(2015)08-2164-06 (in Chinese with English abstract).

Thai Geoscience Journal 2(2), 2021, p. 72-87

ISSN-2730-2695; DOI-10.14456/tgj.2021.7

Additional occurrence report on early Carboniferous radiolarians from southern peninsular Thailand

Katsuo Sashida[1*], Tsuyoshi Ito[2], Sirot Salyapongse[1] and Prinya Putthapiban[1]

[1] *Mahidol University Kanchanaburi Campus, 99 M.9 Lunsaum Kanchanaburi-Sangkraburi Road Sai Yok, Thailand*
[2] *Institute of Geology and Geoinformation, Geological Survey of Japan, AIST, Tsukuba, 305-8567, Japan*
**Corresponding author: dt4mi5@bma.biglobe.ne.jp*
Received 3 May 2021; Accepted 5 July 2021

Abstract

Moderately-preserved radiolarians have been identified from black chert interbedded with layers of medium- to coarse-grained sandstone and variegated siliceous shale outcropped at a quarry near Ka Bang, Songkhla Province, southern peninsular Thailand. The following radiolarians (13 species belonging to seven genera) were identified and systematically investigated: namely *Albaillella* sp., *Ceratoikiscum* sp., *Stigmosphaerostylus variospina*, *Stigmosphaerostylus* cfr. *vulgaris*, *Stigmosphaerostylus* cfr. *delvolei*, *Stigmosphaerostylus* sp., *Stigmosphaerostylus*? sp. A, *Stigmosphaerostylus*? sp. B, *Stigmosphaerostylus*? sp. C, *Trilonche*? sp., *Spongentactnia exilispina*, *Pylentonema antiqia*, and *Archocyrtium* sp. These radiolarians indicate the Tournaisian–Visean, Mississippian (early Carboniferous) in age. The present authors have already reported a Tournaisian radiolarian fauna which is slightly older than the present fauna from black bedded chert in the Saba Yoi--Kabang area. This is an additional report on the occurrence of early Carboniferous radiolarians from southern peninsular Thailand. The radiolarian-bearing chert reported in this study may have been deposited in the upper continental rise to open deep-sea basins within the Paleotethys Ocean on the basis of the lithological and radiolarian characteristics.

Keywords: Carboniferous, depositional setting, paleogeography, Paleotethys Ocean, radiolarian fauna, Sibumasu terrane

1. Introduction

Mainland Thailand tectonically consists the Sibumasu Terrane, Inthanon Zone, Sukhothai Terrane, and Indochina Terrane, from west to east (e.g., Metcalfe, 2017) (Fig. 1 A). Lower Carboniferous siliceous rocks, such as chert and siliceous shale, are distributed in southern peninsular Thailand and the northwestern part of peninsular Malaysia (e.g., Sashida, Salyapongse and Charusri, 2002; Basir and Zaiton, 2011). Several researchers have reported radiolarian occurrences from these siliceous rocks (e.g., Caridroit, Fontaine, Jongkanjanasoontorn, Suteethorn and Vachard, 1990; Sashida, Igo, Hisada, Nakornsri and Ampornmaha, 1993; Sashida, Igo, Adachi, Ueno, Nakornsri and Sardsud, 1998; Sashida, Nakornsri, Ueno and Sardsud, 2000; Sashida et al., 2002; Wonganan and Caridroit, 2005; Wonganan, Randon and Caridroit, 2007; Saesaengseerung, Sashida and Sardsud, 2007a, 2007b, 2015; Kamata et al., 2015). These radiolarian-bearing siliceous rocks are considered to have been deposited on the slope, upper continental rise, and lower continental rise of the Sibumasu Terrane to the ocean basin of the Paleotethys based on their lithological characteristics and radiolarian faunal analysis (Basir and Zaiton, 2011). The present authors already reported the occurrence of early Carboniferous radiolarians from the Saba Yoi-Kabang areas, southern peninsular Thailand (Sashida et al., 2002), and have continued to investigate the area. A new radiolarian assemblage, distinguishable from the previously-reported one, was obtained from a chert layer intercalated within the sandstone–siliceous shale sequence cropping out in a quarry near the locality of Sashida et al. (2002). Further, the lower Carboniferous radiolarian-bearing siliceous rocks shown in this study differ from contemporary siliceous rocks in neighboring areas (e.g., Sashida et al., 1993, 1998; Wonganan et al., 2007) in containing coarse-grained clastic materials. In this article, we describe an early Carboniferous radiolarian

assemblage from a quarry near Ka Bang, southern peninsular Thailand, as an additional occurrence report of the authors' previous study. In addition, we discuss the depositional setting of the radiolarian-bearing siliceous rocks.

2. Previous studies on southern peninsular Thailand and sample locality of this study

Although most of peninsular Thailand is included in the Sibumasu Terrane in the tectonic subdivision map of mainland Southeast Asia by Metcalfe (2017), southern part is in the Inthanon Terrane (Fig. 1A).

Ueno and Charoentitirat (2011) summarized the Carboniferous–Permian stratigraphy in southern Peninsular Thailand (their Lower Peninsular Thailand) and discriminated the Yaha Formation (?Mississippian), Khuan Klang Formation (Mississippian), Kaeng Krachan Group (?latest Pennsylvanian–early Permian), and Ratburi Limestone (early–late Permian). Concerning the Yaha Formation, this formation was first introduced by Muenlek, Meesook, Tongchit, Tipdhonsab and Skulkaew (1985) in the Geological Map of Changwat Narathiwat and Amphoe Takbai for a mainly siliciclastic succession of shale, sandstone, siliceous shale, chert and conglomerate (Ueno and Charoentitirat, 2011). Muenlek et al. (1985) also introduced the Mayo Formation for similar lithologic characters distributed in the North east of Yala and included both formations in the Kaeng Krachan Group with the Mayo Formation in the lower part and the Yaha Formation in the upper. DMR (1999) regarded the Mayo and Haya formations as identical Carboniferous strata, and mapped the Yaha Formation in Yala, Pattani, Songkhla and Phatthalung provinces. Igo (1973) reported the occurrence of late Tournaisian conodonts from a chert–siliceous shale succession at the northern end of Ko Yo in Songkhla Province which substantiated the Mississippian age for the Yaha Formation. Sashida et al. (2002) discriminated Mississippian radiolarians from a sandstone--chert succession exposed in the Saba Yoi--Kabang area near the Songkhla-Yala provincial boundary. Besides these Carboniferous fossils, late Permian and Middle Triassic radiolarians have been reported from two areas where the distributional area of the Yaha Formation according to DMR (1999): the Chana area (Sashida et al., 2000) and the Rattaphum area (Sardsud and Saengsrichan, 2002; Kamata et al., 2008, 2009) in Songkhla Province. Ueno and Charoentitirat (2011) regarded the Yaha Formation only provisionally as Mississippian due to the controversial litho- and chronostratigraphic characterization of the above mentioned Yaha Formation. DMR (2013) discriminated 12 lithological units of Carboniferous sedimentary rocks in Thailand and set up sandstone, shale, siliceous shale with *Posidonia becheri*, chert, and conglomerate around Songkhla and Yala, in the border areas with Malaysia, as Unit Cy.

The Saba Yoi-Kabang area, study area of this article, is located within the distributional area of Unit Cy of DMR (2013) (Fig. 1B). A study section crops out at the quarry along the road, about 15 km west-southwest of Outcrop 1 of Sashida et al. (2002). A column of the section with outcrop photographs is shown in Fig. 2. Rocks at this outcrop strike N–S and dip 30° to 50° west. The total thickness of the formation of this outcrop attains 12 m. Variegated siliceous shale, mainly dark gray, green, brown, white, yellow, and black, predominates in the section. This siliceous shale is thinly bedded with several millimeters to a few centimeter beds, and it is strongly folded and sheared in the middle part of the section. The folded and sheared parts are cut by faults that are almost parallel to the bedding. Sandstone beds in the lower part intercalate with black chert beds and have a total thickness of about 1.5 m. Sandstone in the middle part of the section is coarse--grained and thickly bedded with intercalated very thin shale. Sandstone beds in the upper part are thickly bedded and have about 2.5 m total thickness. Radiolarian-bearing chert is thinly bedded with intercalated thin siliceous shale, and the total thickness is about 30 cm. This chert is black when fresh and brown to yellow on weathered surfaces. The lower and upper limits of this section are not exposed.

3. Materials and methods

We collected more than 10 samples from variegated siliceous shale and other chert layers of the section. Among them, only one sample (SYK-1) yielded radiolarians. Under thin section,

the samples characteristically contain radiolarian and foraminifer shells within matrices consisting of fine-grained quartz and clay minerals (Fig. 3). Foraminiferal shells are concentrated in some parts and their maximum diameter attains 300 μm. The foraminiferal shells were replaced by silica and are infilled with silica.

Radiolarian specimens were extracted from chert by the procedures, which generally established by Pessagno and Newport (1972), as mentioned below. In addition, we recovered the foraminiferal shells during the procedures. Crushed chert of several centimeters size was soaked in a diluted hydrofluoric acid (HF) solution (3–5%) for about 24 hours at room temperature. The sample was washed and sieved by nylon mesh of 36 μm for collecting residue. This procedure was repeated five times for every samples. The residue was dried in an oven. Well--preserved specimens in the residue were placed on scanning electron microscopy (SEM) plugs and coated with platinum in a vacuum evaporator. SEM images of foraminifers are shown in Fig. 4; those of radiolarians are shown in Figs. 5 and 6. Generic and species name of the foraminifers have not been identified. The systematic paleontology of radiolarians will be described in Section 6.

4. Age of radiolarian fauna

We discriminated radiolarians of 13 species belonging to seven genera from the chert sample (SKY-1). Identified radiolarians are *Albaillella* sp., *Ceratoikiscum* sp., *Stigmosphaerostylus variospina* (Won), *Stigmosphaerostylus* cfr. *delvoli* (Gourmelon), *Stigmosphaerostylus* cfr. *vulgaris* (Won), *Stigmosphaerostylus* sp., *Stigmosphaerostylus*? sp. A, *Stigmosphaerostylus*? sp. B, *Stigmosphaerostylus*? sp. C, *Trilonche*? sp., *Spongentactnia exilispina* (Foreman), *Pylentonema antiqua* (Deflandre), and *Archocyrtium* sp.

Stigmosphaerostylus vulgaris and *Stigmosphaerostylus variospina* was originally described by Won (1983) from the lower Carboniferous the Rheinisches Schiefergebirge, Germany. Subsequently, Gourmelon (1987) reported these two species from the Tournaisian of the Montagne Noire and the central Pyrenees in France. Saesaengseerung et al. (2007a) reported the occurrence of these two species from a sequence of chert, siliceous shale, and sandstone from the Pak Chom area, Loei Province, northeastern Thailand. The occurrence of these two species has been reported by Sashida et al. (2002) from the Saba Yoi-Kabang area. *Stigmosphaerostylus delvoli* was first reported from the Tournaisian of the Montagne Noire and Central Pyrenees by Gourmelon (1987). *Spongentactinia exlispina* was described as *Entactinia exlispina* by Foreman (1963) from the Upper Devonian Ohio Shale. Subsequently this species was reported from the Tournaisian of the Montagne Noire by Gourmelon (1987). *Pylentonema antiqua* was first described from the lower Carboniferous of France by Deflandre (1963) and subsequently Holdsworth (1973) and Holdsworth, Jones and Allison (1978) reported this species from the Upper Devonian of Alaska and the lower Carboniferous of Istanbul, Turkey, respectively. Sandberg and Gutshik (1984) reported this species from the Mississippian (lower Carboniferous) of North America. This species is also known from the Montagne Noire, France (Gourmelon, 1987), Southern Thailand (Sashida et al., 2002), and northwestern Peninsular Malaysia (Basir and Zaiton, 2011).

We discriminate poorly preserved species *Albaillella* sp. whose shell features are slightly similar to *Albaillella indensis* Won. According to Aitchison, Suzuki, Caridroit, Danelian and Noble (2017), *Albaillella idensis* has a range from the late Tournaisian to middle Visean (Mississippian) and this species is an index of the boundary between the upper Tournaisian through lower Visean. As mentioned above, our radiolarian fauna is similar to those from the lower Carboniferous Rheinisches Schiefergebirge, Germany (Won, 1983) and the Montagne Noire, France (Gourmelon, 1987).

The geologic age of the chert sample (SKY-1) may be late Tournaisian to early Visean (Mississippian). In our previous study, *Albaillella deflandrei* Gourmelon occurred in all of the samples (Sashida et al., 2002). *Albaillella deflandrei* is regarded as an index species of the late middle Tournaisian by Aitchison et al. (2017); therefore, our present radiolarian is younger than the samples from our previous study.

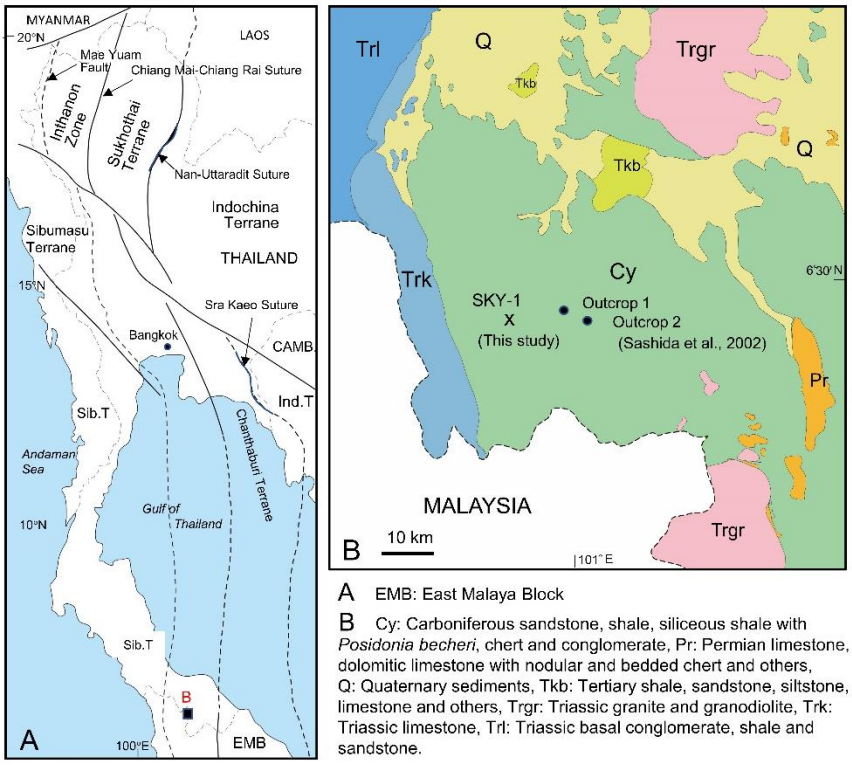

Fig 1: Location map of our study area. A. tectonic subdivision of Thailand and study area. The base map is modified from Metcalfe (2017). B. Location map of our study area, SKY-1, our examined sample. The basic geologic map is modified from DMR (2013).

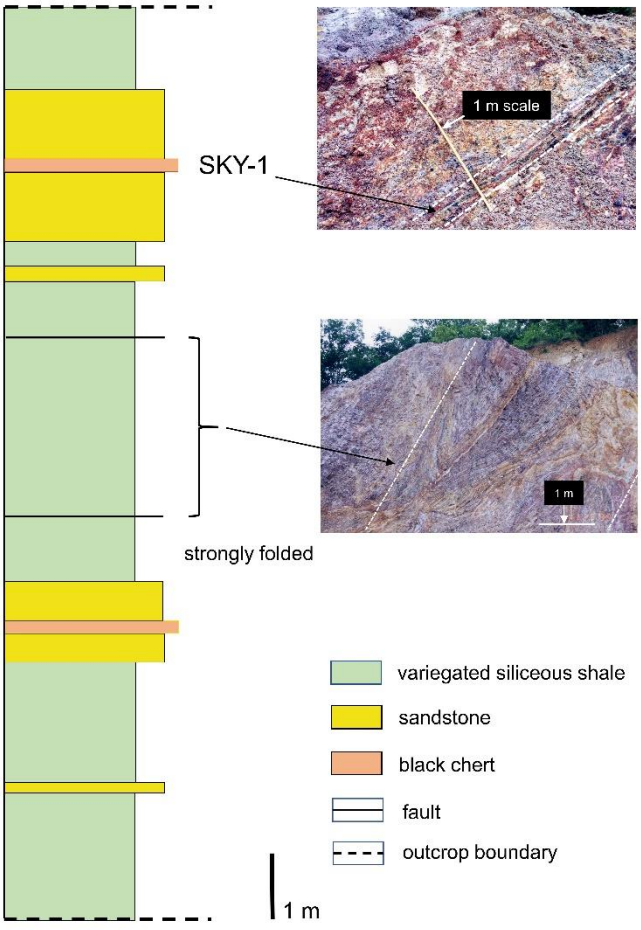

Fig 2: Columnar section and outcrop photos of study section.

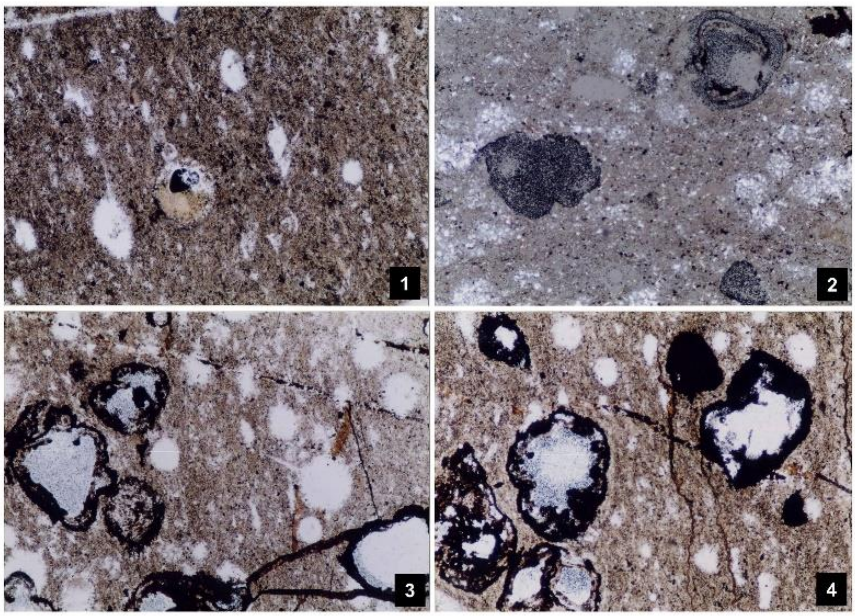

Fig 3: Thin section microphotographs of radiolarian-bearing chert. 1, 3, and 4 are under plane polarized light; 2 is under cross polarized light.

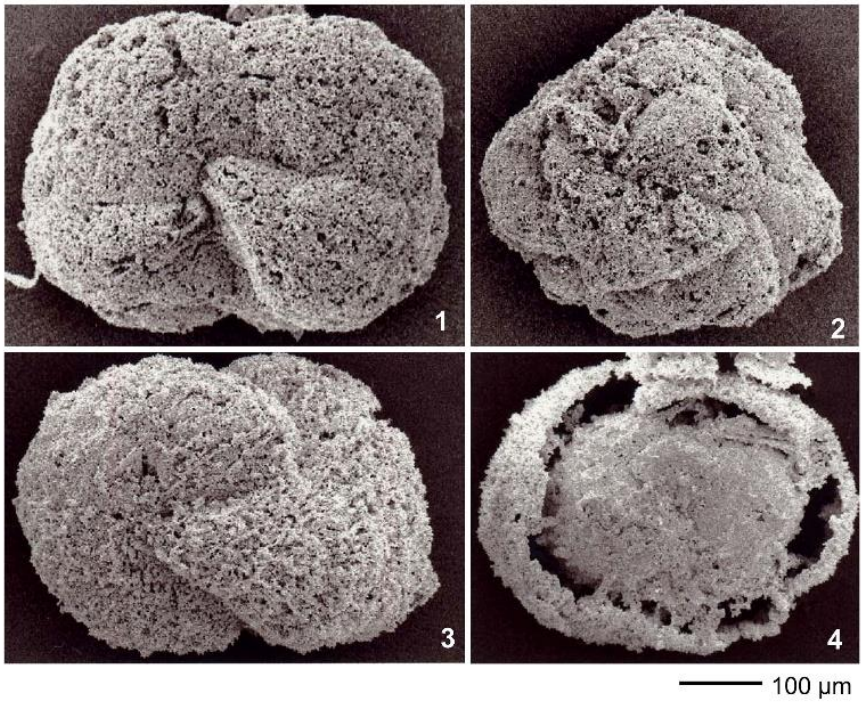

Fig 4: SEM (Scanning Electron Microscope) photos of foraminiferal shells.

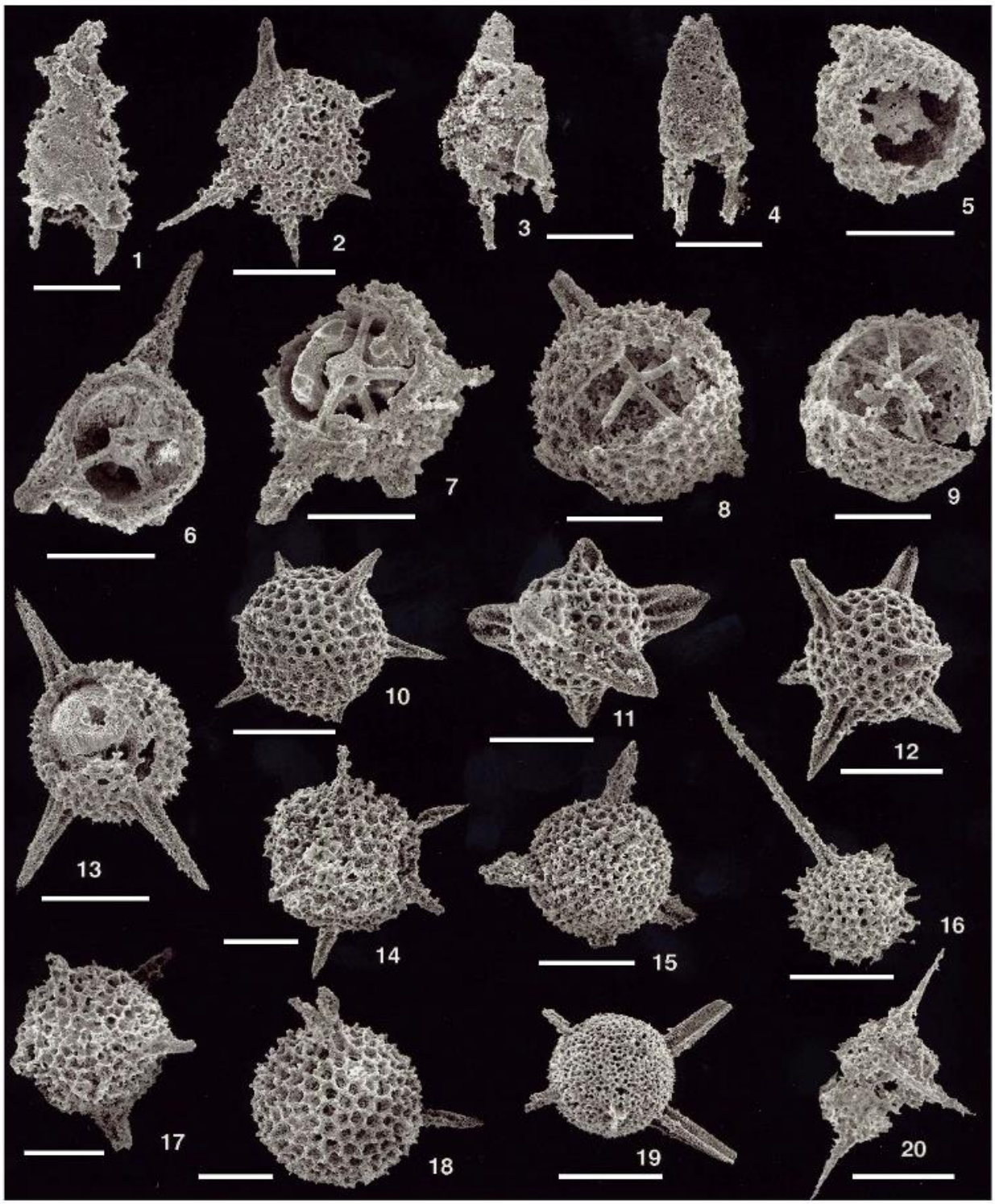

Fig 5: Radiolarian SEM photos of Mississippian chert from southern peninsular Thailand. All scale bars indicate 100 μm. 1, 3, 4. *Albaillell*a sp., 1, EES-KS-ST-0001, 3, EES-KS-ST-0003, 4, EES-KS-ST-0004, 2, 20. *Ceratoikiscum* sp., 2, EES-KS-ST-0002, 20, EES-KS-ST-0020, 5, 6, 7. *Trilonch*e? sp., 5, EES-KS-ST-0005, 6, EES-KS-ST-0006, 7, EES-KS-ST-0007, 8, 9. *Stigmosphaerostylus* sp., 8, EES-KS-ST-0008, 9, EES-KS-ST-0009, 10, 14, 17, 18. *Stigmosphaerostylus*? sp. A, 10, EES-KS-ST-0010, 14, EES-KS-ST-0014, 17, EES-KS-ST-0017, 18, EES-KS-ST-0018, 11. *Stigmosphaerostylus variospina* (Won), EES-KS-ST-0011, 12. *Stigmosphaerostylus* cfr. *vulgaris* (Won), EES-KS-ST-0012, 13. *Stigmoshpaerostylus*? sp. B, EES-KS-ST-0013, 15. *Stigmoshpaerostylus*? sp. C, EES-KS-ST-0015, 16. *Stigmoshpaerostylus* cfr. *delvolei* (Gourmelon), EES-KS-ST-0016, 19. *Spongentactinia exillispina* (Foreman), EES-KS-ST-0019.

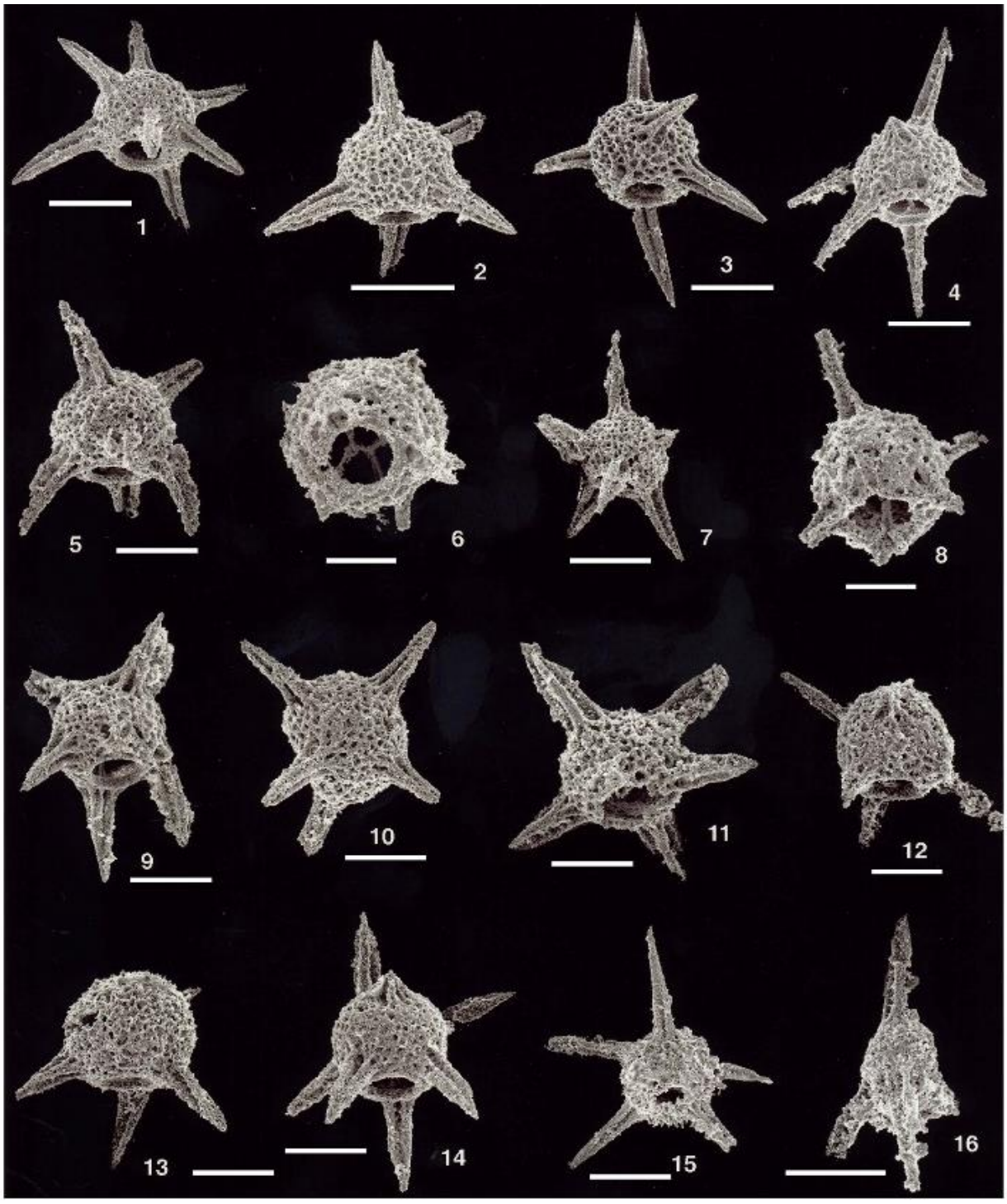

Fig 6: Radiolarian SEM photos of Mississippian chert from southern peninsular Thailand. All scale bars indicate 100 μm. 1–15. *Pylentonema antiqua* Deflandre, 1, EES-KS-ST-2001, 2, EES-KS-ST-2002, 3, EES-KS-ST-2003, 4, EES-KS-ST-2004, 5, EES-KS-ST-2005, 6, EES-KS-ST- 2006, 7, EES-KS-ST-2007, 8, EES-KS-ST-2008, 9, EES-KS-ST-2009, 10, EES-KS-ST-2010, 11, EES-KS-ST-2011, 12, EES-KS-ST-2012, 13, EES-KS-ST-2013, 14, EES-KS-ST-2014, 15, EES-KS-ST-2015, 16. *Archocyrtium* sp., EES-KS-ST-2016.

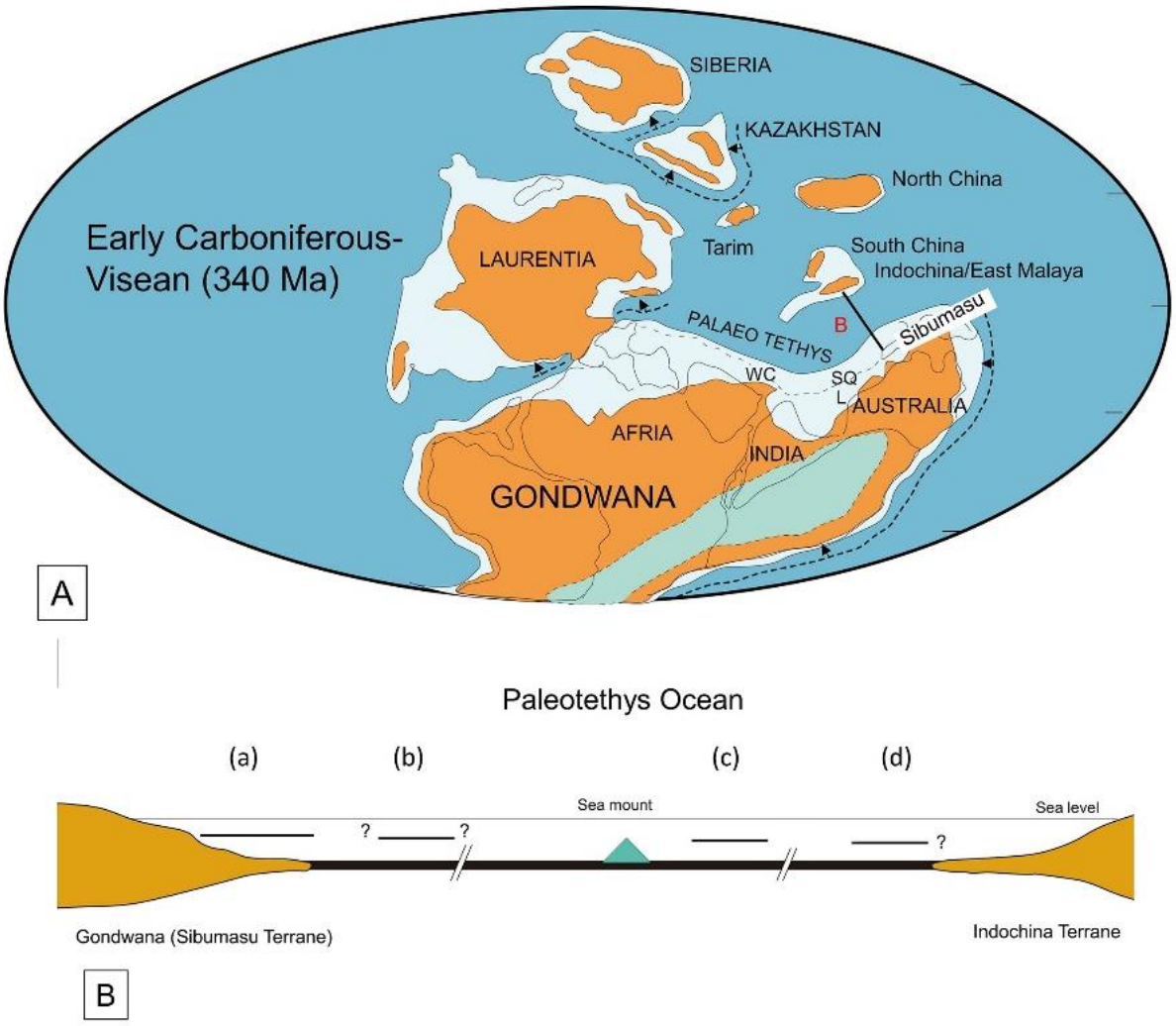

Fig 7: Image of depositional environment of radiolarian bearing siliceous sedimentary rocks. A Paleogeographic map at Mississippian (Tournaisian–Visean: (340 Ma). Map is modified from Metcalfe (2017). B. Image of the depositional sites of radiolarian-bearing sediments across the Paleotethys Ocean. (a): Sashida et al. (2002), Saesaengseerung et al. (2015), The present study. (b): Feng et al. (2004), (c): Sashida et al. (1998), Wonganan and Caridroit (2005), Wonganan et al. (2007), (d): Saesaengseerung et al. (2007a), L=Lhasa, SQ= South Qiangtang, WC=Western Cimmerian

5. Depositional environment of radiolarian--bearing chert

This article reports the late Tournaisian to early Visean (Mississippian) radiolarians from the chert in the Inthanon Zone. Middle–Late Devonian and early Carboniferous radiolarians have been reported from the "Fang Chert" distributed in north of Chiangmai, within the Inthanon Zone (e.g., Ueno, 1999) northern Thailand (Sashida et al., 1993, 1998; Wonganan et al., 2007). These siliceous rock sequence basically does not contain any coarse-grained clastic materials and they are thought to have been deposited in the offshore, far from land and deeper environments of the Paleotethys Ocean (Wonganan et al., 2007). In contrast, the radiolarian--bearing chert is intercalated in the medium to coarse-grained sandstone as described by Sashida et al. (2002) and the present study (Fig. 2). The presence of sandstone beds indicates that the depositional site is near the continent, not far from land. Furthermore, the chert sample (SYK-1) contains foraminiferal shells (Figs. 3 & 4), suggesting that depth of chert accumulation is not deeper than a carbonate compensation depth. Saesaengseerung et al. (2015) discriminated detrital quartz grains in siliceous shale distributed in the Uthai Thani area which means that Devonian to lower Carboniferous radiolarian-bearing siliceous shale has been deposited in hemipelagic, not pelagic

environment. For these reasons, we speculate that the radiolarian-bearing chert of Sashida et al. (2002) and this study deposited on shallower area near land.

In addition to the above-mentioned characteristics, the radiolarian faunal characteristic supports the speculation of the depositional setting. Catalano, Stefano and Kozur (1991), Feng and Ye (1996), Feng, Helmcke, Chonglakmani, Helmcke and Liu (2004), and others mentioned that early Carboniferous radiolarian assemblages from shallow-water sediments are scarce and low diverse: only by members of the Spumellaria and/or Entactinaria usually represented. On the other hand, early Carboniferous radiolarian assemblages from deep-water basins are characterized by abundant and high diversity radiolarians including Spumellaria and/or Entactinaria, Nassellaria, and Albaillellaria, and they usually make radiolarites and/or radiolarian chert. Basir and Zaiton (2011) reported the occurrence of early Carboniferous (Tournaisian) radiolarians from Peninsular Malaysia. They discriminated following three radiolarian assemblages based on the faunal composition and lithology: the *Stigmosphaerostylus*, *Archocyrtium*, and *Albaillellara* assemblages. The *Stigmosphaerostylus* Assemblage is characterized by the occurrence of *Stigmospharostylus variospina* and spherical entactinarians but its specific diversity is very low. The *Archocytrium* Assemblage is characterized by moderate diversity and is dominated by cone-shaped archocyrtiids such as *Archocyrtium*. This assemblage consists of 20 radiolarian species. The *Albaillella* assemblage is characterized by the common occurrence of *Albaillella* and high species diversity (more than 34 species identified). Basir and Zaiton (2011) inferred that The *Stigmosphaerostylus* Assemblage is due to the shallow water environment (upper continental rise), the *Archocyrtium* Assemblage is rather deeper environment (continental rise), and the *Abaillella* Assemblage is open deep-sea marine environment (Ocean basin). They recognized the radiolarian absence in the fauna is attributed to a strong diagenesis and selective dissolution (O'Dogherty, Rodriguez-Canero, Gursky, Matin-Algarra, and Caridroit, 2000). Our examined radiolarian fauna from the chert sample is correlated to the transitional assemblage between the *Arhcocyrtium* and *Albaillella* assemblages based on radiolarian faunal similarity, implying that the chert has been deposited in the upper continental rise to the open deep-sea marine environment (Ocean basin).

The depositional sites of the Devonian to lower Carboniferous radiolarian-bearing siliceous rocks in Thailand are located in roughly four sites in the Paleotethys Ocean based on the lithological characteristics and present geological settings (Fig. 7). The radiolarian-bearing chert reported in this study may have been deposited in the upper continental rise to the open deep-sea basins within the Paleotethys Ocean on the basis of the lithological and faunal characteristics. Seamount consisting of basaltic rocks and carbonate rocks completely lacks of coarse-grained terrestrial materials which may indicate that it formed far from land in the Paleotethys Ocean.

6. Systematic paleontology

Radiolarian description was made by K. S. and T. I. All specimens treated in this paper are stored at the Earth Evolution Sciences, University of Tsukuba, Japan with registered EES-KS. Taxonomic scheme of radiolarians is followed from that of Noble et al (2017).

Order Albaillellaria Deflandre, 1953
Family Albaillellidae Deflandre, 1953 sensu Holdsworth (1977)
Genus *Albaillella* Deflandre, 1952
Type species. - *Albaillella paradoxa* Defladre, 1952

Albaillella sp.
Figs. 5.1, 5.3, 5.4

Remarks. - We collected more than 10 specimens attributed to this species. However, all of them are poorly preserved. Our examined specimens may have cylindrical shell with a smooth surface and conical apical part, and a well-developed H-frame. At the pseudo-abdomen, ventral and dorsal wing may be present. Although we cannot compare precisely our specimens, their outer shell features, short conical and short wing are slightly similar to those of *Albaillella indensis* Won. Our specimens may be distinguished from *Albaillella deflandre* Gourmelon by having above mentioned shell characters.

Sample, occurrence, and range. - This species occurs from Sample SKY-1 and is known from southern Thailand. Mississippian (Tournaisian–Visean).

Family Ceratoiksicidae Holdsworth, 1969
Genus *Ceratoikiscum* Deflandre, 1953
Type species. - *Ceratoikiscum avimexpectans* Deflandre, 1953

Ceratoikiscum sp.
Figs. 5.2, 5.20

Remarks. - Three incomplete specimens were examined. Our specimens are characterized by having a sturdy and conical a.a (a-rod: extra-triangular) and long needle-like i.d (intersector: extratriangular), i.v. (intersetor: extratriangular) and a.p. (a-rod: extratriangular) (nomenclature of *Ceratoikiscum* is from Holdsworth, 1969). However, cavaeal ribs are not clear which may be covered by spongy patagial structure.

Sample, occurrence, and range.- This species occurs from Sample SKY-1 and is known from southern Thailand. Mississippian (Tournaisian–Visean).

Order Entactinaria Kozur and Mostler, 1982
Family Entactiniidae Riedel, 1967
Genus *Spongentactinia* Nazarov, 1975
Type species. - *Spongentactinia fungosa* Nzarov, 1975

Spongentactinia exilispina (Foreman, 1963)
Fig. 5.19

1963 *Entactinia exilispina* Foreman, p. 273, pl. 1, fig. 8.
1987 *Spongentactinia exilispina* (Foreman), Gourmelon, p. 56, 57, pl. 5, figs. 6-8.

Remarks. - We identified only one specimen of this species. Our specimen is characterized by having a spongy spherical shell with may be six spines which are three bladed. Although our examines specimen is an incomplete one, general outer shell features are identical to those of *S. exilispina*.

Sample, occurrence, and range.- This species occurs from Sample SKY-1 and is known from Ohio shale and Montagne Noire, France. Upper Devonian (Famennian) to Mississippian (Tournaisian–Visean).

Genus *Stigmosphaerostylus* Rüst, 1892
Type species. - *Stigmosphaerostylus notabilis* Rüst, 1892

Stigmosphaerostylus variospina (Won, 1983)
Fig. 5.11

1983 *Palaeoxyphostylus variospina* Won, p. 156, 156, pl. 8, figs. 1–4, 6–22.
1986 *Entactinia variospina* (Won), Gourmelon, pl. 4, fig. 1.
1987 *Entactinia variospina* (Won), Gourmelon, p. 49, 50, pl. 3, figs.6, 11.
1989 *Entactinia variospina* (Won), Braun, p. 368, pl. 2, figs. 3, 4, pl. 4, fig. 5.
1990 *Entactinia variospina* (Won), Braun, pl. 7, figs. 4.1–4.13, 4.14.
1994 *Entactinia variospona* (Won), Kiessling and Tragelehn, p. 236, pl. 4, figs. 23, 24.
1995 *Entactinia variospina* (Won), Basir, p. 78, pl. 1, figs.2–4.
1996 *Entactinia variospina* (Won), Spiller, pl. 2, figs. 7, 8.
1997 *Entactinia variospina* (Won), Feng et al., p. 86, pl. 3, figs. 12, 13.
1998 *Entactinia variospina* (Won), Sashida et al., p. 13, 15, figs. 9.1–9.10.
1998 *Entactinia variospina* (Won), Wang et al., pl. 2, figs. 6, 7.
1998 *Entactinia variospina* (Won), Won, p. 238, pl. 2, fig. 18.
2000 *Entactinia variospina* (Won), Sashida et al., p.83, figs. 6.5–6.12.
2002 *Stigmosphaerostylus variospina* (Won), Spiller, p. 43, pl. 6, figs. g, h, i.
2002 *Stigmosphaerostylus variospina* (Won), Sashida et al., p. 132, 133, pl. 1, figs. 18,22,23, pl. 3, fig.12?
2007a *Stigmosphaerostylus variospina* (Won), Saesaengseerung et al., p. 115, 116, figs. 8,7, 8.8, 8.17.
2011 *Stigmosphaerostylus variospina* (Won), Basir and Zaiton, pl. 1, figs. 1–4.
2015 *Stigmosphaerostylus variospina* (Won), Saesaengseerung et al., p. 123, pl. 2, figs. 1–14.

Remarks. - Only one specimen was examined. Our specimen has a spherical shell with short, and sturdy six spines. Shell has many small circular pores surrounded by pentagonal to circular shell frames. Length of spines is generally half of the shell diameter. Won (1983) showed the various types of the spines; number, shape and length of this species. Our examined specimen has shorter and more sturdy spines compared with any of her examined specimens. Gourmelon (1987) also showed several shell morphology of this species. Our specimen is similar to his specimens (pl. 3, figs. 7, 8) which have shorter spines. Our specimen is also similar to the species reported by Saesaengseerung et al. (2007) by having short and sturdy three-bladed spines. This species is distinguished from *E. vulgaris* by having above mentioned shell characters.

Sample, occurrence, and range.- This species occurs from Sample SKY-1 and is known from northern and southern Thailand, Peninsular Malaysia, Europe, and South China. Upper Devonian (Famennian) to Mississippian (Tournaisian–Visean).

Stigmosphaerostylus cfr. *delvolei* (Gourmelon, 1987)
Fig. 5.16

cfr.
1987 *Entactinia*? *delvolvei* Gourmelon, p. 45, 46, pl. 7, figs. 8–10.

Remarks. - Two specimens attributed to this species have been identified. Examined specimens characteristically have a spherical shell with 6 to 7? thin and long spines with small needle-like bi-spines. Illustrated specimen has a long and thin spine whose length is almost twice as the diameter of a spherical shell. Our specimens are similar to the type species of this species which has only two long spines. Our specimens are incomplete, therefore we identified this species with cfr.

Sample, occurrence, and range. - This species occurs from Sample SKY-1 and is known from the Montagne Noire, France. Mississippian (Tournaisian).

Stigmosphaerostylus cfr. *vulgaris* (Won, 1983)
Fig. 5.12

cfr.
1983 *Entactinia*? *vulgaris* Won, pl. 4, figs. 1-3
1986 *Entactinia vulgaris* Won, Gourmelon, p. 184, pl. 2, fig. 4.
1987 *Entactinia vulgaris* Won, Gourmelon, p. 50, 51, pl. 4, figs. 1-6.

Remarks. - We examined two specimens. An illustrated specimen has a spherical shell with 6 three-bladed long conical spines. Many small circular pores surrounded by pentagonal to circular frames are present on the surface of the shell. The original specimens attributed to this species by Won (1983) have more sturdy and longer spines. Therefore, we put cfr. for our specimens.

Sample, occurrence, and range.- This species occurs from Sample SKY-1 and is known from Germany and France, Mississippian (Tournaisian–Visean).

Stigmosphearostylus sp.
Figs. 5.8, 5.9

Remarks. - Several incomplete specimens were examined. Illustrated specimens have a rather small spherical shell with may be six or seven spines. Small circular pores surrounded by square to circular pore frames are present. Thin to moderately thick internal spicule systems consisting of six-rayed spicules are observed in our specimens. Internal spicule system does not have median bar, point centered. This species is distinguished from *S.* sp. B of the present study by having smaller spherical shell.

Sample, occurrence, and range.- This species occurs from Sample SKY-1 and is known from southern Thailand. Mississippian (Tournaisian–Visean).

Stigmosphaerostylus? sp. A
Figs. 5.10, 5.14, 5.17, 5.18

Remarks. - Seven specimens of this species were examined. This species has a spherical shell with six, short, three-bladed and conical spines. This

species is similar to *S. deflendrei* (Won, 1991) described from Germany in general shell feature. However, latter species has longer and more sturdy spines. This species also resembles *S. vulgaris* (Won, 1983), but it differs from the latter by smaller and shorter spines. We questionably assigned this species in *Stigmosphaerostylus* because the internal shell structure cannot be detected.

Sample, occurrence, and range.- This species occurs from Sample SKY-1 and is known from southern Thailand. Mississippian (Tournaisian--Visean).

Stigmosphaerostylus? sp. B
Fig. 5.13

Remarks. – One specimen has been identified. This species is characterized by a spherical shell with may be six or seven spines. Spherical shell is thick and has many and small circular pores on its outer surface. Small conical spines are present at the junction of each neighboring pore flame. Spines are three-bladed and sturdy and long conical shale. We cannot observe the inner side of the spherical shell and determine the presence of spicule system or inner shell. Therefore, we questionably assigned this species in *Stigmosphearostylus*. This species is distinguished from *Stigmosphearostylus*? sp. A of the present study by having longer and more sturdy spines.

Sample, occurrence, and range.- This species occurs from Sample SKY-1 and is known from southern Thailand. Mississippian (Tournaisian–Visean).

Stigmosphaerostylus? sp. C
Fig. 6.15

Remarks. – Only one specimen has been examined. This species has a spherical shell with more than four spines whose length is almost two-thirds of the diameter of shell. Shell has many small circular pores surrounded by polygonal to circular frames. This species similar to *Stigmosphaerostylus*? sp. A of the present study but it has thicker spines.

Sample, occurrence, and range.- This species occurs from Sample SKY-1 and is known from southern Thailand. Mississippian (Tournaisian--Visean).

Genus *Trilonche* Hinde, 1899 sensu Aitchison and Stratford, 1997
Type species.- *Trilonche vetusta* Hinde, 1899

Trilonche? sp.
Figs. 6.5, 6,7

Remarks. - Three specimens were examined. This species has a spherical shell with three to more three-bladed spines and an internal spherical shell. Inner and outer shells are connected by six three--bladed thick spines. The presence of an internal spicule system cannot be determined. The outer shell is thick and has many small pores on the surface of the outer shell. The internal surface of the outer shell is fine sponge. Inner shell has a circular phylome. We questionably placed this species in *Trilonch* because we did not observe the internal spicules in the inner shell and the inner shell has a pylome.

Sample, occurrence, and range.- This species occurs from Sample SKY-1 and is known from southern Thailand. Mississippian (Tournaisian--Visean).

Family Pylentonemidae Deflandre, 1963
Genus *Pylentonema* Deflandre, 1963 sensu Holdsworth et al., 1978
Type species.- *Acanthopyle antiqua* Deflandre, 1960

Pylentonema antiqua (Deflandre, 1960)
Figs. 6.1–6.15

1960 *Acanthopyle antiqua* Deflandre, p. 216, pl. 1, fig. 14
1963 *Pylentonema antiqua* (Deflandre), p. 3981–3984, figs. 1–5.
1973 *Pylentonema antiqua* (Deflandre), Holdsworth, p. 122-125, pl. 1, fig. 4.
1978 *Pylentonema antiqua* (Deflandre), Holdsworth et al, p. 785, figs. 3d, 3e.
1984 *Pylentonema antiqua* (Deflandre), Sandberg and Gutshick, pl. 6, figs. P, T.
1986 *Pylentonema antiqua* (Deflandre), Gourmelon, p. 188-189, pl. 1, figs. 7, 8.

1987 *Pylentonema antiqua* (Deflandre), Gourmelon, p. 102, pl. 15, figs. 1–6.
1998 *Pylentonema antiqua* (Deflandre), Won, p. 255, 256, pl. 6m figs. 9–14, 16.
2002 *Pylentonema antiqua* (Deflandre), Sashida et al., P. 131, 132, pl. 1, figs. 14–17, 20–22, pl. 2, fig. 2, pl. 3, figs. 2, 6, 8, 9, 11?.

Remarks. - More than 30 specimens identified to this species have been obtained. Our forms are characterized by having a spherical shell with 7 spines, among which one is generally small and others are three bladed and sturdy, and their length is almost same as the diameter of spherical shell. Small circular pores surrounded by pentagonal to circular pore rim are present. Internal surface of spherical sell is generally spongy. A large circular pylome is present surrounded by a narrow pylome rim. We can see the internal spicule system (e.g., fig. 6.6), but the presence of inner shell is not sure due to the mesh structure of the internal surface of spherical shell. Position of spines around pylome is variable as discussed by Won (1998), but the type of four spines around pylome (her type Bs and Bd) may be most predominate.

Sample, occurrence, and range.- This species obtained from Sample SKY-1 and is known from Germany, France, North America, Turkey, Thailand. Upper Devonian (upper Famennian) to Mississippian (Tournaisian–Visean).

Order Nassellaria Ehrenberg, 1875
Family Archocyrtidae Kozur and Mostler, 1981
Genus *Archocytrium* Deflandre, 1972 sensu Holdsworth (1973)
Type species. - *Archocyrtium riedeli* Deflandre, 1960

Archocyrtium sp.
Fig. 6.16

Remarks. - Three specimens attributed this species were identified. An illustrated specimen has a subspherical cephalis with three bladed apical horn and three three-bladed feet. Length of apical horn is almost equal with the diameter of cephalis. Small pores are observed on the surface of cephalis. Length of three feet are not known. Our specimens may have week pyrome. This species is similar to *Arhocyrtium venustum* Cheng and *A. riedeli* Deflandre, however, precise comparison cannot be made.

Sample, occurrence, and range. - This species occurs from Sample SKY-1 and is known from southern Thailand. Mississippian (Tournaisian--Visean).

7. Conclusions

1. Radiolarians of 13 species belonging to seven genera have been identified from a black chert bed intercalated within sandstone and variegated siliceous shale at the Kabang area, Songkhla Province, southern peninsular Thailand.
2. The age of the radiolarians may indicate the Tournaisian to Visean, Mississippian (early Carboniferous). The age is slightly younger than that of the previously reported radiolarians in the Saba Yoi-Kabang area in our previous study.
3. The radiolarian-bearing chert characteristically contains foraminiferal shells and therefore the chert may have been deposited in shallower ocean than the carbonate compensation depth. The chert is intercalated within sandstone beds, so that the chert was deposited near land.
4. The radiolarians from the chert sample is correlated to the transitional assemblage between the *Arhcocyrtium* and *Albaillella* assemblages. Consequently, the chert has probably been deposited in the upper continental rise to the open deep-sea marine environment.
5. On the basis of the lithological and radiolarian faunal characteristics, the radiolarian-bearing chert may have been deposited in the upper continental rise to the open deep-sea basins within the Paleotethys Ocean. However, further study such as sedimentary structure and zircon provenance analyses are required to clarify this interpretation.

Acknowledgements

The first author (K.S.) would like to express his sincere thanks to the Mahidol University Kanchanaburi Campus for offering facilities to

carry out our research. The authors also thank to Drs. Sardsud, A. and Saesaengseerung, D. of the DMR (Department of Mineral Resources of Thailand) for giving us various suggestions for our investigations in Thailand. The authors further express our thanks to Dr. Suzuk N. of the Tohoku University for offering important radiolarian literature. We would like to acknowledge three anonymous reviewers for critical reading the manuscript and giving us many constructive suggestions that improved our manuscript.

References

Aitchison, J.C. & Stratoford, J.M.C. (1997). Middle Devonian (Givetian) radiolarians from eastern New South Wales, Australia: A reassessment of the Hinde (1899) funa. *Neues Jarbuh Fur Geologie und Palaeontologie, Abhandlung*, 203, 369–390.

Aitchison, J.C., Suzuki, N., Caridroit, M., Danelian, T. & Noble, P. (2017). Paleozoic radiolarian biostratigraphy. *Geodiversitas, 39*, 419–502.

Basir, J. (1995). Occurrence of bedded radiolarian chert in the Kubang Pasu Formation, North Kedah, Peninsular Malaysia. *Warta Geologi, 21*, 73–79.

Basir, J. & Zaiton, H. (2011). Lower Carboniferous (Tournaisian) radiolarians from peninsular Malaysia and their significance. *Bulletin of the Geological Society of Malaysia, 57*, 47–54.

Braun, A. (1989). Unterkarbonishe Radiolarien aus Kieslschifergeronllen des Marine bei Frankfurt am Main. *Jahresber, Mitt. Oberrhein. Geologische, 71*, 357–380.

Braun, A. (1990). Radiolarien aus dem Unter-Karbon Deutschlands. Courier *Forschung-sinstitute Senckenberg, 133*, 1–177.

Caridroit, M., Fontaine, H., Jongkanjanasoontorn, Y., Suteehorn, V. & Vachard, D. (1990). First results of a palaeontological study of Northwest Thailand. In Fontaine, H. ed., Ten Years of CCOP *Research on the Pre-Tertiary of East Asia*. CCOP/TP, 20, 337–350.

Catalano, R., Stefano, P.D. & Kozur, H. (1991). Permian circumpacific deep-water faunas from western Tethys (Sicily, Italy)-new evidence for the position of the Permian Tethys. *Palaeogeography, Palaeoclimatology, Palaeoecology*, 87, 75–108.

Deflandre, G. (1952). *Albaillella* nov. gen., radiolaire fossile du Carbonifere inferieur, type d7ne lignee aberrante eteinte. *Comptes Rendus hebdomadaires des Seances delAcademie des Sciences (Paris), Serie D: Sciences naturelles, 234*, 872–874.

Deflandre, G. (1953). Radiolaires fossils. In Grasse P. P. ed., *Traite de Zoologie*. Masson, Paris, 389–436.

Deflandre, G. (1960). A propos du developpment des recherches sur les Radiolaires fossils. Revue de *Micropaleonotologie*, 2, 212–218.

Deflandre, G. (1963). Pylentonema, nouveau genre de Radiolarie du Viseen: Sphaerellaire ou Nassellaire? *Comptes Rendus hebdomadaires des Seanace de lAcademie des Sciences (Paris), Serie D: Science naturelles, 257*, 3981–3984.

Deflandre, G. (1972). Le systeme trabeculaire interne chez les pylentonemides et les Popofskyllides, Radiolaires du Paleozoique. Pylogenese des Nassellaries. Comptes *Rendus Academie des Sciences, Paris 274, series D*, 3535–3540.

DMR (Department of Mineral Resources of Thailand). (1999). *Geological Map of Thailand, Scale 1:1,000,000*. Geological Survey Division, Department of Mineral Resources of Thailand, Bangkok.

DMR (Department of Mineral Resources of Thailand). (2013). *Geological Map of Thailand, Scale 1:1,000,000*. Geological Survey Division, Department of Mineral Resources of Thailand, Bangkok.

Ehrenberg, C.G. (1876). Fortestzung der mikro-geologischen Studien als Gesammt-Uebersichtder mikroskopischen Palaontologie gleichartig analysirter Gebigsarten der Erde, mit specieller Rucksicht aud den Polycystine-Megel von Barbados. *Abhandlungender koniglichen preussichen-Akadeie der Wissenschaften zur Berlin, 1875*, 1–225.

Feng, Q. & Ye, M. (1996). Devonian to Triassic Tethys in Western Yunnan, China, In Fan, N. & Feng, Q., eds. *Sedimentologic, stratigraphic and maicropaleontologic studies on Changning-Menglian Orogenic belt*, 15–22.

Feng, G, Ye, M., & Zhang, Z. (1997). Early Carboni-ferous radiolarians from western Yunnan. *Acta Micropalaeontologica Sinica*, *14*, 79–92.

Feng, Q., Helmcke, D., Chonglakmani, P., Helmcke, I. & Liu, B. (2004). Early Carboniferous radiolarians from North-West Thailand. Palaeogeographical implications. *Palaeontology*, 47, 377–393.

Foreman, H.P. (1963). Upper Devonian Radiolaria from the Huron Member of the Ohio Shale. *Micropale-ontology*, 9, 267–304.

Gourmelon, F. (1986). Etude des Radiolaires dun nodule pjhosphate du Carboniferieur de Bareilles, Hautes Pyrenees, France. *Geobios, 19*, 179–197.

Gourmelon, F. (1987). Les radiolaires tournaisiens des nodulesphtoshate de la Montagne noire et des Pyrenees. *Baiostratigraphie du Paleozoique, 6*, 1–172.

Hinde, G.J. (1899). On the Radiolaria in the Devonian rocks of New South Wales. *Quarterly Journal of the Geological Society of London, 55*, 38–64.

Holdsworth, B.K. (1969). Namurian Radiolaria of the genus *Ceratoikiscum* from Staffordshire and

Derbyshire, England. *Micropaleontology, 15*, 221–229.

Holdsworth, B.K. (1973). The Radiolaria of the Baltalimani Formation, Lower Carboniferous, Istanbul. *In* Kaya, Q., ed., *Paleozoic of Istanbul*, 117-134, Ege Universites Fen Fakaltesi Kitaplor, 40.

Holdsworth, B.K. (1977). Paleozoic Radiolaria of the genus Ceratoikiscum from Staffordshire and Derbyshire, England. *Micropaleontology, 15*, 221–229.

Holdsworth, B.K., Jones, D.L. & Allison, C. (1978). Upper Devonian radiolarians separated from chert of the Ford Lake Shale, Alaska. *Journal of Research, U.S. Geological Survey, 6*, 775–788.

Igo, H. (1973). Lower Carboniferous conodonts from Ko Yo, Songkhla, peninsular Thailand. *Geology and Paleontology of Southeast Asia, 12*, 29–42.

Kamata, Y., Ueno, K., Saengsrichan, W., Sardsud, A., Charoentitirat, T., Charsiri, P., & Hisada, K. (2008). Stratigraphy and geological ages of siliceous sedimentary rocks distributed in the Hat Yai area, southern peninsular Thailand. In Choowong, M. & Thitimakorn, T., eds. *Proceedings of International Symposium on Geoscience Resources and Environ--ments of Asian Terranes (Great 2008), 4th IGCP516, and 5th APSEG. Bangkok, 24–26, November 2008* (pp. 349–352). Bangkok, Thailand.

Kamata, Y., Ueno, K., Hara, H., Ichise, M., Charoentitirat, T., Charusiri, P., Sardsud, A., & Hisda, K. (2009). Classification of the Sibumasu and Paleo-Tethys tectonic division in Thailand using chert lithofacies. *Island Arc, 18*, 21–31.

Kamata, Y., Kato, M., Ueno, K., Miyahigashi, A., Charoentitirat, T. & Sardsud, A. (2015). Middle-Late Devonian radiolarians from Klaeng District, Rayong Province, southeastern Thailand. Geotectonic signify-cance of the Rayong area as a continental margin of the Sibumasu Block. *Journal of Asian Earth Sciences, 104*, 197–204.

Kiessling, W. & Tragelehn, H. (1994). Devonian radiolarian faunas of conodont-dated localities in the Frankenwald (northern Bavaria, Gemany). *Abhand-lungen der Geologischen Bundesnanstalt, 50*, 219–255.

Kozur, H. & Mostler, H. (1981). Beitrage zur Erforschnung der mesozoischen Radiolarien. Teil IV: Thalasso-spharacea Haeckel, 1862, Hexastylacea Haeckel 1882, emend. Petrushevskaya, 1979, Sponguracea Haeckel, 1862 emend, und weitere triassische Lithocycliacea, Trematodiscaea, Actiommadea und Nassellaira. *Gologische-Palaontologische Mitteilungea Innsbruck, Sonderband, 1*, 1–208.

Kozur, H. & Mostler, H. (1982). Entactinaria suborder nov., a new radiolarian suborder. *Geologische-Palaontologische Mitteilugen Innsbruck*, 11/12, 399–414.

Metcalfe, I. (2017). Tectonic evolution of Sundaland. *Bulletin of the Geological Society of Malaysia, 63*, 27–60.

Muenlek, S., Meesook, A., Tongchit, P., Tipdhonsab, C., & Skulkaew, P. (1985). *Geologic Map of Changwat Narathiwat and Amphoe Takbai (Sheet NB 47-8,5, Scale 1:250,000)*. Geological Survey Division, Department of Mineral Resources, Bangkok.

Nazarov, B.B. (1975). Radiolaria of the Lower-Middle Paleozoic of Kazakhstan. Trudy *Geologischeskii Institut Akademia Nauk SSSR, 275*, 203 p.

Noble, P., Aitchison, J.C., Danelian, T., Dumitrica, P., Maletz, J., Suzuki, N., Cuvelier, J., Caridroit, M., & O'Dogherty, L. (2017). Taxonomy of Paleozoic radiolarian genera. *Geodiversitas, 39*, 419–502.

O'Dogherty, L., Rodriguez-Canero, R., Gursky, H.J., Matin-Algarra, A. & Caridroit, M. (2000). New data on Carboniferous stratigraphy and palaeogeography of the Malaguide complex (Betic Cordillera, southern Spain). *Comptes Rendus-Academie des Sciences, Serrie II: Sciences de la Terra, et des Planetes, 331*, 533–541.

Pessagno, E.A. and Newport, R. L. (1972). A technique for extracting Radiolaria from radiolarian cherts. *Micropaleontology, 18*, 231–234.

Riedel, W.R. (1967). Some new families of Radiolaria. *Proceedings of the Geological Society of London, 1640*, 148–149.

Rüst, D. (1892). Beitrage zur Kenntnis der fossilen Radiolarien aus Gesteinen der Trias und der palaeozoischen. *Schichten. Palaeontolographica*, 38, 107–192.

Saesaengseerung, D., Sashida, K., & Sardsud, A. (2007a). Late Devonian to early Carboniferous radiolarian fauna from the Pak Chom area, Loei Province, northeastern Thailand. *Paleontological Research, 11*, 109–121.

Saesaengseerung, D. Sashida, K., & Sardsud, A. (2007b). Devonian to Triassic radiolarian faunas from northern and northeastern Thailand. In Tantiwanit, W. ed., *Proceedings of the International Conference on Geology of Thailand: Towards Sustainable Development and Sufficiency Economy* (pp. 54–71). Bangkok, Thailand.

Saesaengseerung, D., Kawinae, T., & Pothichaiya, C. (2015). Discovery of Devonian to Carboniferous radiolarians from central Thailand and its significance of these fauna in Thailand and Laos. *The 3rd Lao-Thai Technical Conference, July 8-8, 2015* (pp. 115–134). Bangkok, Thailand.

Sandberg, C. & Gutschick, R.C. (1984). Distribution, microfauna and source-rock potential of Mississippian Della Phosphatic member of Woodman Formation and equivalents, Utah and adjacent states. In Woodward, J. et al. (Eds.), *Hydrocarbon source rocks of the Greater Rocky Mountain region* (pp. 135–178),

Rocky Mountain Association of Geologists, Denver, Colorado.

Sardsud, A. & Saengsrichan, W. (2002). *Geological Map of Amphoe Hat Yai Sheet (5023II)*. Department of Mineral Resources, Technical report, no. 16, 1–77. (in Thai with English summary)

Sashida, K., Igo, H., Hisada, K., Nakornsri, N., & Amprnmaha, A. (1993). Occurrence of Paleozoic and Early Mesozoic Radiolaria in Thailand (preliminary report). *Journal of Southeast Asian Earth Sciences*, 8, 97–108.

Sashida, K., Igo, H., Adachi, S., Ueno, K., Nakornsri, N., & Sardsud, A. (1998). Late Paleozoic radiolarian faunas from northern and northeastern Thailand. Science *Reports of the Institute of Geosciences, University of Tsukuba, section B, 19*, 1–27.

Sashida, K., Nakornsri, N., Ueno, K., & Sardsud, A. (2000). Carboniferous and Triassic radiolarian fauna from the Saba Yoi area, southernmost part of peninsular Thailand and their paleogeographic significance. *Science Reports of the Institute of Geoscience, University of Tsukuba, section B, 21*, 71–99.

Sashida, K., Salyapongse, S., & Charusri, P. (2002). Lower Carboniferous radiolarian fauna from the Saba Yoi-Kabang area, southernmost part of peninsular Thailand. *Micropaleontology, 48*, supplement 1, 129–143.

Spiller, F.C.P. (1996). Late Paleozoic radiolarians from the Bentong-Raub suture zone, Peninsular Malaysia. *The Island Arc, 5*, 91–103.

Spiller, F.C.P. (2002). Radiolarian biostratigraphy of Peninsular Malaysia and implications for regional palaeotectonic and palaeogeography. Palaeontographica Abteilung A: *Palaeozoologie-Stratigraphie, 266*, 1–91.

Ueno, K. (1999). Gondwana/Tethys divide in East Asia: solution from Late Paleozoic foraminiferal paleobiogeography. In Ratanasthien, B. & Rieb, S.L. (Eds.), *Proceedings of the International Symposium on Shallow Tethys (ST) 5*, (pp. 45–54), Chiang Mai, Thailand.

Ueno, K. & Charoentitirat, T. (2011). Carboniferous and Permian. In Ridd, M.F. et al., eds., *The Geology of Thailand*, 71–136, The Geological Society, London.

Wakita, K. & Metcalfe, I. (2005). Ocean plate stratigraphy in East and Southeast Asia. *Journal of Asian Earth Sciences, 24*, 679–702.

Wang, Y.J., Luo, H., Kuang, G., & Li, J. (1998). Late Devonian-Late Permian strata of cherty facies at Xiadong and Banchen countries of the Qinzhou area, SE Guangxi. *Acta Micropalaeonotoliglca Sinica, 15*, 351–366.

Won, M.Z. (1983). Radiolarian aus dem Unterkarbon des Rheinischen Schiefergebireges. *Palaeontographica, Abteilung A: Palaozoologie-Stratigraphie, 182*, 116–175.

Won, M.Z. (1991). Lower Carboniferous radiolarians from siliceous boulders in western Germany. *Journal of Paleontological Society of Korea, 7*, 77-106.

Won, M. (1998). A Tournaisian (Lower Carboniferous) radiolarian zonation and radiolarian of the A. pseudoparadoxa Zone from Oese (Rheinische Schifergebirege) Germany. *Journal of Korean Earth Science Society, 19*, 216–259.

Wonganan, N. & Caridroit, M. (2005). Middle and Upper Devonian radiolarian faunas from Chiang Dao area, Chiang Mai Province, northern Thailand. *Micropaleontology, 51*, 39–57.

Wonganan, N., Randon, N. & Caridroit, M. (2007). Mississippian (early Carboniferous) radiolarian biostratigraphy of northern Thailand (Chang Dao area). *Geobios, 40*, 875–888.

THAI GEOSCIENCE JOURNAL

If you are interested in earth sciences
Support geoscience with a subscription to

Thai Geoscience Journal

The **Thai Geoscience Journal** publishes original research and review articles from the international community in all fields of geological sciences such as

- Engineering Geology
- Petrology
- Medical Geology
- Paleontology
- Economic Geology
- Geophysics
- Tectonics
- Structural Geology
- Geochemistry

All articles published by the **Thai Geoscience Journal** are made freely and permanently accessible online immediately upon publication, **without subscription charges or registration barriers.**

Please scan for

VISIT US

ARTICLES SUBMISSION

SUBSCRIPTION TO TGJ AND MORE INFORMATION

Contact
Mineral Resources Research and Development Center
Department of Mineral Resources 75/10 Rama VI Road,
Ratchatewee, Bangkok 10400 Phone: +66 2-6219731
Website : https://www.dmr.go.th/tgjdmr/
E-mail : tgj.2020@gmail.com

Published by

CONCEPT DESIGN

This logo composes of Abbreviations of Thai Geoscience Journal

T = THAI G = GEOSCIENCE J = JOURNAL

Coexistence of 3 abbreviations design in a concept of modernity blend with a Thainess
Modification of G alphabet in a shape of ammonoid shows relevance to geology
and infinite development of Thai Geoscience Journal

- **SCOPE AND AIM OF THAI GEOSCIENCE JOURNAL (TGJ):** TGJ is an international (Thai and English) journal publishing original research articles dealing with the geological sciences. It focuses, mainly but not exclusively, on: Sedimentology and Geomorphology, Palaeontology, Quaternary, Geology and Environment Change, Geological Hazards, Environmental Geosciences, Geophysics, Mineral and Petroleum Geology, Tectonics and Structural Geology, Geochemistry and Geochronology, Metamorphic Geology and Volcanic and Igneous Geology. Two types of articles are published in the Journal: Research Articles and Reviews. Research Articles are new original articles, normally not exceeding 25 pages. Review Articles are those papers that summarize the current state of knowledge on specific fields or topics of geosciences. They analyze and discuss previously published research results, rather than report new results. TGJ Aim is to provide valuable geoscience knowledge and information and push more inspiration for readers and researchers to produce treasure research in the future.
- **FEEDBACK AND CONTACT:** We welcome your feedback, comments and suggestions for the development of TGJ

Please contact: Dr. Apsorn Sardsud (Editor-in-Chief, TGJ)
Department of Mineral Resources
75/10 RamaVI Road Ratchathewee Bangkok 10400, Thailand

Phone: +66 (0)2 6219731

Email: tgj.2020@gmail.com

Website: http://www.dmr.go.th/tgjdmr

TGJ Contributors

Assoc. Prof. Dr. Apichet Boonsoong	Chiang Mai University, Thailand
Dr. Apsorn Sardsud	Department of Mineral Resources, Thailand
Prof. Dr. Che Aziz bin Ali	Universiti Kebangsaan Malaysia, Malaysia
Prof. Dr. Clive Burrett	Mahasarakham University, Thailand
Assoc. Prof. Dr. Danupon Tonnayopas	Prince of Songkla University, Thailand
Dr. Dhiti Tulyatid	Coordinating Committee for Geoscience Programmes in East and Southeast Asia, Thailand (CCOP)
Dr. Ian Watkinson	University of London, England
Mr. Jittisak Premmanee	Department of Mineral Resources, Thailand
Prof. Dr. Katsumi Ueno	Fukuoka University, Japan
Prof. Dr. Katsuo Sashida	Mahidol University, Kanchanaburi campus, Thailand
Prof. Dr. Ken-Ichiro Hisada	University of Tsukuba, Japan
Assoc. Prof. Dr. Kieren Howard	Kingsborough Community College, City University of New York, USA
Prof. Dr. Koji Wakita	Yamaguchi University, Japan
Assoc. Prof. Dr. Kriengsak Srisuk	Khon Kaen University, Thailand
Assoc. Prof. Dr. Lindsay Zanno	North Carolina State University, USA
Dr. Mallika Nillorm	Department of Mineral Resources, Thailand
Dr. Martin Smith	Global Geoscience, British Geological Survey, UK
Adj. Prof. Dr. Michael Ryan King	Western Colorado University, Thailand
Prof. Dr. Montri Choowong	Chulalongkorn University, Thailand
Assoc. Prof. Dr. Mongkol Udchachon	Mahasarakham University, Thailand
Prof. Dr. Nigel C. Hughes	University of California, Riverside, USA
Mr. Niwat Boonnop	Department of Mineral Resources, Thailand
Asst. Prof. Nussara Surakotra	Khon Kaen University, Thailand
Asst. Prof. Dr. Passkorn Pananont	Kasetsart University, Thailand
Dr. Phumee Srisuwan	Department of Mineral Fuels, Thailand
Prof. Dr. Pitsanupong Kanjanapayont	Chulalongkorn University, Thailand
Dr. Pol Chaodumrong	Geological Society of Thailand, Thailand
Dr. Pradit Nulay	Department of Mineral Resources, Thailand
Dr. Prinya Putthapiban	Mahidol University Kanchanaburi Campus, Thailand
Prof. Dr. Punya Charusiri	Department of Mineral Resources, Thailand
Asst. Prof. Dr. Rattanaporn Hanta	Suranaree University of Technology, Thailand
Assoc.Prof. Rungruang Lertsirivorakul	Khon Kaen University, Thailand
Assoc. Prof. Dr. Sachiko Agematsu-Watanabe	University of Tsukuba, Japan
Dr. Sasiwimol Nawawitphisit	Department of Mineral Resources, Thailand
Dr. Seung-bae Lee	Korea Institute of Geoscience and Mineral Resources, Republic of Korea
Dr. Siriporn Soonpankhao	Department of Mineral Resources, Thailand
Asst. Prof. Dr. Sombat Yumuang	Geo-Informatics and Space technology Development Agency, Ministry of Science and Technology (GISTDA), Thailand
Mr. Somchai Chaisen	Department of Mineral Resources, Thailand
Dr. Surin Intayos	Burapha University, Chanthaburi Campus, Thailand
Mr. Sutee Chongautchariyakul	Department of Mineral Resources, Thailand
Dr. Tawatchai Chualaowanich	Department of Mineral Resources, Thailand
Mr. Thananchai Mahatthanachai	Department of Mineral Fuels, Thailand
Assoc. Prof. Dr.Thasinee Charoentitirat	Chulalongkorn University, Thailand
Dr. Toshihiro Uchida	Retired geophysicist, Japan
Mr.Tritip Suppasoonthornkul	Department of Mineral Fuels, Thailand
Dr. Weerachat Wiwegwin	Department of Mineral Resources, Thailand
Assoc. Prof. Dr. Yoshihito Kamata	University of Tsukuba, Japan

Thai Geoscience Journal
Vol. 2 No. 2
July 2021
ISSN 2730-2695

CONTENTS

Published by
Department of Mineral Resources
Geological Society of Thailand
Coordinating Committee for Geoscience Programmes in East And Southeast Asia (CCOP)